SURFACE ZETA POTENTIAL AS A BIOMARKER FOR MONITORING HUMAN RED BLOOD CELLS

BY

BRANDON K. EBERL

A Dissertation Submitted to the Graduate Faculty of

WAKE FOREST UNIVERSITY GRADUATE SCHOOL OF ARTS AND SCIENCES

Partial Fulfillment of the Requirements

for the Degree of

DOCTOR OF PHILOSOPHY

Biomedical Engineering

May 2026

Winston-Salem, North Carolina

Approved By:

Erin Henslee, Ph.D., Advisor and Committee Chair

James Jordan, Ph.D.

Rafael Davalos, Ph.D.

Daniel Kim-Shapiro, Ph.D.

Oleg Kim, Ph.D.

Acknowledgements

I want to first and foremost thank my Lord and Savior, Jesus, for His faithfulness every day and for getting me through this major life and career milestone.

To my PhD Advisor, Dr. Erin Henslee, words can't begin to describe how incredibly blessed I am to have spent the past three-and-a-half years under your mentorship, and how blessed I am for your unwavering support of me throughout my entire graduate school journey. Thank you for pushing me every single day (both with constructive criticism where needed, and with enthusiastic encouragement, celebrating the "little wins") to achieve my full potential personally and professionally. I am a certainly a better doctoral researcher, biomedical engineer, and human being because of your friendship and your incredible mentorship.

To my other committee members: Dr. Jordan, Dr. Davalos, Dr. Kim-Shapiro, and Dr. Kim, thank you for your tremendous support, encouragement, and the countless technical insights you each have provided to me throughout the last three-and-a-half years, especially during the preparation of this dissertation.

To (future Dr.) Sydney Joseph, thank you for being an awesome lab and office mate and for selflessly subjecting yourself to repeated needle sticks (and many, many bruises) to draw your blood for my experiments (thank you Dr. Henslee for your blood too). I am excited to continue watching you develop into an amazing researcher, engineer, and doctoral scholar over the remainder of your graduate school career. To (now Dr.) Malaena White (Khoury), you were the first grad student and friend I met during orientation in August 2019. I am forever grateful for your friendship, and for the countless times you

provided empathy and encouragement to me, especially during the long, hard days of my lab transition.

To Dr. Gross, Dr. Yazdani, Dr. VanderKam, Dr. Kenny, and the rest of the Wake Forest Department of Engineering faculty, thank you for allowing me to contribute to the growth and development of the nascent WFU Engineering program over the past 7 years as a Graduate Teaching Assistant for numerous classes, and an Adjunct Teaching Professor (in Spring 2022). I have enjoyed learning from each of you and contributing to the growth of our program and the undergraduate student body at Wake Forest University.

To all my clinical mentors in cardiology (Drs. Michael Walsh, Carmen Kiper, and R. Brandon Stacey), pediatric cardiothoracic surgery (Drs. Yoshi Ootaki, Joe Turek, and Ross Ungerleider) and cardiovascular perfusion (Drs. Rob Baker and Tony Shackleford, Jillian and John Holler, and Matt Wilder) thank you for your unwavering support and mentorship, reminding me of the potential clinical impact of my *ex vivo* research, and of my goal from day 1 of graduate school— *use my passion for medicine, engineering design, and entrepreneurship to develop medical devices with the goal of providing hope and healing to pediatric patients at their greatest point of need*.

To my countless friends, and my church and young adult small group family, thank you for your standing by my side, for your countless prayers and support (and coffee and snack outings) throughout my PhD journey. To my family, especially my mother, Karen Taylor, you are my rock, and my first best friend and my biggest cheerleader. WE would have not achieved this PhD dream together without your never-ceasing prayers and Bible verses to encourage me, along with the cute kitten and ducking Instagram reels, and more Starbucks coffee runs than I can count. To (my future stepdad) Rob Padgett, your countless

prayers and encouragement mean the world to me. I am so thankful to have you in my life, and for your support during my PhD journey. To my twin sister, Brianna Eberl, thank you for being my biggest fan since day one (literally) and for the many lunch and dinner dates over the years. I love you so much. To my brother, Bryan Eberl, thank you for taking me along on your crazy adventures, both in North Carolina and abroad, and for your willingness to drive over three hours during your off weeks just to hang out with me. I am incredibly grateful for your friendship. I love each of you so much! Lastly, these acknowledgements would not be complete without a quote from my engineering role model, Thomas Eddison:

"Our greatest weakness lies in giving up. The most certain way to succeed is always to try just one more time."

Table of Contents

List of Figures and Tables

CHAPTER 2:

Figures:

CHAPTER 3:

Figures:

CHAPTER 4:

Figures:

Tables:

CHAPTER 5:

Figures:

Tables:

List of Abbreviations

3DEP	Three-Dimensional Dielectrophoresis
ATP	Adenosine Triphosphate
Ca^{2+}	Calcium Ion
CAT	Catalase
C_{EFF}	Effective Membrane Capacitance
Cl^-	Chloride Ion
CO_2	Carbon Dioxide
σ_{CYT}	Cytoplasmic Conductivity
DMSO	Dimethyl Sulfoxide
ECMO	Extracorporeal Membrane Oxygenation
EDL	Electric Double Layer
ELS	Electrophoretic Light Scattering
EM	Electrophoretic Mobility
ESR	Erythrocyte Sedimentation Rate
G_{EFF}	Effective Membrane Conductance
GLUT1	Glucose Transporter 1
GPX	Glutathione Peroxidase
H_2O_2	Hydrogen Peroxide
Hb	Hemoglobin
HBSS	Hanks' Balanced Salt Solution
HCO_3^-	Bicarbonate
Hct	Hematocrit
K^+	Potassium Ion
MCV	Mean Corpuscular Volume
Na^+	Sodium Ion
OD	Optical Density
OS	Oxidative Stress
PBS	Phosphate Buffered Saline
PIXIE	Affinity Pixie™ Membrane Oxygenator
pO_2	Partial Pressure of Oxygen
RBC	Red Blood Cell
ROS	Reactive Oxygen Species

SA_{free}	Free (unbound) sialic acid
tBHP	Tert-butyl Hydroperoxide
ζ-potential	Surface Zeta Potential

Abstract

Red blood cells (RBCs) are the most abundant cell in the human body. RBCs play a critical role maintaining physiologic homeostasis through oxygen and carbon dioxide exchange. Negative surface charge is an important property of RBCs that prevents them from clumping and adhering to vessels or other cells via the repulsive, negative force. During normal circulation and in disease processes (e.g., cardiovascular disease and RBC-related diseases) RBCs can be damaged and membrane surface charge can be impacted. This damage can be induced by oxidative stress (OS) as well as exposure to mechanical shear stress produced by physiologic circulation and mechanical circulatory support devices. Conventionally, erythrocyte sedimentation rate (ESR) has been used to quantify surface charge-induced RBC aggregation, by measuring the time required for RBCs to settle at the bottom of a glass tube. However, ESR cannot directly measure the electrostatic forces responsible for causing RBC aggregation.

Surface zeta potential is an alternate technique that offers the ability to directly measure the cell's surface charge and repulsive forces. While surface zeta potential has been shown to be sensitive in healthy human RBCs, as well as in RBC-related disease processes, the mechanistic sensitivity and specificity of surface zeta potential response for RBCs exposed to OS and mechanical shear stress remains largely unknown. This work aims to investigate surface zeta potential for use as a biomarker to monitor human RBCs exposed to OS and mechanical shear stress, as well as demonstrate applicability of surface zeta potential as a real-time biomarker for RBC monitoring in extracorporeal membrane oxygenation (ECMO) cardiopulmonary bypass systems.

This will be achieved through two primary research studies. In the first study, the mechanistic sensitivity and specificity of surface zeta potential will be examined through the treatment of human RBCs to three oxidizing agents with different mechanistic pathways. In the second study, the impact of mechanical shear stress exposure on the surface zeta potential of human RBCs will be investigated. Through this study, a clinical application of zeta potential monitoring of human RBCs in ECMO will be demonstrated. This is the first application of surface zeta potential in the real-time monitoring of ECMO systems.

Collectively, this work demonstrates surface zeta potential's ability to detect subtle changes in human RBCs during physiologically relevant processes. Importantly, storage duration of whole blood is the most consistent variable impacting RBC health and surface zeta potential in our studies. This can have significant implications for RBC storage protocols since all our experiments are conducted within the allowable storage duration in clinical settings.

Chapter 1: Introduction

DISSERTATION SIGNIFICANCE AND AIMS

Red blood cells (RBCs) are the most abundant cell in the human body. RBCs play a critical role maintaining physiologic homeostasis through oxygen and carbon dioxide (CO_2) exchange. RBC cell size, shape, and volume, as well as surface charge are important properties for monitoring RBC health and disease progression. Negative surface charge is an important property of RBCs that prevents them from clumping and adhering to vessels or other cells via the repulsive, negative force. During both normal circulation and in disease (e.g., cardiovascular disease and RBC-related diseases) RBCs can be damaged and surface charge can be impacted. This damage can be induced by chemical oxidative stress[1–3] and due to exposure to mechanical shear stress, often caused by both physiologic blood circulation and produced by mechanical circulatory support devices[4,5].

Conventionally, erythrocyte sedimentation rate (ESR) has been used by clinicians and researchers to quantify RBC aggregation by measuring the time required for RBCs to settle at the bottom of a glass tube[6,7]. While ESR can detect the presence of underlying disease contributing to reduced surface charge, it cannot directly measure the electrostatic forces responsible for causing RBC aggregation. Further, ESR measurements are highly influenced by factors such as cell size, leading to wide variability in measurements across studies[8–10].

Surface zeta potential (ζ-potential) is a method used to directly quantify RBC surface charge by measuring particles moving under the influence of an applied electric

field. Surface ζ-potential has been shown to exhibit sensitivity in healthy RBCs during physiologic processes (e.g., circadian rhythmicity)[11] and during RBC-related diseases[12–14] (e.g. malarial anemia and cardiovascular disease). However, the mechanistic sensitivity and specificity of ζ-potential under oxidative and mechanical stressors remains largely unknown.

The primary aim of this dissertation was to investigate changes in the surface ζ-potential of human red blood cells (RBCs) for use as a biomarker to monitor RBCs exposed to chemical and mechanical stressors. This was accomplished through two primary research studies with the following aims:

Research Aim 1: Develop an understanding of mechanistic sensitivity and specificity of ζ-potential response to oxidative stress in human RBCs.

Research Aim 2: Develop an understanding of ζ-potential response to flow-induced mechanical shear stresses in human RBCs.

Research Aim 3: Apply ζ-potential as a tool for monitoring human RBCs in extracorporeal membrane oxygenation (ECMO) bypass circuits.

BACKGROUND

Introduction to ζ-potential: Surface zeta potential (ζ-potential) is an electro-physical property of charged particles placed in suspension[15,16]. It offers the ability to directly measure the particle's surface charge and repulsive forces. In the field of colloidal

science, ζ-potential is used to predict the stability and likelihood of particles to aggregate. ζ-potential has been applied in a wide variety of both biological and industrial settings[17]. For example, ζ-potential has been applied in the development of curcumin nanocrystals to improve *in vivo* drug solubility and particle stability via tunable surface charge.

In other biological contexts, ζ-potential has been used to characterize the biochemical composition of yeast and coconut milk, specifically investigating how the pH of solution alters the surface chemistry of these proteins, and applications for improving beverage stability[18]. In industrial settings and materials science[19], nanoparticle design and optimization have been a major focus of scientific studies. One such application of nanoparticle-based ζ-potential characterization is the development and optimization of ionic liquids [20]. At present, the effects of thermal conductivity and viscosity of ionic-liquids have revealed differences in the thermal-physical properties based on the shape of nanoparticles, such as aluminum oxide[21,22].

Recently, there has been a growing interest to study the effects of nanoparticle properties (e.g., size, shape, etc.) on ζ-potential response to further enhance the stability and heat transfer properties of ionic liquids. Although my dissertation work presented is specifically focused on RBC applications, the results presented in my dissertation may inform other applications of ζ-potential and further contribute to the broader field of colloidal science.

ζ-potential as a Tool for RBC Monitoring: Beyond the industrial and biological applications discussed above**,** ζ-potential can play an important role in improving human

health. One primary application of this is in the study of red blood cells (RBCs). Beginning with the seminal 1940s work of Ponder *et al*[23] and Wright *et al*[24], ζ-potential, has gained increasing attention for its application in monitoring RBCs. ζ-potential is important for monitoring RBCs because it offers the potential to predict changes in cell surface properties before disease occurs, unlike other measurements of RBCs.

Measurement of ζ-potential cannot be performed directly, rather, it must be obtained using mathematical models and experimental measurements of the particle's electrophoretic mobility (EM) defined as the movement of charged particles under the influence of an applied electric field. Experimentally, the ζ-potential of RBCs is measured using electrophoretic light scattering technique (ELS). ELS allows for repeatable ζ-potential with high measurement precision (± 0.1 mV). ELS-based ζ-potential measurement is performed using a commercial ζ-potential analyzer (e.g., Malvern Zetasizer)[25,26]. As described in *Chapter 3,* experimental ELS works by first measuring the frequency of scattered light emitted as RBCs move under an applied electric field. The light frequency is then converted to EM, used to quantify RBC ζ-potential using the Helmholtz-Smoluchowski approximation (Equation 1.1):

$$\zeta = \frac{4\pi\eta}{\varepsilon} \cdot \mu_p f(\kappa\alpha) \tag{1.1}$$

where η and ε are the viscosity (in Pa·s) and dielectric constant of the suspending media (in F/m) respectively, and μ_p is the electrophoretic mobility (in $m^2/V{\cdot}s$). The dimensionless Henry function, denoted by $f(\kappa\alpha)$ above, relates particle radius to electric double layer

thickness (described in *Chapter 3*). For RBCs, the value of the Henry function[27] is approximated to be $f(\kappa\alpha)$ =1.5, based on their cell diameter of ~8 μm.

For the work presented in this dissertation all ζ-potential were carried out at a temperature of 25 °C, and a maximum of 30 ζ "sub-runs" per technical replicate were collected (decreased from the automated software cap of 100 "sub-runs" to mitigate risk of RBC sedimentation). This was preceded by a temperature equilibration time of 60 seconds. Specific methods for RBC sample preparation and the application of drug treatment (*Chapter 4*) and mechanical shear stress (*Chapter 5*) are described in the individual chapters.

DISSERTATION ORGANIZATION

The dissertation is organized into 5 subsequent chapters. Descriptions of each chapter are provided below:

Chapter 2 – RBC Physiology and Electrophysiological Measurement: This chapter introduces basic concepts of RBC physiology, particularly how it pertains to cellular electrophysiology. Additionally, a brief description of normal RBC physiologic processes and RBC-related diseases (e.g., cell aging, eryptosis, and hemostasis) are discussed. Finally, this chapter concludes with a section on the electrophysiological measurement of human RBCs.

Chapter 3 – ζ-potential Theory, RBC Applications, and Measurement Optimization:

This chapter begins with a review of electrokinetic principles influencing ζ-potential measurement (electro-osmosis, streaming potential, charge density, and EDL thickness). A mathematical derivation of the classical Smoluchowski formula is provided along with the assumptions applied for characterizing RBCs. Although electrophoretic light scattering (ELS) is used in this dissertation for measuring ζ-potential, I briefly describe alternative techniques for ζ-potential measurement, such as microelectrophoresis and optical tweezers, including applications of each for monitoring RBCs. Next, a review of ζ-potential RBC applications (cardiovascular disease, blood storage, and RBC-related diseases) is conducted to provide a framework for where my work sits within the broader scope of RBC monitoring. Lastly, to carry out robust, reliable ζ-potential experiments throughout this work, several experimental parameters were optimized, including the conductivity of the iso-osmotic suspending medium and RBC concentration. These optimization experiments informed all subsequent experiments presented in this dissertation.

Chapter 4 – ζ-potential for Monitoring Human RBCs in Oxidative Stress: The first experimental study presented investigates the electrophysiologic response of human RBCs to chemical oxidative stress (OS), and probes the mechanisms of action driving oxidative processes in RBCs. This chapter begins with a literature review describing the significance, current approaches, and limitations of monitoring OS in RBCs. Experimental methods used to chemically induce OS, and the specific experimental technique (e.g., intracellular Ca^{2+}, free sialic acid, etc.) to monitor the RBC biophysical response are described in detail.

Standard methods for monitoring the electrophysiologic response of RBCs using a commercial Zetasizer (ζ-potential) and 3DEP (for σ_{CYT}, C_{EFF}, and G_{EFF}) are also described. The effect of drug concentration, as well as a comparison of different OS agents and their impacts on the ζ-potential response and biophysical properties of RBCs is explored.

Chapter 5 – ζ-potential for Monitoring Human RBCs in ECMO and Shear Stress:

The second experimental study investigates effects of blood circulation time and blood storage duration on the ζ-potential response of human RBCs circulating through a benchtop extracorporeal membrane oxygenation (ECMO) circuit. The effects of mechanical shear stress and exposure time, and magnitude on the ζ-potential response of human RBCs was also investigated, along with consideration for the compounding effects of blood storage duration. This chapter starts with a review of the literature on clinical relevance of ECMO, current approaches and limitations for blood monitoring in ECMO systems, and potential implications of ζ-potential for RBC monitoring in ECMO. Next, the methods for ECMO circuit setup/operation, and data collection are outlined, including ζ-potential, hemolysis and microscope imaging for comparison of blood circulation effects, and blood storage effects (stored up to 49 days as whole blood) on the ζ-potential and biophysical responses of human RBCs. Additionally, to probe the sensitivity of ζ-potential in RBCs exposed to mechanical shear stress, RBCs were exposed to high (123 Pa) shear stress over increasing shear duration up to 6s. The effects of shear stress magnitude on the ζ-potential of human RBCs were also investigated by comparing high and low shear stress (61.25 Pa) at maximum shear duration. Finally, the compounding effects of blood storage duration

(stored up to 49 days as whole blood) on the ζ-potential response of RBCs exposed to mechanical shear stress was also explored.

Chapter 6: Conclusions and Future Work: The final chapter summarizes major findings from each of the research studies. To address the study limitations discussed in *Chapters 4-5* several future studies are proposed as follows:

Future Work on RBC Monitoring in OS:

- Determine effects of incubation time on the ζ-potential response at physiologically relevant treatment dosage (e.g., below 0.5 mM).
- Determine mechanistic contributions of glutathione and catalase for RBC repair, observed through the lens of ζ-potential modulation.
- Determine biophysical mechanisms responsible for sialic acid removal in oxidative processes, comparing removal of sialic acid by viral agents (e.g. neuraminidase) to cleavage by drug-induced ROS.

Future Work on RBC Monitoring in Mechanical Shear Stress:

- Determine ζ-potential response of human RBCs to mechanical shear stress in physiologically relevant fluids, to accurately mimic rheological properties observed in *vivo*.
- Determine the effects of heparin concentration on ζ-potential response of human RBCs exposed to mechanical shear stress.

- Determine the ζ-potential response of human RBCs exposed to peak mechanical shear stress.

Future Work on RBC Monitoring in ECMO:

- Determine the time-based response of oxygenator protective effects in ECMO.
- Determine the compounding effect of oxygen on ζ-potential response in ECMO.
- Determine effects of circuit components on ζ-potential response in ECMO.

REFERENCES

1. McNamee, A. P., Horobin, J. T., Tansley, G. D. & Simmonds, M. J. Oxidative stress increases erythrocyte sensitivity to shear-mediated damage. *Artif. Organs* **42**, 184–192 (2018).

2. Bayer, R. & Waßer, G. Effects of oxidative stress on erythrocyte deformability. in vol. 2678 333–341 (SPIE, 1996).

3. Chiu, D. T.-Y. & Liu, T. Z. Free radical and oxidative damage in human blood cells. *J. Biomed. Sci.* **4**, 256–259 (1997).

4. Avcı, M., O'Rear, E. A., Foster, K. M. & Papavassiliou, D. V. Sublethal damage to erythrocytes during blood flow. *Fluids* **7**, 66 (2022).

5. McNamee, A. P., Tansley, G. D. & Simmonds, M. J. Sublethal mechanical trauma alters the electrochemical properties and increases aggregation of erythrocytes. *Microvasc. Res.* **120**, 1–7 (2018).

6. Bedell, S. E. & Bush, B. T. Erythrocyte sedimentation rate. From folklore to facts. *Am. J. Med.* **78**, 1001–1009 (1985).

7. Levinsky, H., Rothman, G., Lapidot, M. & Allalouf, D. Red blood cell membrane and serum sialic acid in relation to erythrocyte sedimentation rate. *Acta Haematol.* **64**, 276–280 (1980).

8. Penev, M., Doukova-Peneva, P. & Kalinov, K. Study on long-term biological variability of erythrocyte sedimentation rate. *Scand. J. Clin. Lab. Invest.* **56**, 285–288 (1996).

9. Rourke, M. D. & Ernstene, A. C. A method for correcting the erythrocyte sedimentation rate for variations in the cell volume percentage of blood. *J. Clin. Invest.* **8**, 545–559 (1930).

10. Grønlie, M. & Hjortdahl, P. The erythrocyte sedimentation rate; its use and usefulness in primary health care. *Scand. J. Prim. Health Care* **9**, 97–102 (1991).

11. Henslee, E. A. *et al.* Rhythmic potassium transport regulates the circadian clock in human red blood cells. *Nat. Commun.* **8**, 1978 (2017).

12. Tokumasu, F., Ostera, G. R., Amaratunga, C. & Fairhurst, R. M. Modifications in erythrocyte membrane zeta potential by Plasmodium falciparum infection. *Exp. Parasitol.* **131**, 245–251 (2012).

13. Gaikwad, S. S., Avari, J. G. & Patil, M. L. Zeta potential as a diagnostic tool to determine the angina risk. *Apolipoproteins Triglycerides Cholest.* 1–8 (2020).

14. Karemore, M. N. & Avari, J. G. Alteration in zeta potential of erythrocytes in preeclampsia patients. in *Prediction of maternal and fetal syndrome of preeclampsia* (IntechOpen, 2019).

15. DEMİR, A. The Importance Of Zeta Potential In Biological Cells. *Prof Dr Hasan Akgül Prof Dr Engin Şahna Prof Dr Zeliha Selamoğlu* 19 (2024).

16. Hughes, M. P. The cellular zeta potential: cell electrophysiology beyond the membrane. *Integr. Biol.* **16**, zyae003 (2024).

17. Kamble, S. *et al.* Revisiting zeta potential, the key feature of interfacial phenomena, with applications and recent advancements. *ChemistrySelect* **7**, e202103084 (2022).

18. Cano-Sarmiento, C. *et al.* Zeta potential of food matrices. *Food Eng. Rev.* **10**, 113–138 (2018).

19. Serrano-Lotina, A. *et al.* Zeta potential as a tool for functional materials development. *Catal. Today* **423**, 113862 (2023).

20. Katana, B. *et al.* Masking specific effects of ionic liquid constituents at the solid–liquid interface by surface functionalization. *Phys. Chem. Chem. Phys.* **22**, 24764–24770 (2020).

21. Main, K. *et al.* Nanoparticles shape effect on viscosity and thermal conductivity of ionic liquids based nanofluids. in (Begel House Inc., 2020).

22. Main, K. *et al.* Nanoparticles shape effect on viscosity and thermal conductivity of ionic liquids based nanofluids. in *ASTFE Digital Library* (Begel House Inc., 2020).

23. Furchgott, R. F. & Ponder, E. Electrophoretic studies on human red blood cells. *J. Gen. Physiol.* **24**, 447 (1941).

24. Horan, F. E., Hirsch, F. G., Wood, L. A. & Wright, I. S. SURFACE EFFECTS ON BLOOD-CLOTTING COMPONENTS AS DETERMINED BY ZETA-POTENTIALS. I. *J. Clin. Invest.* **29**, 202–211 (1950).

25. Cotner, P., Serrallach, E., Catsimpoolas, N. & Valeri, C. *Electrophoretic Light Scattering: Instrumentation and Application to the Measurement of the Electric Charge of Human Blood Cells.* (1982).

26. Josefowicz, J. Y. Electrophoretic light scattering and its application to the study of cells. in *Methods of Cell Separation* 67–91 (Springer US Boston, MA, 1979).

27. Henry, D. C. The electrophoresis of suspended particles. IV. The surface conductivity effect. *Trans. Faraday Soc.* **44**, 1021–1026 (1948).

Chapter 2: Red Blood Cell Physiology and Electrophysiological Measurement

RED BLOOD CELL PHYSIOLOGY

Red blood cells (RBCs) are the most abundant type of cell in the human body. A healthy RBC (**Figure 2.1 A**) is approximately 8μm in diameter with a thickness of 2 μm. Geometrically, RBCs are shaped as biconcave disks which results in a large surface area to volume ratio (1.50 ± 0.12), and is favorable for both gas exchange and deformability through small capillaries[1,2]. Although RBCs are classified as eukaryotic, mature RBCs shed their nucleus to maximize space for oxygen exchange.

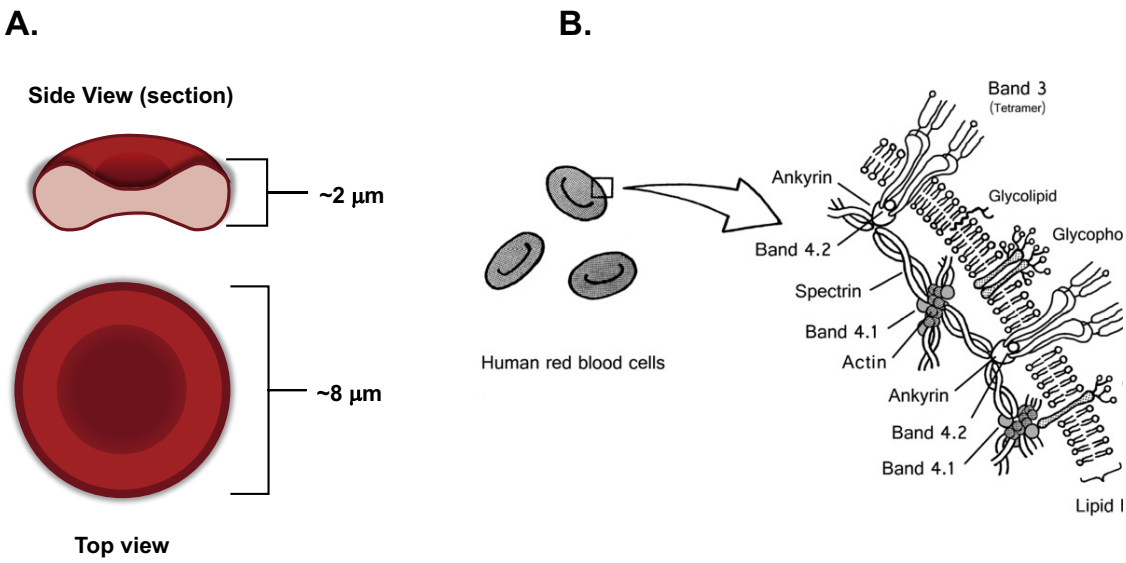

Figure 2.1 Schematic showing structure of healthy red blood cell (RBC). (A) Bi-concave shape of RBC allowing for optimal oxygen delivery to tissues. (B). Lipid bilayer of RBC membrane with integral proteins and peripheral proteins supports regulation of cell deformability, volume, and ion flux (adapted from Aoki et al[3]).

Cell Membrane: The RBC membrane is comprised of a lipid bilayer separating the intra-cellular space from the extra-cellular space. The lipid bilayer consists of phospholipids (made up of hydrophilic, phosphate heads and two hydrophilic lipid tails). The phospholipids self-arrange to form a double (bi-)layer membrane with the phosphate head groups facing outward, and the lipid tails facing towards one another. This configuration allows the cell to be selectively permeable to specific ions and other solutes.

To maintain its biconcave shape, the RBC cytoskeleton is comprised of an interwoven network of α-spectrin and β-spectrin proteins. The cytoskeleton is anchored to the lipid bilayer via ankyrin proteins that play an important role in maintaining cellular deformability and gives RBCs their flattened biconcave shape. However, in disease processes, such as oxidative stress, discussed extensively in *Chapter 4*, the cytoskeleton has been shown to be irreversibly altered, via formation of spectrin-globin complexes[4]. This reduces overall membrane deformability and impairs oxygen delivery.

Further, the RBC membrane contains carbohydrates, along with peripheral proteins and integral proteins. Peripheral proteins temporarily attach to the outside (periphery) of RBC membrane to perform specialized functions. RBC peripheral proteins include ankyrin, spectrin and Band 4.1[5]. The former two help to anchor the cytoskeleton to the lipid bilayer. In contrast, integral proteins are permanently attached (integrated) into the cell membrane (**Figure 2.1**) Integral proteins provide structural integrity, gas exchange, and adhesion capabilities and include Band 3 (anion exchanger 1), glycophorins (A, B, and C), and glucose transporter (GLUT1)[6]

Hemoglobin and Gas Transport: Oxygen is fundamental to aerobic respiration and critical for sustaining human life. RBCs facilitate oxygen transport by binding oxygen molecules to hemoglobin proteins located within the cell cytoplasm. Hemoglobin (Hb) is composed of four polypeptide chains, two alpha (α) chains and two beta (β) chains. Each subunit contains one heme molecule, and thus, can bind four oxygen molecules per hemoglobin complex (**Figure 2.2**).

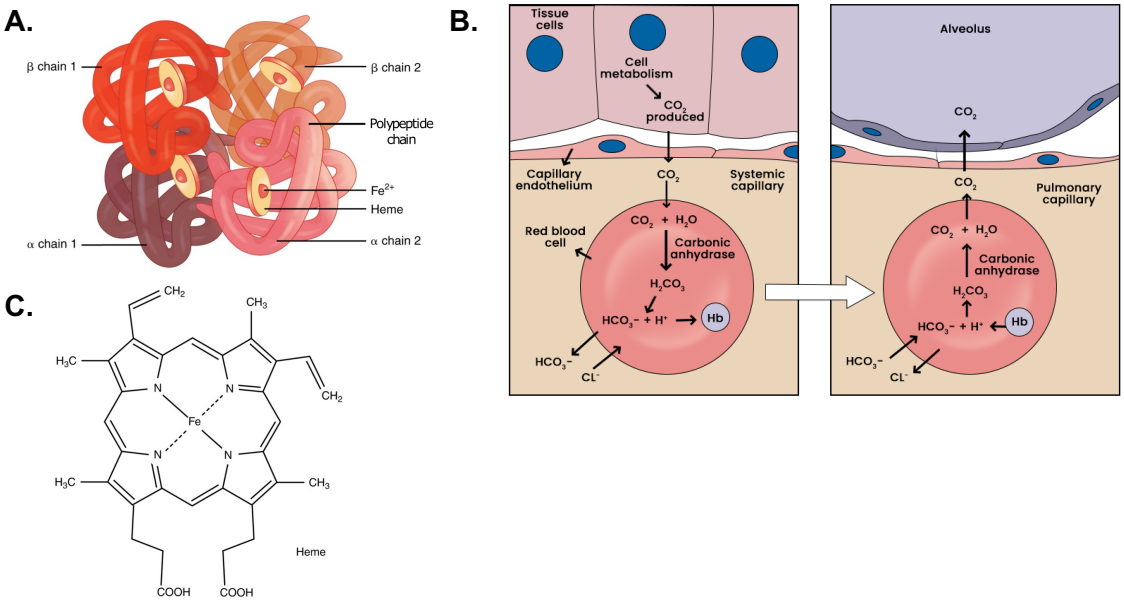

Figure 2.2: (A.) Physical structure of hemoglobin molecule in RBCs. (B.) Gas transport of oxygen from RBCs to tissues in the body, and (C.) Chemical structure of hemoglobin molecule.

Oxygen binds to heme by ferrous iron (Fe^{2+}) in a reversible process. Hb proteins exist in two configurations: tight (T-state) with a low affinity for oxygen, and relaxed configuration (R-state) with a high affinity for oxygen. In deoxygenated RBCs, no oxygen molecules are bound to heme groups, and therefore (deoxy)hemoglobin is in a constrained T-state. However, when RBCs encounter the lung alveoli and oxygen begins to bind to heme groups, it results in a conformational change in the polypeptide chains resulting in an R-

state and increased oxygen affinity. Oxygen binding to hemoglobin is dictated by the partial pressure of oxygen (pO_2). In the lungs pO_2 is high, promoting tight binding of oxygen to Hb. Conversely, the pO_2 is low in the tissues, promoting unloading of oxygen molecules from Hb. The relationship between oxygen binding (saturation) and partial pressure, represented by the oxygen-hemoglobin dissociation curve (**Figure 2.3:**) is important for monitoring oxygen delivery in RBCs. A right-ward shift in the oxygen-hemoglobin curve indicates that hemoglobin has a lower affinity for oxygen, making it easier for oxygen to unload into tissues, whereas a left-ward shift in the curve means that hemoglobin has a higher affinity for oxygen, releasing it less easily.

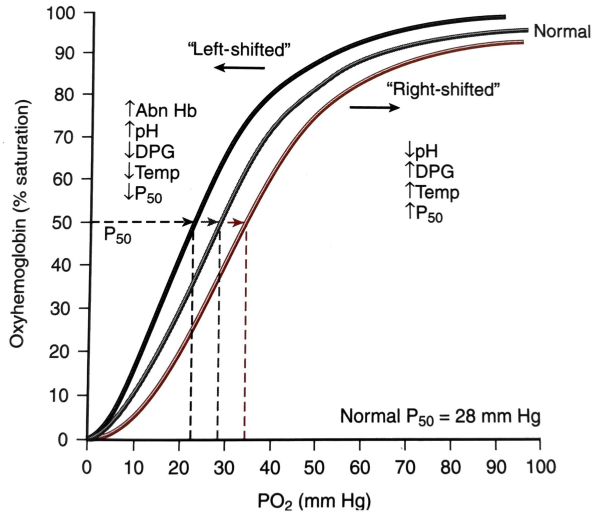

Figure 2.3: Schematic of standard Oxygen-Hemoglobin Dissociation Curve. Figure reproduced from Harmening *et al*[9].

OVERVIEW OF RED BLOOD CELL ELECTROPHYISOLOGY

RBC electrophysiology describes the study of RBC electrical properties, membrane potential, and mechanisms regulating ion transport across the cell membrane. Since mature RBCs lack a nucleus, RBCs use ion channels and a membrane potential to manage their structural integrity, flexibility, and deformation. RBCs act as oxygen sensors, releasing signals (like ATP) in low-oxygen environments to improve blood flow, a process linked to membrane potential. Due to the lack of nuclei, mature RBCs cannot synthesize new proteins or repair genetic damage, their electrical and structural integrity depends on the existing membrane machinery. Dysfunction in electrophysiology can cause an overload in Ca^{2+} (or dehydration), leading to rigid, damaged cells that are removed from circulation early. RBC electrophysiology also aids in their interactions with endothelial cells, platelets, and the immune system. By studying the electrical properties of the RBC membrane, researchers can identify early, subtle markers of diseases like malaria[10], sickle cell anemia[11], and cardiovascular conditions[12] before physical changes occur.

Ion Channels: Due to the impermeability of the RBC membrane to cations, regulation of cell size, shape, and volume is accomplished by careful control of ion flux across the cell membrane via transmembrane proteins, referred hereafter as ion channels (**Figure 2.4:**).

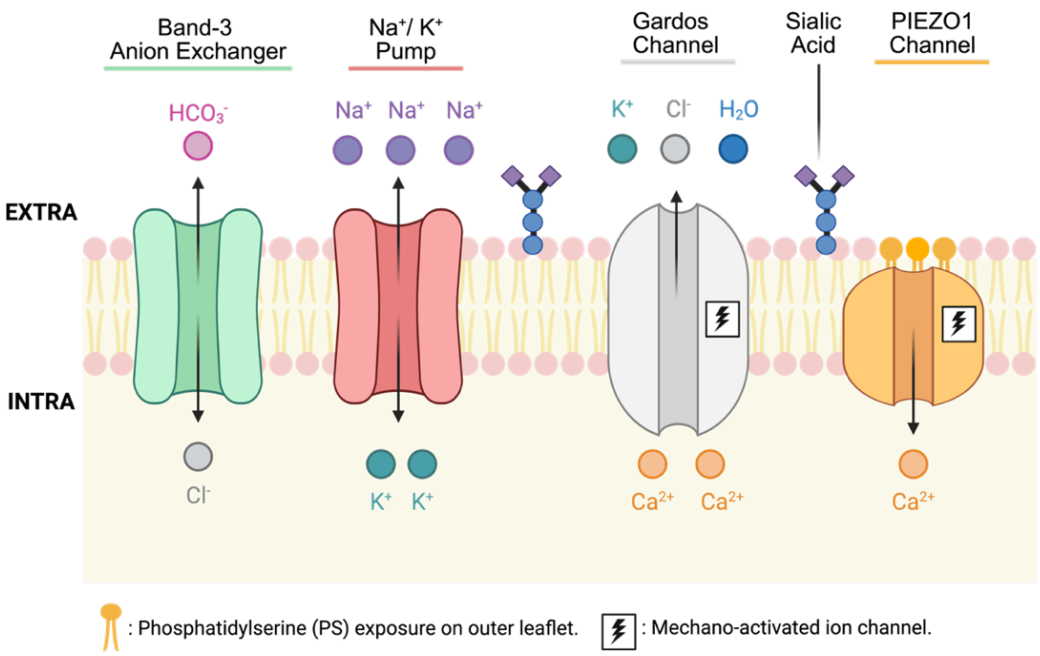

Figure 2.4: Schematic showing cell membrane and major transmembrane proteins responsible for modulating cell surface charge and ζ-potential in human RBCs.

The **anion exchanger Band-3** is the most abundant transmembrane protein in RBCs with approximately 1.2 x 10^6 units per cell. Band-3 provides structural support by anchoring to cytoskeletal proteins (ankyrin and Band 4.1). Additionally, the rapid exchange of bicarbonate (HCO_3^-) with chloride ions (Cl^-) by Band 3 facilitates gas exchange. Specifically, when CO_2 enters the RBC, it is converted to HCO_3^- and H^+ ions by the enzyme carbonic anhydrase. The increase in HCO_3^-, combined with the influx of Cl^- pushes HCO_3^- out of the cell cytoplasm due to the charge balance. This process in turn facilitates release of bound oxygen to the tissues.

Of relevance to the work in this dissertation is the relationship between the chloride shift, HCO_3^-/ Cl^- and ζ-potential of RBCs. As noted by Ramsey *et al*[13], when the cations in blood plasma interferes with the RBC surface, influx of Cl^- into the cell is impaired,

decreasing the distance between the membrane surface charge and the Stern layer, and decreasing ζ-potential magnitude.

The **Na^+/K^+ pump**, which is activated by the enzyme ATPase, transports three Na^+ ions out of the cell in exchange for two K^+ ions. Inhibition of the Na^+/K^+ pump has been associated with ion leakage into the surrounding plasma, which decreases extracellular serum pH and can neutralize the cell's surface charge, accelerating cell aggregation. Maintaining intracellular calcium (Ca^{2+}) is important for RBC function, as an increase of Ca^{2+} concentration can lead to dehydration and cell lysis.

Intracellular Ca^{2+} is regulated by the **Gardos Channel**. When intracellular concentration of Ca^{2+} increases, either due to exposure to mechanical shear stress or other biological factors, the Gardos Channel opens allowing an efflux of K^+, Cl^- and water from the cytoplasm. This process causes the cell to shrink, improving it's deformability and ability to traverse narrow capillaries. Beyond the regulation of cell volume/deformability, the Gardos channel has been shown to be an important player in the cellular processes such as RBC clearance via sensence[14].

Unlike the prior two ion channels which are controlled by enzymatic processes and changes in intracellular ion concentrations, the **PIEZO1 Channel** is mechano-activated. This means when the RBC membrane is exposed to mechanical forces (e.g., flow-induced shear stress) the channel opens resulting in Ca^{2+} influx into the cytoplasm. Activation of PIEZO1 plays an important role in promoting blood clot formation, as the influx of Ca^{2+}

subsequently promotes exposure of the pro-coagulant factor, phosphatidylserine (PS) on the membrane's surface[15].

Cell Surface Charge: Cell surface charge is an important property of RBCs because it allows the cells to repel each other when in suspension, which prevents cells from adhering to each other or to blood vessel walls. In RBCs, two proteins are responsible for the cell's net negative surface charge—**Band-3** and **sialic acid**. As described above, Band-3 functions as both a HCO_3^-/Cl^- exchanger and provides structural support to the membrane. Band-3 also contributes to ~25-30% of the cell's surface charge[16]. Sialic acid (SA) is a class of nine-carbon negatively charged sugar molecules located on the terminal end of Glycophorin A proteins on the surface of every mammalian cell. To date, over 50 sialic species of SAs have been identified, including N-acetylneuraminic acid (Neu5Ac), N-glycolylneuraminic acid (Neu5Gc) and their derivatives[17]. SAs have been shown to contribute to up to 70% of the total negative surface charge on the RBC membrane[18].

ELECTROPHYSIOLOGIC MEASUREMENT OF RED BLOOD CELLS

Patch Clamp Measurement of RBCs: Electrophysiologic measurement of RBCs involves measuring transmembrane potential using electrical impedance (resistance), or voltage clamp to measure ion flux. Voltage clamp technique works by holding (i.e., "clamping") the cell's transmembrane potential at a constant voltage, simultaneously measuring the ion flow needed to maintain that constant voltage. The **patch clamp** technique, developed by German physicist, Erwin Neher, and cell physiologist Bert Sakmann, refines limitations of voltage clamp (which requires the entire cell to be

clamped) by allowing for single-channel measurement of ion flux[19]. Patch clamp uses a glass micropipette to create a tight vacuum seal on a portion of membrane and electrical current in and out of the cell is measured with a recording device (**Figure 2.5***:*).

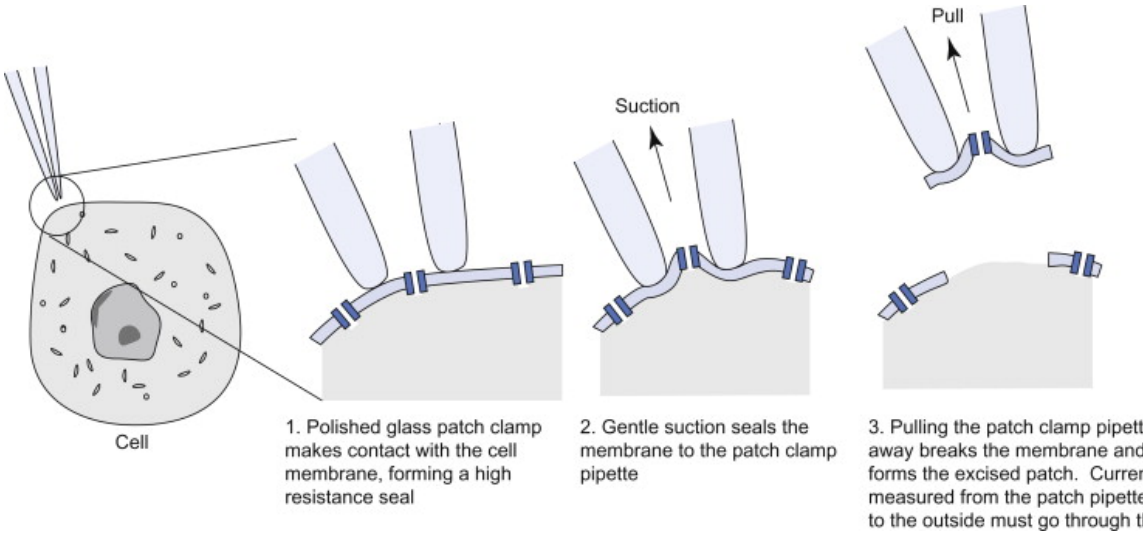

Figure 2.5: Schematic of whole-cell patch clamp technique for measuring ion flux across the cell membrane.

The patch clamp technique has been used to characterize chloride ion channel function in RBCs infected with Plasmodium falciparum[20], the bacteria causing malaria infection. Other authors have investigated the effects of membrane deformations on Ca^{2+} channel function using whole-cell patch clamp[21]. Collectively these studies have advanced the field of cell electrophysiology and our understanding of long-term impacts of disease pathology on the RBC membrane[22].

Dielectrophoresis-based Measurement of RBCs: Dielectrophoresis (DEP) is an electrokinetic technique that relies on the electrophysiologic properties of cells, properties of the suspending medium, and the geometry of the applied electric field to induce cell

movement in a non-uniform electric field. Since the early needle-based experiments conducted by Pohl *et al*[23,24] DEP-based measurement has evolved to utilize micro-scale devices, providing a means of automated, rapid, and low-cost electrophysiologic measurement of RBCs. Additionally, the commercially available DEP cytometry platform, 3DEP, allows for characterization of RBC membrane properties: membrane conductance, G_{EFF} (resistance of the cell membrane to ion flux), membrane capacitance, C_{EFF} (indicates cell morphological changes), and cytoplasmic conductivity σ_{CYT} (ion storage in the cytoplasm) within a bulk, often heterogeneous cell population. To date members of our laboratory have used DEP techniques to investigate the effects of laboratory handling conditions on RBC intracellular properties (unpublished), RBC monitoring in circadian rhythmicity[25], and RBC monitoring in oxidative stress (described in *Chapter 4* of this dissertation). Other authors have applied DEP-based approaches for cell sorting, including separation of cancer cells from whole blood[26,27], and characterization of RBC sub-populations for investigating the impact of blood storage lesions[28,29] and RBC aging[30] on intracellular electrical properties. Collectively these studies have demonstrated the ability for DEP techniques to discriminate subtle shifts in RBC membrane function (e.g., changes in ion flux) which can occur in parallel, and often prior to, more distinguishable changes in mechanical properties, which may provide early detection of RBC-related diseases.

Surface ζ-potential Measurement of RBCs: Compared to DEP approaches which characterize intracellular (e.g., membrane and cytoplasm) electrical properties, surface ζ-potential is an electro-physical property of cells in suspension, used to characterize the repulsive force between cells as a function of membrane surface charge. Surface ζ-

potential has been extensively used to characterize RBCs, specifically how cell aggregation impacts the progression/severity of cardiovascular disease and blood disorders including sickle cell disease[31], β-thalassemia[32] , and hydronephrosis[33]. As discussed in *Chapter 3*, results from these studies can be difficult to interpret, at least in the broader context of ζ-potential as a biomarker for RBC monitoring, given the wide variability in measurements likely due to differing experimental conditions (e.g., buffer conductivity and viscosity).

PHYISOLOGIC PROCESSESSES IMPACTING RED BLOOD CELLS

Erythropoiesis and Cell Aging: RBCs are produced in the red bone marrow via a multi-step process called **erythropoiesis**. Initially, hematopoietic stem cells (HSCs) differentiate into more specialized cells known common myeloid progenitor (CMP) cells. CMP cells can further differentiate into any type of blood cell (e.g., RBCs, leukocytes, or platelets). CMPs that become RBCs are known as megakaryocyte erythroid progenitor (MEP) cells. The maturation process from an MEP to a fully developed RBC is depicted in **Figure 2.6.**

During the maturation process (approximately 3-5 days) RBCs eject their organelles to make room for iron and hemoglobin, at which point the reticulocyte will exit the bone marrow to enter circulation. The last organelle to be shed is the nucleus, at which point a fully mature RBC is produced. Since mature RBCs lack a nucleus and other organelles, they must use anaerobic respiration which helps facilitate oxygen transport.

The process of erythropoiesis is controlled by a hormone called erythropoietin, produced in the kidneys. Interestingly, for patients supported by cardiopulmonary bypass

and ECMO support systems hypoxia, indicated by a decrease in oxygen tissue perfusion (dO_2) has been associated with a high risk of developing acute kidney failure. The reasoning for this is because dissolved oxygen tightly controls the production of erythropoietin, and in turn RBC production.

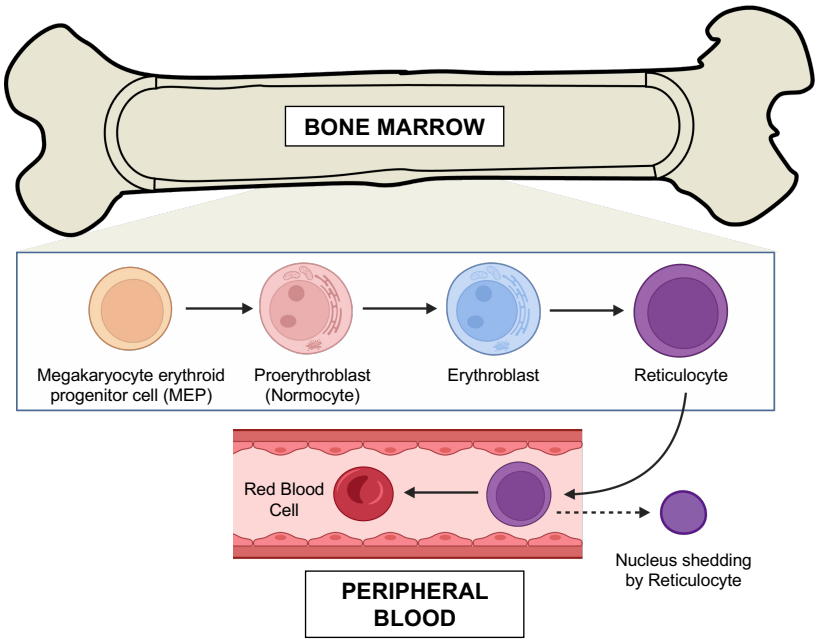

Figure 2.6: Schematic showing process of erythropoiesis (RBC production) beginning in the red bone marrow (megakaryocyte erythroid progenitor cell) and ending in the peripheral circulation (reticulocyte).

Circulating RBCs have an average lifespan of ~120 days. As RBCs age, they undergo several functional and biochemical changes, such as decreasing deformability, decreasing ATP production, and increased exposure to oxidative damage. Relevant to the work in this dissertation, Huang *et al* also demonstrated that during aging RBCs exhibit a reduction in membrane surface charge and ζ-potential[34] which has further implications for increased cell aggregation and clot formation.

Eryptosis: During their lifespan, RBCs will frequently be exposed to both oxidative and mechanical shear stresses as they circulate the macro- and micro-vasculature. When cells age or become damaged from exposure to stressors, they require clearance from the circulation which can be accomplished by a process known as eryptosis. **Eryptosis**, the process of suicidal programmed death in RBCs is characterized by cell shrinkage and cell membrane blebbing triggered by an influx of intracellular Ca^{2+}. Quantifying eryptosis is important to understanding disease processes such as malarial anemia and the effects of external mechanical shear stress on RBCs.

Hemolysis: In addition to programmed cell death (eryptosis), circulating RBCs can be destroyed via an abnormal breakdown of cells, known as hemolysis. Unlike eryptosis which involves a systematic breakdown of the cell membrane by enzymatic processes, hemolysis occurs due to sudden rupture/bursting of the cell membrane, releasing hemoglobin into the blood plasma. Hemolysis can occur due to disease processes (e.g., oxidative stress, sickle cell disease) as well as exposure to external (mechanical shear) stressors. Sikora *et al* further showed a strong positive correlation between ATP release, mechanical shear stress exposure, and increase in percent hemolysis[35]. ATP production is crucial for control of ion flux; thus, these findings have the potential to inform our understanding of hemolysis effects on RBC function beyond oxygen transport (e.g., hemoglobin release).

Hemostasis: Hemostasis describes the body's ability to prevent blood loss caused by vascular injury and is critical for wound healing. Hemostasis can be divided into two stages: primary hemostasis (platelet plug formation), and secondary hemostasis (coagulation cascade) depicted in **Figure 2.7**.

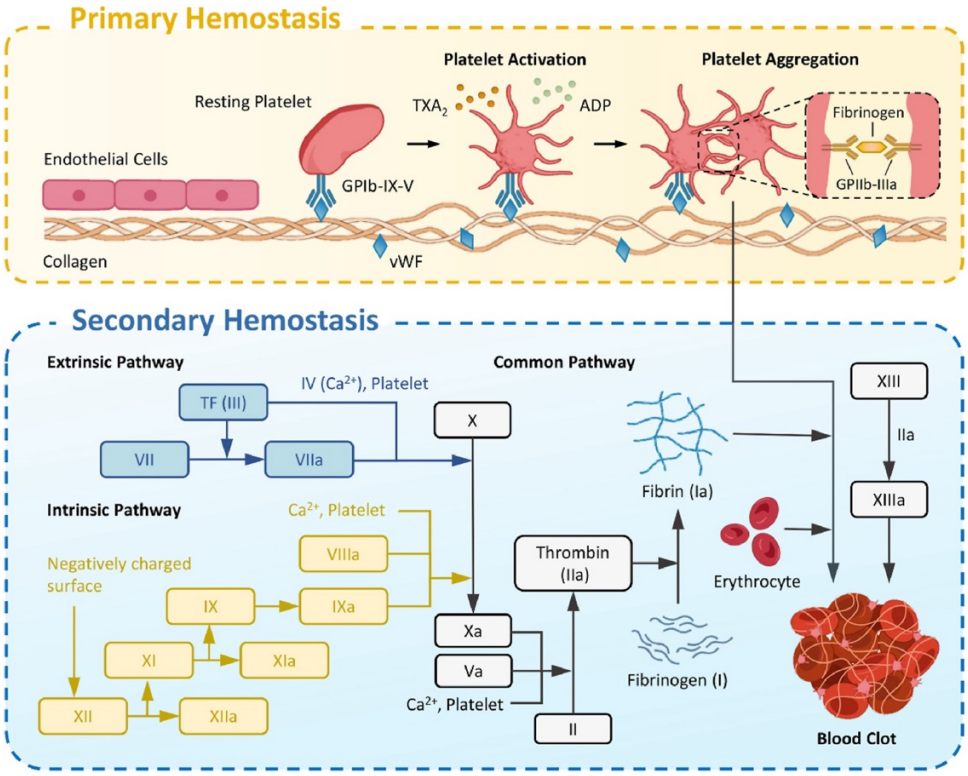

Figure 2.7: Schematic showing Primary Hemostasis and Secondary Hemostasis (i.e., coagulation cascade) processes leading to the formation of a blood clot (fibrin mesh with entrapped RBCs). Figure used under creative common license.

Upon injury to the blood vessel wall, vasoconstriction immediately occurs to mitigate blood loss. Next, circulating platelets are exposed to collagen fibers and von Willebrand factor proteins within the vessel wall causing the platelets to become activated

and change their shape, as well as recruit additional platelets to the site of injury. This process results in the formation of a platelet plug. Secondary hemostasis, also known as the coagulation cascade, is a "waterfall-like" sequence, where one clotting factor protein activates a subsequent clotting factor in sequence ultimately resulting in the formation of a stable blood clot. The coagulation cascade can be sub-divided into three pathways: extrinsic, intrinsic and common pathway. Both the extrinsic and intrinsic pathways operate in parallel (activated by different triggers) but converge at a common pathway.

The **extrinsic pathway** is triggered by injury to the blood vessel wall exposing and activating tissue factor protein (Factor IIIa) found in the endothelial cells of the vessel wall. Factor IIIa binds to calcium ions and Factor VIIa, both of which are released by platelets, creating which activates Factor Xa. In contrast to the external trigger (e.g., tissue injury) of the extrinsic pathway, the **intrinsic pathway.** Factor Xa initiates the common pathway, via the prothrombinase complete (Factor Xa with co-factors Ca_{2+} and Factor Va) to convert prothrombin (Factor II) to its activated form, thrombin (Factor IIa.

Thrombin molecules, which circulate through the bloodstream activate platelets and activate co-factors V, VIII, and IXa which cleaves fibrinogen (Factor I) into its activated form, fibrin (Factor Ia). While thrombin is important for maintaining the structural integrity of blood clots, thrombin-induced platelet activation has been associated with platelet fragmentation after just 30 minutes of incubation with thrombin, which has implications for blood clot integrity.

The final step of the coagulation cascade is the conversion of fibrinogen to fibrin. Fibrin forms long fiber-like protein chains which interweave to create a mesh network that stabilizes the platelet plug and entraps circulating RBCs. Entrapment of RBCs in the fibrin mesh is beneficial for the stabilization of the clot (via compression forces exerted by fibrin causing RBCs to conform to polyhedral shapes) and prevents clot breakdown (fibrinolysis). Fibrinogen binding to RBC membrane receptors is another mechanism that stabilizes blood clots. Relevant to our study of ζ-potential in RBCs, several studies have shown that the surface charge density on the RBC membrane can increase fibrinogen binding[36,37]. RBC-fibrinogen interactions, and surface charge density are further influenced by cell aging, which has implications for our current work and for early prediction of RBC aggregation and blood clot formation.

RBC-Biomaterial Surface Interactions: Medical devices (e.g., stents, prosthetic heart valves, and mechanical blood pumps) help to restore normal physiology and blood flow for millions of patients suffering from cardiovascular disease worldwide. However, extensive research has shown that when RBCs contact solid, artificial surfaces their membrane morphology is altered from the normal high surface area-to-volume 'doughnut' shape to echinocytes (spiked cells) or stomatocytes (cup-shape) due to an imbalance in pH[38–40].

Further, while cobalt is a crucial component of vitamin B12 as well as the production (erythropoiesis) and metabolism of RBCs, studies have shown that metallic implants can leach excess cobalt ions into the systemic circulation, resulting in anemia due to RBC loss. In fact, a retrospective analysis by Shenghao Xu *et al* demonstrated an

increase in blood cobalt concentration resulted in significantly higher risks of developing angina pectoris, arrhythmia, and heart failure. This underscores the importance of accounting for cobalt toxicity in cardiovascular disease[41].

Polymer materials used in many medical devices induce RBC aggregation which is said to occur either by two co-existing "models"—bridging and depletion. As described by Moreno *et al*[42], the bridging mechanism of cell aggregation involves the binding of macromolecules (e.g., fibrinogen or other plasma proteins) to the RBC membrane surface and forming a "bridge" connecting two or more cells. In contrast, in the depletion model RBC aggregation occurs due to absence of macromolecules between RBCs, leading to osmotic pressure gradient that draws the cells towards one another.

DISEASES IMPACTING RED BLOOD CELLS

Diabetes Melitus: Diabetes melitus is a chronic metabolic disease characterized by high blood sugar caused by either the insufficient production or metabolism of insulin Diabetes detrimentally impacts RBCs by increasing glycation and oxidative stress which reduces RBCs deformability, cell shape, and increases the potential for cell aggregation[43]. For example, Adak *et al*[12] compared the ζ-potential and mechanical properties of RBCs in patients with and without diabetes melitus. They found that in addition to reduced membrane deformability and fluidity, the ζ-potential magnitude of RBCs in diabetic patients decreased significantly compared to healthy controls. Biophysically, the ζ-potential decrease was attributed to oxidative damage and a reduction in membrane surface charge. Other studies investigating human RBCs under hypoglycemic conditions also reported a decrease in ζ-potential magnitude due to removal of sialic acid[44]

Malaria Infection: Malaria, another RBC-related disease which impacts nearly 249 million people worldwide each year, is caused by infecting the host organism with *Plasmodium falciparum* parasites which remodels the host RBCs impairing oxygen delivery and cell deformability. Further, *Plasmodium* remodeling has been shown to cause the formation of knob-like structures on the RBC surface which can alter the cell's surface charge, and leads to adhesion of infected cells (cytoadherence) to the host's vascular wall, blocking blood flow. To better understand cytoadherence of RBCs, Tokumasu *et al* [10] investigated the *impact of P. falciparum* infection on ζ-potential of human RBCs and found the infected RBCs had a reduced ζ-potential magnitude (-14.6 mV) compared to non-infected RBCs (-15.7mV), with the variations in ζ-potential attributed to altered binding sites due to parasite-derived knob proteins on the surface. While further work is needed to explore other biophysical mechanisms (e.g., intracellular Ca^{2+} increase) in malaria-infected RBCs, this study provides a solid foundation for understanding the importance of ζ-potential monitoring in malaria disease progression.

Anemia and Preeclampsia: Anemia is a disease condition in RBCs characterized by general loss of RBCs due to a myriad of diseases (e.g., bacterial infections viral infections, and cardiovascular disease)[45,46] as well as medical device-induced RBC loss[47]. While no *ex vivo* studies have directly compared the effect of generalized anemia on ζ-potential response in RBCs, Pérez-Pacheco *et al*[48] used a pulsed photoacoustic technique to characterize changes in RBC sedimentation in patients with and without hemolytic anemia. Observations from this study revealed RBCs with hemolytic anemia had faster

sedimentation rate due to cell clustering, attributed to decreases in cell size/shape, compared to healthy cells which formed long uniform pearl chains. This study underscores the importance of accounting for cell morphology and cell-to-cell interactions when studying surface charge and ζ-potential response in RBCs.

Preeclampsia is a disease arising after the 20th week of pregnancy and is characterized by elevated blood pressure, protein in urine and the potential for organ damage due to abnormal development of the placenta causing widespread endothelial damage. Due to the risk for hypertension-induced hemolytic anemia, RBC monitoring is import for predicting disease progression and informing treatment of preeclampsia. Recently, Karemore *et al*[49] applied surface ζ-potential for monitoring RBCs as a novel diagnostic tool in preeclampsia. Pregnant women with preeclampsia exhibited a reduction in ζ-potential magnitude of RBCs compared to healthy pregnant participants (Preeclampsia: -15.13 ± 0.1393 mV versus Healthy: -21.64 ± 0.3122 mV). While the authors suggest that changes in ζ-potential are due to oxidative damage and removal, which is likely based on similar trends observed in other RBC-related diseases, damage to RBCs during pregnancy alone are multi-factorial, thus a follow up study to investigate the underlying impact of pregnancy should be considered before translation to clinical practice. Nevertheless, this study provides a solid foundation for applying ζ-potential as real-time tool for monitoring RBCs. This study also serves as a benchmark for further bench-to-bedside translational RBC electrophysiology studies.

REFERENCES

1. Secomb, T. Red blood cell mechanics and capillary blood rheology. *Cell Biophys.* **18**, 231–251 (1991).

2. Chien, S. Red cell deformability and its relevance to blood flow. *Annu. Rev. Physiol.* **49**, 177–192 (1987).

3. Aoki, T. A comprehensive review of our current understanding of red blood cell (RBC) glycoproteins. *Membranes* **7**, 56 (2017).

4. Snyder, L. *et al.* Effect of hydrogen peroxide exposure on normal human erythrocyte deformability, morphology, surface characteristics, and spectrin-hemoglobin cross-linking. *J. Clin. Invest.* **76**, 1971–1977 (1985).

5. Pasini, E. M., Lutz, H. U., Mann, M. & Thomas, A. W. Red blood cell (RBC) membrane proteomics—Part I: Proteomics and RBC physiology. *J. Proteomics* **73**, 403–420 (2010).

6. Tanner, M. J. 1 The major integral proteins of the human red cell. *Baillières Clin. Haematol.* **6**, 333–356 (1993).

7. Grygorczyk, R. & Orlov, S. N. Effects of hypoxia on erythrocyte membrane properties—implications for intravascular hemolysis and purinergic control of blood flow. *Front. Physiol.* **8**, 1110 (2017).

8. Jensen, F. B. Red blood cell pH, the Bohr effect, and other oxygenation-linked phenomena in blood O2 and CO2 transport. *Acta Physiol. Scand.* **182**, 215–227 (2004).

9. Harmening, D. *Clinical Hematology and Fundamentals of Hemostasis*. (FA Davis, 2024).

10. Tokumasu, F., Ostera, G. R., Amaratunga, C. & Fairhurst, R. M. Modifications in erythrocyte membrane zeta potential by Plasmodium falciparum infection. *Exp. Parasitol.* **131**, 245–251 (2012).

11. Barodka, V. M. *et al.* New insights provided by a comparison of impaired deformability with erythrocyte oxidative stress for sickle cell disease. *Blood Cells. Mol. Dis.* **52**, 230–235 (2014).

12. Adak, S., Chowdhury, S. & Bhattacharyya, M. Dynamic and electrokinetic behavior of erythrocyte membrane in diabetes mellitus and diabetic cardiovascular disease. *Biochim. Biophys. Acta BBA-Gen. Subj.* **1780**, 108–115 (2008).

13. Purnell, M. C. & Ramsey, R. D. The influence of the golden ratio on the erythrocyte. in *Erythrocyte* (IntechOpen, 2019).

14. Klei, T. R. *et al.* The Gardos effect drives erythrocyte senescence and leads to Lu/BCAM and CD44 adhesion molecule activation. *Blood Adv.* **4**, 6218–6229 (2020).

15. Evtugina, N. G. *et al.* Activation of Piezo1 channels in compressed red blood cells augments platelet-driven contraction of blood clots. *J. Thromb. Haemost.* **21**, 2418–2429 (2023).

16. Steck, T. L. The band 3 protein of the human red cell membrane: a review. *J. Supramol. Struct.* **8**, 311–324 (1978).

17. Doostkam, A. *et al.* Sialic acid: an attractive biomarker with promising biomedical applications. *Asian Biomed. Res. Rev. News* **16**, 153 (2022).

18. Zhang, X. *et al.* Red blood cells in biology and translational medicine: natural vehicle inspires new biomedical applications. *Theranostics* **14**, 220 (2024).

19. Neher, E. & Sakmann, B. The patch clamp technique. *Sci. Am.* **266**, 44–51 (1992).

20. Akkaya, C. *et al.* The Plasmodium falciparum-induced anion channel of human erythrocytes is an ATP-release pathway. *Pflüg. Arch.-Eur. J. Physiol.* **457**, 1035–1047 (2009).

21. Dyrda, A. *et al.* Local membrane deformations activate Ca2+-dependent K+ and anionic currents in intact human red blood cells. *PloS One* **5**, e9447 (2010).

22. Kaestner, L. & Bernhardt, I. Ion channels in the human red blood cell membrane: their further investigation and physiological relevance. *Bioelectrochemistry* **55**, 71–74 (2002).

23. Pohl, H., Pollock, K. & Crane, J. Dielectrophoretic force: A comparison of theory and experiment. *J. Biol. Phys.* **6**, 133–160 (1978).

24. Pohl, H. A. & Crane, J. S. Dielectrophoresis of cells. *Biophys. J.* **11**, 711–727 (1971).

25. Henslee, E. A. *et al.* Rhythmic potassium transport regulates the circadian clock in human red blood cells. *Nat. Commun.* **8**, 1978 (2017).

26. Duncan, J. L. & Davalos, R. V. A review: Dielectrophoresis for characterizing and separating similar cell subpopulations based on bioelectric property changes due to disease progression and therapy assessment. *Electrophoresis* **42**, 2423–2444 (2021).

27. Sano, M. B., Henslee, E. A., Schmelz, E. & Davalos, R. V. Contactless dielectrophoretic spectroscopy: examination of the dielectric properties of cells found in blood. *Electrophoresis* **32**, 3164–3171 (2011).

28. Almizraq, R., Tchir, J. D., Holovati, J. L. & Acker, J. P. Storage of red blood cells affects membrane composition, microvesiculation, and in vitro quality. *Transfusion (Paris)* **53**, 2258–2267 (2013).

29. Lavi, E. D. Investigating the Impact of Refrigeration and Autologous Transfusions on Human Red Blood Cell Electrical Properties Using Dielectrophoresis and Inductively Coupled Mass Spectroscopy. (2023).

30. Chen, Y., Feng, Y., Wan, J. & Chen, H. Enhanced separation of aged RBCs by designing channel cross section. *Biomicrofluidics* **12**, (2018).

31. Tripette, J. *et al.* Red blood cell aggregation, aggregate strength and oxygen transport potential of blood are abnormal in both homozygous sickle cell anemia and sickle-hemoglobin C disease. *haematologica* **94**, 1060 (2009).

32. Doltchinkova, V. *et al.* Electrokinetic properties of healthy and β-thalassemia erythrocyte membranes under in vitro exposure to static magnetic field. *Front. Chem.* **11**, 1197210 (2023).

33. Chang, C.-C., Chen, J.-S., Huang, C.-C., Yang, Y.-N. & Chen, C.-C. Hydronephrosis-Induced Polycythemia with Low Erythropoietin Level: A Case Report and Literature Review. *Children* **11**, 1534 (2024).

34. Huang, Y. *et al.* Human red blood cell aging: correlative changes in surface charge and cell properties. *J. Cell. Mol. Med.* **15**, 2634–2642 (2011).

35. Sikora, J., Orlov, S. N., Furuya, K. & Grygorczyk, R. Hemolysis is a primary ATP-release mechanism in human erythrocytes. *Blood J. Am. Soc. Hematol.* **124**, 2150–2157 (2014).

36. Carvalho, F. A., de Oliveira, S., Freitas, T., Gonçalves, S. & Santos, N. C. Variations on fibrinogen-erythrocyte interactions during cell aging. *PLoS One* **6**, e18167 (2011).

37. Fuss, C., Palmaz, J. C. & Sprague, E. A. Fibrinogen: structure, function, and surface interactions. *J. Vasc. Interv. Radiol.* **12**, 677–682 (2001).

38. Hasper, D., Hummel, M., Hetzer, R. & Volk, H. Blood contact with artificial surfaces during BVAD support. *Int. J. Artif. Organs* **19**, 590–596 (1996).

39. Eriksson, L. G. On the shape of human red blood cells interacting with flat artificial surfaces—the 'glass effect'. *Biochim. Biophys. Acta BBA-Gen. Subj.* **1036**, 193–201 (1990).

40. Grzhibovskis, R. *et al.* Shape of red blood cells in contact with artificial surfaces. *Eur. Biophys. J.* **46**, 141–148 (2017).

41. Xu, S. *et al.* Association between blood cobalt ion concentrations and anemia and cardiovascular diseases: novel evidence of toxicity resulting from metal implants. *Front. Nutr.* **12**, 1614771 (2025).

42. Moreno, N. *et al.* Aggregation and disaggregation of red blood cells: Depletion versus bridging. *Biophys. J.* **124**, 1285–1297 (2025).

43. Ebenuwa, I. *et al.* Altered RBC deformability in diabetes: clinical characteristics and RBC pathophysiology. *Cardiovasc. Diabetol.* **23**, 370 (2024).

44. Gaikwad, S. S., Karemore, M. N. & Avari, J. G. Alterations in zeta potential and osmotic fragility of red blood cells in hyperglycemic conditions. *Pharm. Biosci. J.* 25–30 (2018).

45. Pernow, J., Mahdi, A., Yang, J. & Zhou, Z. Red blood cell dysfunction: a new player in cardiovascular disease. *Cardiovasc. Res.* **115**, 1596–1605 (2019).

46. McCullough, J. RBCs as targets of infection. *Hematol. 2014 Am. Soc. Hematol. Educ. Program Book* **2014**, 404–409 (2014).

47. Bilodeau, K. S., Saifee, N. H. & Chandler, W. L. Causes of red blood cell loss during extracorporeal membrane oxygenation. *Transfusion (Paris)* **63**, 933–941 (2023).

48. Pérez-Pacheco, A. *et al.* Study of erythrocyte sedimentation in human blood through the photoacoustic signals analysis. *Photoacoustics* **37**, 100599 (2024).

49. Karemore, M. N. & Avari, J. G. Alteration in zeta potential of erythrocytes in preeclampsia patients. in *Prediction of maternal and fetal syndrome of preeclampsia* (IntechOpen, 2019).

Chapter 3: Surface Zeta Potential of Human Red Blood Cells: Theory, Applications, and Optimization of Experimental Measurement

ZETA POTENTIAL THEORY

Surface ζ-potential, as defined in *Chapter 1*, is an electro-physical property of particles in suspension and offers the ability to directly measure the particle's surface charge and repulsive forces. Characterization of ζ-potential is governed by a principle known as the electric double layer (EDL).When RBCs, which possess a net negative charge, are suspended in an aqueous electrolyte solution, anions (positive charged ions) are attracted to the negative membrane surface forming a thin, fixed layer (known as the Stern layer) to neutralize the negative surface charge (**Figure 3.1**). Beyond the Stern layer, a second diffuse layer of cations and anions forms. The ions in the Stern layer are not attached as closely to the particle surface and able to move more freely.

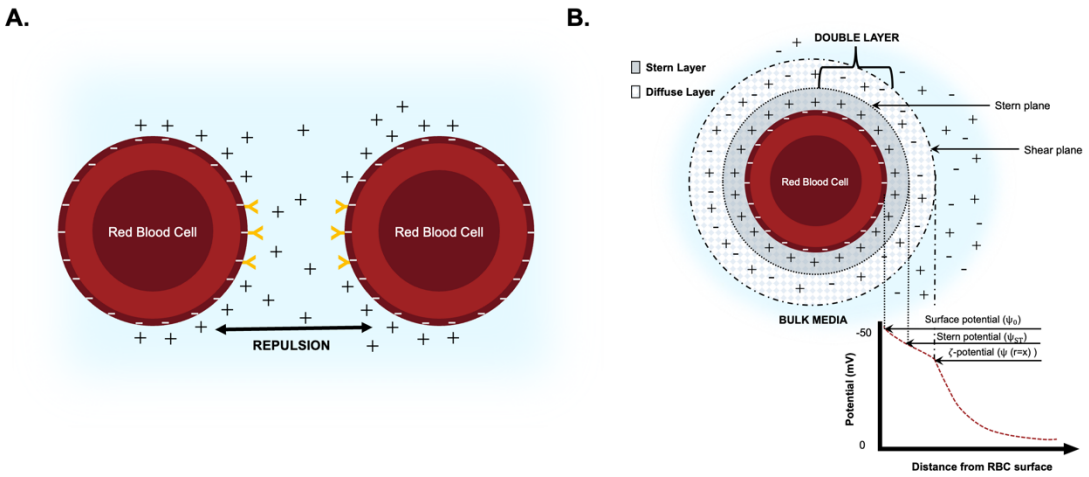

Figure 3.1: Schematic showing (A.) repulsive forces between RBCs resulting from negative surface charge. (B.) RBC ζ-potential measured as the differential of charge between the RBC surface and bulk media.

This diffuse layer of charge separates the fixed Stern layer from the cloud of ions known as the 'bulk media'. Collectively, the two layers of charge (i.e., Stern layer and Diffuse layer) are known as the "electric double layer" (EDL). A hypothetical plane located at the edge of the Diffuse layer separates the diffuse ions from the bulk media. This plane is known as the slipping/shear plane and ζ-potential is the electrokinetic potential at this point (i.e., difference in potential between the particle-bulk media interface) under applied electrophoresis. To derive the ζ-potential for RBCs it is important to briefly review several concepts central to the formation of EDLs.

Electro-osmosis and Streaming Potential: Electroosmosis describes the movement of fluid through a porous material in response to an applied voltage. In 1809 Ferdinand Friedrich Reuss documented electro-osmosis experimentally by observing the flow of water through a clay plug following the application of a voltage[1]. These experiments were accompanied by investigations of electrophoresis as demonstrated by the migration of charged clay particles in response to an applied electric field. In the context of the EDL, when an external electric field is applied tangential to a charged, fixed surface, the mobile portion of the Diffuse layer will flow due to excess charges. Using the Poisson's Equation, a relationship between the flow due to electro-osmosis, the EDL at shear plane, and applied electric field can be derived:

$$\nabla^2\psi_x = -4\pi\rho/\varepsilon \tag{3.1}$$

where ∇^2 is the Laplace operator, ψ_x is the electrokinetic potential of the EDL at a distance x from the particle surface, ρ is the net charge per unit volume and ε is dielectric constant of the suspending media. Further, when applying an electric field of strength E, the fluid will also experience a force, F_1 at a distance x from the particle surface:

$$F_1 = E\rho\, dx \tag{3.2-a}$$

As described by Oliver *et al*: "*At steady state, the viscous drag on the liquid layer will be contributed by adjacent layers that are moving at a different velocity*. At this layer, a retarding (resistance) force, F_{ret}, defined by Equation 3.2-b, will be applied at a distance x, and an acceleration force, F_{acc} (Equation 3.2-c) will be applied at distance $x + dx$.

$$F_{ret}(x) = -\eta \cdot (\mathrm{d}v/\mathrm{d}x)_x \tag{3.2-b}$$

$$F_{acc}(x) = \eta \cdot (\mathrm{d}v/\mathrm{d}x)_{x+\mathrm{d}x} \tag{3.2-c}$$

The net frictional force on the fluid layer is:

$$F_2 = \eta \cdot \left(\frac{\mathrm{d}v}{\mathrm{d}x}\right)_{x+\mathrm{d}x} - \eta \cdot \left(\frac{\mathrm{d}v}{\mathrm{d}x}\right)_x \tag{3.2-e}$$

Assuming steady state (total force on EDL is zero) laminar flow of counterions within the EDL, as well as a constant dielectric constant and fluid viscosity, η, through the moving portion of the EDL, we arrive at the following expression:

$$\mathrm{E}\rho\,\mathrm{d}x = \eta \cdot \left(\frac{\mathrm{d}^2\mathrm{v}}{\mathrm{d}^2x}\right)\mathrm{d}x \tag{3.3-a}$$

Substituting Equation 3.1 into Equation 3.3-a, the net charge per unit volume, ρ, given by Equation 3.1, and recognizing that for a planar surface, Poison's Equation is:

$$\nabla^2\psi_x = \left(\frac{\mathrm{d}^2\mathrm{v}}{\mathrm{d}^2x}\right)\mathrm{d}x \tag{3.3-b}$$

We obtain Equation 3.3-c:

$$-\left(\frac{ED}{4\pi}\right)\frac{\mathrm{d}^2\psi}{\mathrm{d}^2x} = \eta \cdot \left(\frac{\mathrm{d}^2\mathrm{v}}{\mathrm{d}^2x}\right)\mathrm{d}x \tag{3.3-c}$$

Integrating Equation 3.3-c twice over the whole fluid from the shear plane to infinity (i.e., $x = \infty$):

$$-\left(\frac{E\varepsilon}{4\pi}\right)\psi = \eta\mathrm{v} \tag{3.4}$$

Recognizing that at $x = \infty$, $\psi = 0$, and $\mathrm{v} = \mathrm{v_p}$ (the electro-osmotic velocity), and $\psi = \zeta$ and $v_e = 0$ at the shear plane, combining like terms we obtain the classical Smoluchowski formula (Equation 3.5)[2,3]:

$$\mathrm{v_p} = \mathrm{E}\varepsilon\zeta/4\pi\eta \tag{3.5}$$

Under the assumptions described above, the electro-osmotic flow given by an applied voltage at the shear plane is equivalent to the electrophoretic velocity, and hence the ζ-potential of the particle. This generalized Smoluchowski formula has been extensively applied for solid particles throughout the literature including for RBCs.

Another important concept to our understanding of ζ-potential is the **streaming potential**. Streaming potential is described by Oliver *et al* as "the voltage difference, E_s, developed between the ends of a capillary tube or porous diaphragm through which liquid is forced to flow by an applied pressure difference, P[4]. An expression relating E_s, P, and ζ-potential is given in Equation 6, and its accompanying derivation can be found in the original manuscript by Oliver *et al*[5]. Streaming potential has further been described by the charge displacement within the EDL due to electro-osmotic flow past a charged stationary surface.

Charge Density and EDL Thickness: The distribution of ions, both within the EDL and concentration of bound charges on the particle surface, are important for characterizing ζ-potential as they determine both the aggregation and separation between particles. According to the Gouy-Chapman model[6], the thickness of the double layer (also known as the Debye length) denoted by κ^{-1}, is given by:

$$\kappa^{-1} = \sqrt{\frac{\varepsilon \kappa_B T}{\sum_i c_i z_i^2 e^2}} \tag{3.6}$$

Here ε is the dielectric constant, κ_B is the Boltzmann's constant (1.38 x 10^{-23} J/K), T is absolute temperature (in Kelvin), c_i is the molecular concentration of counterions, z_i is valency of counterions in EDL and e is elementary charge of counterions (in Columbs). Due to the continuous movement of ions across the cell membrane, counterion concentration within the EDL, as well as the total charge density, are important considerations in the study of RBC ζ-potential. To express ζ-potential in terms of charge

density (i.e., electric charge per unit area), σ, (measured in C/m^2) the Smoluchowski formula can be re-written using the linearized form of the Poisson-Boltzmann equation (also referred to as the Debye-Hückel approximation), as follows:

General Poisson Equation $$-\nabla^2\psi = \frac{\sigma}{\varepsilon} \Rightarrow \frac{\mathrm{d}\psi^2}{\mathrm{dx}^2} = \frac{\sigma}{\varepsilon} \tag{3.7-a}$$

Where the potential only varies in the *x* direction for a planar surface.

$$\sigma \approx -\varepsilon\kappa^2 \cdot \psi \tag{3.7-b}$$

Where κ is the Debye screening parameter. Substituting into Equation 3.7-a:

Linearized Poisson-Boltzmann $$\frac{\mathrm{d}\psi^2}{\mathrm{dx}^2} = \kappa^2 \cdot \psi \tag{3.7-c}$$

Differentiating Equation 3.7-c in terms of *x* yields the following general solution:

$$\psi(x) = C_1 e^{-\kappa x} + C_2 e^{-\kappa x} \tag{3.7-d}$$

Applying the boundary condition, where the $x = \infty$, $C_2 = 0$, thus:

$$\psi(x) = C_1 e^{-\kappa x} \tag{3.7-e}$$

At the RBC's charged surface, where surface boundary condition $x = 0$, Gauss' law gives:

$$-\varepsilon \frac{\mathrm{d}\psi}{\mathrm{dx}}\Big|_{x=0} = 4\pi\sigma \tag{3.7-f}$$

Computing the derivative of Equation 3.7-f, evaluating again at $x = 0$, and then solving for C_1, yields:

$$C_1 = \frac{4\pi\sigma}{\varepsilon\kappa} \tag{3.7-g}$$

Finally, substituting C_1 into Equation 7-e, and evaluating $\psi(x)$ at $x = 0$, recalling that $\psi(0) = \zeta$ gives the final expression in terms of ζ-potential, Equation 3.7-h:

$$\zeta = \frac{4\pi\sigma}{\varepsilon\kappa} \tag{3.7-h}$$

Brooks *et al*[7] sought to compare this non-linear Poisson-Boltzmann equation, re-written in terms of the Smoluchowski formula (Equation 3.5), to relate the electric charge per unit area (i.e., charge density) σ to the ζ-potential:

Non-linear P-B (general form) $$-\nabla \cdot (\varepsilon \nabla \psi) = \sigma \tag{3.8-a}$$

where σ is given by: $$\sigma = -(\sigma_{fixed} + \sigma_{ion}) \tag{3.8-b}$$

P-B (with Smoluchowski) $$\zeta = \frac{2\kappa_B T}{e} \sin h^{-1}\left(\frac{2\pi e\sigma}{\varepsilon\kappa_B T}\right) \tag{3.8-c}$$

- The final expression shown in Equation 3.8-c considers several assumptions with respect to RBCs:
- The RBC membrane is a spherical particle with uniform surface charge distribution.
- The suspending medium is composed of a 1:1 electrolyte composition (e.g., NaCl).
- ζ-potential is assumed to be small (i.e., <25 mV) and the RBC size is large relative to EDL thickness.

While this section outlines the mathematical derivations to obtain ζ-potential, including the relationship between ζ-potential and surface charge density. The final mathematical expression used for all experimental ζ-potential measurements presented in this dissertation is based on the Equation 3.10. This equation accounts for the effects of particle size (based on Henry function) on ζ-potential, as measured in a bulk cell suspension.

ζ-POTENTIAL MEAUREMENT

Measurement of ζ-potential cannot be performed directly, rather, it must be obtained using mathematical models and experimental measurements of the particle's electrophoretic mobility (EM, also referred simply as "mobility")[8,9]. Recall from *Chapter 1* that EM is characterized as the movement of charged particles under the influence of an applied electric field. The EM of a charged particle is considered positive if moving *towards* the negative electrode, denoting an attraction force. Likewise, EM is negative if moving *away from* the negative electrode, denoting a repulsion force. Mathematically, the EM, denoted by μ_p and measured in units of μm/sV·cm is given by:

$$\mu_p = v_p/E \tag{3.9}$$

where v_p is velocity of the particle (in μm/s) and E is the applied electric field (in V/cm). Experimentally, ζ-potential is measured by exposing charged particles to an applied electric field and measuring the movement of the particles over a defined distance. The Henry equation (Equation 3.10) relates measured EM to ζ-potential by[10]:

$$\zeta = \frac{4\pi\eta}{\varepsilon} \cdot \mu_p f(\kappa\alpha) \tag{3.10}$$

where η and ε are the viscosity (in Pa·s) and dielectric constant of the suspending media (in F/m) respectively, and μ_p is the electrophoretic mobility (in $m^2/V{\cdot}s$). The dimensionless Henry function, denoted by $f(\kappa\alpha)$ above relates particle radius to EDL thickness. The value of the Henry function is dependent on the composition of the suspending media and particle size. For small particles (<1 μm in diameter) suspended in non-polar media (e.g., fats, oils) $f(\kappa\alpha) = 1$. Likewise, for large particles (>1 μm) suspended in non-polar media

(e.g., fats, oils) f(κα) = 1.5. (**Figure 3.2**). Considering RBCs are ~8 μm in diameter, f(κα) of 1.5 is used for all ζ-potential measurements presented in this dissertation.

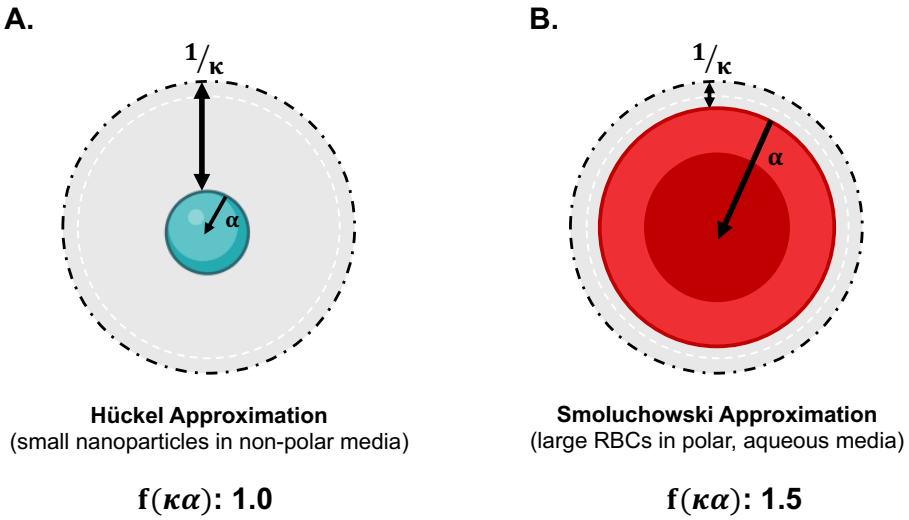

Figure 3.2: Schematic showing relationship between the electric double layer thickness and particle size and comparing the Henry function for (A.) small nanoparticles, using Hückel Approximation, and (B.) large particles such as RBCs, using Smoluchowski Approximation.

Microelectrophoresis: The velocity of charged particles can be measured using an apparatus comprised of a microscope and a thin-walled transparent cuvette equipped with platinum electrodes in which the particles of interest are analyzed. A voltage source is applied to the cuvette, and particles move in response to the applied voltage. The particles' velocity, and it's electrophoretic mobility as a function of electric field strength, is inferred by observing the time it takes for the particle to traverse a defined distance. Traditional microelectrophoresis requires samples with high optical clarity and are subject to inter-operator variability in measurement interpretation. Equipment used in microelectrophoresis possess two sets of electrodes (**Figure 3.3:**). Platinum electrodes

integrated into the cuvette are used to measure the potential drop while zinc electrodes are used to induce particle movement.

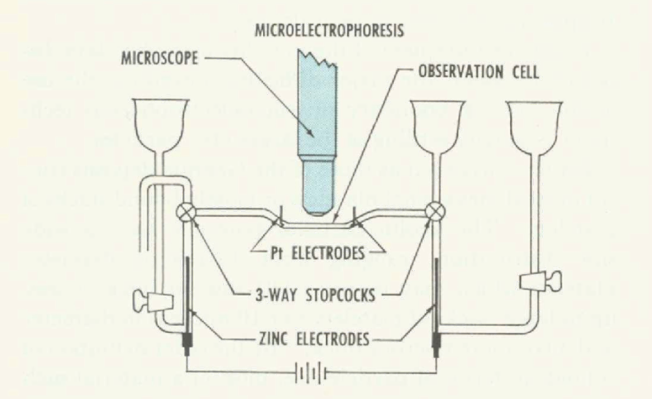

Figure 3.3: Schematic of microelectrophoresis apparatus for early characterization of ζ-potential as described by Oliver *et al*[5].

Electrophoretic Light Scattering: Beginning in the 1970s laser doppler electrophoresis[11,12], also referred to as electrophoretic light scattering (ELS), emerged as an alternative technique for measuring ζ-potential[13]. Unlike conventional microscope-based microelectrophoresis which is limited to single-cell, highly variable EM measurements, ELS allows for repeatable ζ-potential with high precision (± 0.1 mV). ELS-based ζ-potential measurement is performed using a commercial ζ-analyzer (e.g., Malvern Zetasizer). ELS is the most widespread technique used in commercialized applications of ζ-potential measurement and the approach used for all research aims in this dissertation. As depicted in **Figure 3.4*:* A**, experimental ELS works by first measuring the frequency of scattered light emitted as RBCs move under an applied electric field. The light frequency is then converted to particle velocity using the mathematical expression in **Figure 3.4*:* B**. Particle velocity is then converted to an electrophoretic mobility, **Figure 34C**. Lastly,

electrophoretic mobility is used to quantify RBC ζ-potential using the Helmholtz-Smoluchowski equation (**Figure 3.4*: D***).

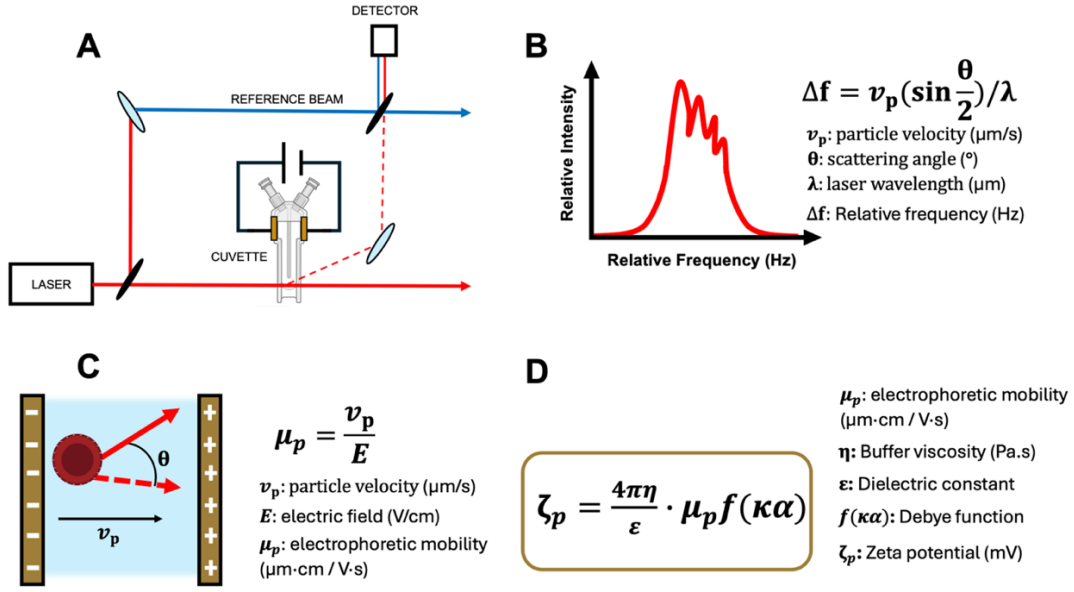

Figure 3.4: Experimental workflow showing application of electrophoretic light scattering (ELS) technique for measuring ζ-potential of human RBCs.

Optical Tweezers: First developed by Ashkin *et al* in the 1970s, later refined to its present form by Ashkin *et al* and Chu *et al*, optical tweezers (OTs), depicted in **Figure 3.5**: is a novel technique used to characterize the ζ-potential of particles for biological applications[14,15]. OTs work based on photon momentum transfer by trapping and suspending a charged particle within an infrared laser beam, allowing for fine-tuned manipulation and characterization of the particle's mechanical properties (e.g., elasticity) and electrical properties (e.g., ζ-potential). OTs have been used in many biological applications. For example, Silva *et al*[16] applied OTs to investigate the ζ-potential of RBCs stored for up to 36 days. The authors found that prolonged blood storage resulted in a 142%

decrease in ζ-potential magnitude from baseline (-14.5 ± 0.7 mV), due to storage-induced oxidative damage.

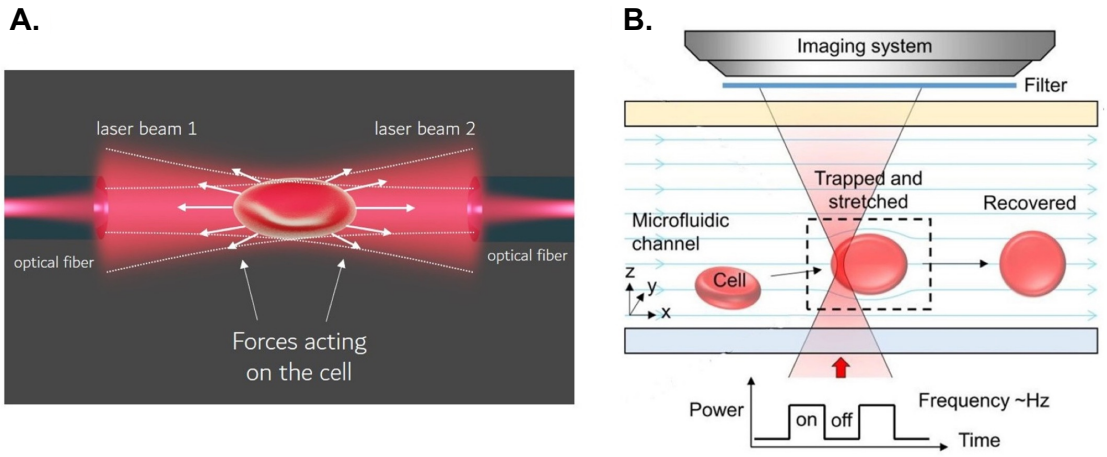

Figure 3.5: Schematic showing RBCs trapped and stretched between two infrared lasers in the optical tweezers apparatus. Image reproduced from Avsievich et al[17].

FACTORS INFLUENCING ζ-POTENTIAL MEASUREMENT

Across the literature, ζ-potential values of healthy RBCs range from (-25 to -45 mV). Experimental conditions, RBC handling, and donor variability all contribute to the ranges found in these works. Additionally, overall RBC health and disease progression also impacts ζ-potential. Ranges of ζ-potential values found in RBC-related diseases have been reported from -10 to -20 mV. (**Figure 3.6***:*). This section will describe the major contributors of ζ-potential in RBCs.

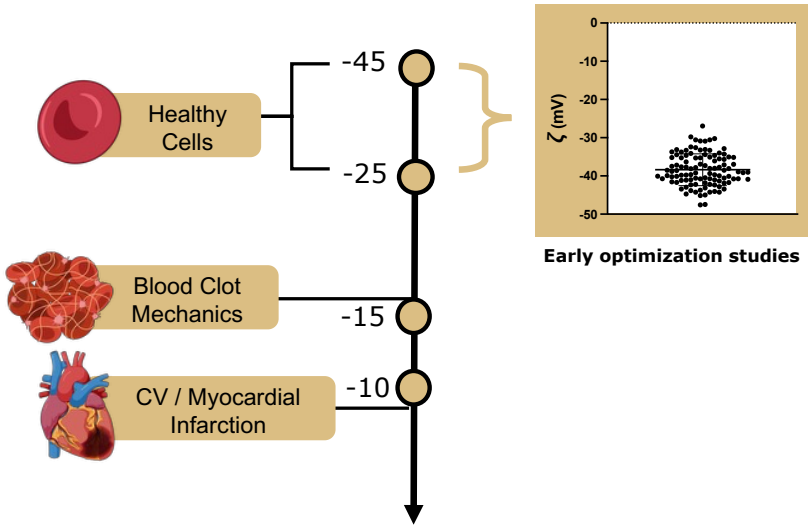

Figure 3.6: Schematic showing range of ζ-potential values for healthy RBCs and various disease conditions as reported in literature.

pH of Buffer: The pH is an important factor impacting the ζ-potential of charged particles suspended in aqueous solution. Changing the pH of the suspending medium directly effects the ζ-potential magnitude of negatively charged RBCs by altering the membrane surface chemistry and negative charge distribution. For example, adding cations (e.g., H^+, Ca^{2+}, Na^+) to the suspending medium, will increase the pH and cause a decrease in ζ-potential magnitude (less negative) due to attraction and cations to the membrane surface. This reduces the available negative charge binding sites on the surface, resulting in the potential for cell aggregation. Lowering the pH by adding anions (e.g., OH^-, Cl^-, SO_4^{2-}) to the suspending media results in an increase (more negative) in ζ-potential magnitude due to absorption of OH^- groups to the membrane surface, increasing the repulsive forces between cells. The pH value at which a negatively charged RBC possesses a net neutral charge (ζ=0 mV) and will not move in response to an applied electric field, is called the **isoelectric point** (IEP), shown in **Figure 3.7***:* .

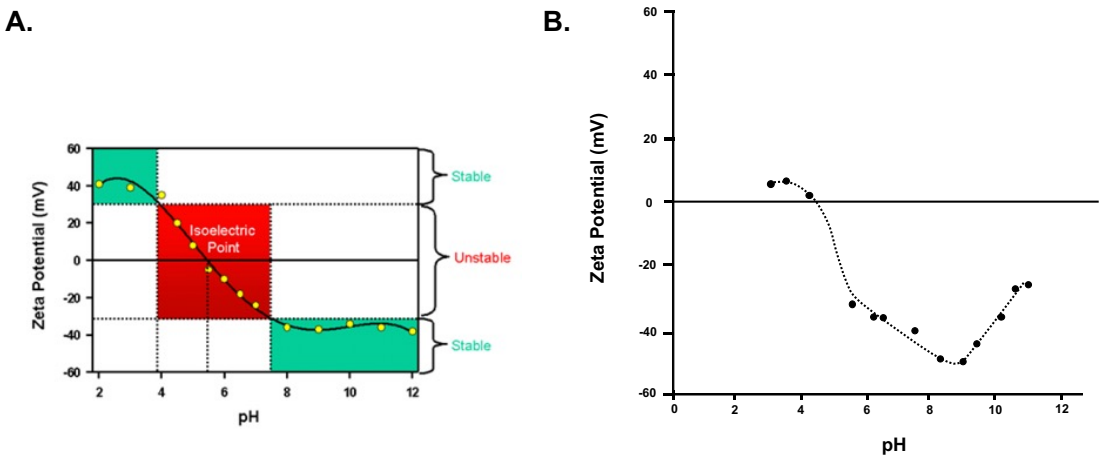

Figure 3.7: Schematic showing the relationship between ζ-potential and buffer pH. (A). Generalized ζ-potential-pH relationship for a spherical particle. (B). Plot of ζ-potential-versus-pH for human RBCs, adapted from Riddick et al[18].

Effects of Buffer Conductivity: In addition to pH, changes in surface ζ-potential magnitude of negatively charged RBCs are influenced by the concentration of ions (conductivity) of the suspending media. For example, when the conductivity of the suspending media is raised (through the addition of cations) the additional positive charges "screen" the RBC's negative surface charge, compressing the EDL, and reducing the ζ-potential magnitude and repulsive force between two cells. Conversely, when the conductivity of the suspending media is lowered (through the addition of anions) the dissolved ions are repelled from the particle surface, the EDL expands due to addition of negative charges, and ζ-potential magnitude and repulsive force between two cells is increased. Moreover, the valency of ions in aqueous suspending media can contribute to changes in ζ-potential magnitude.

Effects of Temperature and Buffer Viscosity: Both the temperature and the viscosity of the buffer are important properties when measuring ζ-potential of charged particles. Temperature effects on ζ-potential have been extensively characterized, but vary depending on the material of interest[19]. For example, in silver nanoparticles, ζ-potential magnitude becomes more negative as temperature increases from 37 to 50 °C, resulting in greater particle stability (reduced susceptibility to aggregation) at higher temperatures[20]. For RBCs, studies directly investigating temperature effects on ζ-potential are limited.

Nevertheless, temperature impacts can be inferred based on the cell's biophysical response to temperature. For example, cooling cells from normothermic (~37°C) to refrigeration (~4°C) temperature causes an increase in the absorption energy of RBC aggregates, leading to stacking and pearl chain (rouleaux) formation. Investigating the effects of heat exposure on RBCs is of equal importance as heat-related illness can lead to anemia due to oxidative damage and hemolysis.

Other authors have reported increases in cytoplasmic conductivity when heating RBCs at 10, 15, 20, 25, 30 and 37°C[21]. As discussed in *Chapter 2*, RBC cytoplasmic conductivity is related to ζ-potential, such that changes in cytoplasmic conductivity correlates with direct changes in ζ-potential magnitude. In the study above K^+ and Na^+ had the highest intracellular ion concentration (K^+: 0.095 mol/L, and Na^+: 0.0186 mol/L, respectively). Thus, it is expected the ζ-potential magnitude to increase (become more negative) with increases in temperature, due to an influx of positive ions into the cell (i.e., the extra-cellular suspending medium becoming more negatively charged).

Viscosity, defined as "a fluid's resistance to flow and shear deformation", is another important factor influencing ζ-potential measurements[22]. The viscosity of aqueous solutions is highly influenced by the presence of protein-to-protein interactions (PPI). In low ionic solutions, electrostatic repulsive force (dictated by the particles surface charge) is greater than Van der Waals attraction forces between protein molecules, preventing aggregation and lowering buffer viscosity. However, with the addition of cations to the suspending media, the electrostatic repulsive force is "screened", allowing Van der Waals attraction forces to dominate. This results in the formation of protein clusters and increases the viscosity of suspending media. Viscosity and ζ-potential are related by the Henry equation (Equation 3.10) described in the proceeding section. Although high buffer viscosity will reduce the particle's velocity, and therefore its electrophoretic mobility, for large particles, an increase in buffer viscosity results in a greater negative ζ-potential magnitude due to minimal changes in electrophoretic mobility compared to viscosity of suspending media.

ζ-POTENTIAL APPLICATIONS RELATED TO RED BLOOD CELLS

Cardiovascular Disease: Cardiovascular disease (CVD) is the leading cause of death worldwide. Over the past two decades, ζ-potential has increasingly been used as a biomarker to monitor CVD risk and disease progression. Adak *et al* conducted a series of experiments to understand how RBC ζ-potential is altered in patients with diabetes mellites and cardiovascular disease, to offer the potential to inform disease monitoring. They reported a significant decrease in ζ-potential magnitude (from -37.24 ± 1.5 mV to -28.44

± 1.34 mV, then further decrease to -22.21 ± 1.21 mV) in healthy controls, diabetic, and CVD patients respectively. Gaikwad *et al* observed a similar, yet more pronounced decrease in RBC ζ-potential magnitude (from -22.13 ± 0.2789 mV to 8.559 ± 0.4864mV) in patients with diabetic hypoglycemia, a condition linked to increased CVD risk. A subsequent study by the same research group focused on measuring ζ-potential as a tool for angina risk in pulmonary hypertension and myocardial infarction showed agreement with earlier work.

Additionally, others have investigated RBC-fibrinogen interactions, effects of cell aggregation, the effects of flow-mediated shear stresses, and the influence of earthing and grounding on cell surface charge and ζ-potential[23]. Collectively these studies provide a foundation for understanding the role of ζ-potential in cardiovascular disease.

Blood Banking and Red Blood Cell Aging: Blood banking and storage and RBC aging have gained considerable attention due to the high number of annual blood transfusions required worldwide[24]. Prolonged blood storage causes storage lesions which deleteriously affect cellular function and RBC membrane integrity, including cleavage of sialic acid and decreased cell membrane elasticity and deformability[25]. Huang *et al*[26] found young RBCs to have a higher charge density (and thus higher ζ-potential) compared to old RBCs. Silva *et al* used optical tweezers[16] to characterize the RBC zeta potential response due to blood storage. They reported that the changes in ζ-potential are due to oxidative damage as noted by the significant decrease with blood storage duration (from Day 1: -14.5 ± 0.7 mV to Day 29/36: -8.5 ± 0.4 mV). These findings demonstrate the importance of monitoring

glycophorin stability (via surface charge and ζ-potential) for to improve blood storage and transfusion protocols for critically ill patients.

Red Blood Cell Function and Disease Progression: To gain a deeper understanding of the biophysical significance of ζ-potential pertaining to the RBC membrane, Eylar *et al*[27] conducted a series of experiments to determine the relationship between sialic acid glycoproteins and the inherent negative charge present on the surface of RBCs. Results from Eylar's experiments focused on measuring the electrophoretic mobility and ζ-potential of packed RBCs from five animals, revealed significant reductions in both electrophoretic mobility and ζ-potential following treatment with neuraminidase due to removal of sialic acid surface proteins. Subsequent studies have demonstrated the important contribution of sialic acids for modulating the RBC ζ-potential response. Beyond normal physiologic processes the ζ-potential response of RBCs has been studied to understand disease progression in malarial anemia[28], β-thalassemia[29], and sickle cell disease[30].

OPTIMIZATION OF METHODS FOR MEASURING ζ-POTENTIAL

To ensure repeatability and reproducibility of my ζ-potential measurements preliminary experiments were conducted to optimize parameters that may in results, including effect of buffer conductivity, and duration cells sit in suspending media, effect of cell concentration, and comparison of hematocrit for translation to real-world clinical applications.

Optimization of Suspending Media Conductivity: Low-conductivity, iso-osmotic media has been used for monitoring RBC electrophysiological properties, with the recipe optimized to minimize ion leakage[31,32]. However, ion flux has been shown to occur immediately following RBC suspension in the media and therefore has the potential to alter ζ-potential measurements on short time scales. Considering this, I sought to compare our current 100 μS/cm media to a higher conductivity media (~400 μS/cm used in previous DEP work)[31,33,34] to determine which buffer conductivity produced the most consistent ζ-potential measurements between trials. Briefly, 2 mL of human whole blood was obtained by venipuncture from a single healthy donor. Isolation of healthy packed RBCs, along with preparation of the iso-osmotic buffer and final cell suspensions, were performed as described in *Chapter 4*. Measurement of RBC ζ-potential was performed using a Zetasizer Pro (Malvern Analytical, Inc.) commercial ζ-potential analyzer. The default setting in the ζ-potential analyzer software consists of a maximum of 100 ζ runs per trial, and a temperature equilibration duration of 120 seconds. However, due to the propensity for RBC sedimentation, the maximum ζ runs per trial was adjusted to 30 runs, and the temperature equilibration time was set to 30 seconds.

As shown in **Figure 3.8***:* , 400 μS/cm produced the most consistent results between ζ-potential trial replicates as well as the most consistent results between media conductivities. These findings are important because they provide a foundation to ensure measurement reproducibility for the research aims conducted in this dissertation. In addition, the ζ-potential values obtained at 400μS/cm are more closely aligned with other RBC ζ-potential values found in literature[32,35,36].

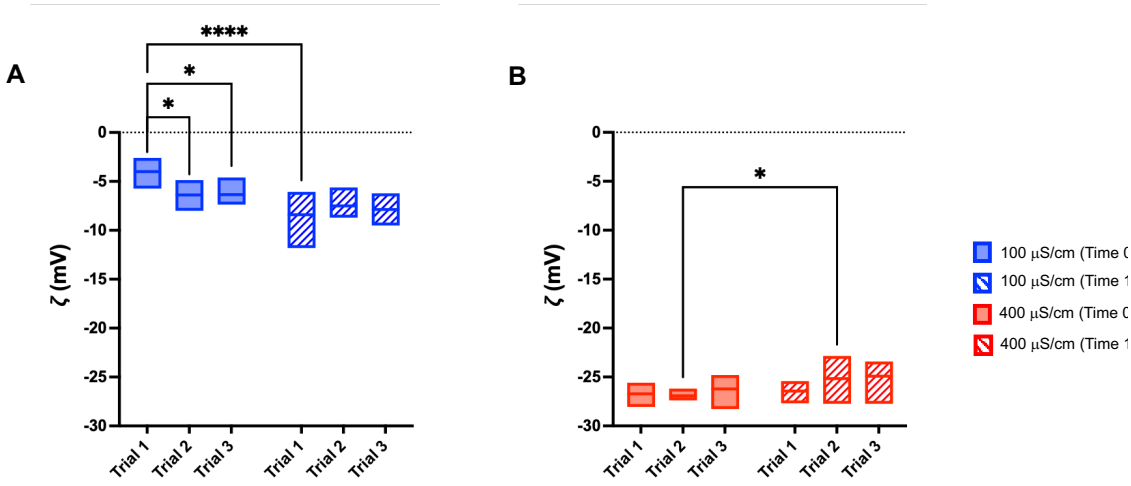

Figure 3.8: Media Conductivity Experiment - (A.) Significant changes in ζ-potential magnitude were observed between trials in 100 µS/cm media at both 0 hr and after 1 hr of cells sitting in suspension. (B.) No changes in ζ-potential magnitude were observed between trials in 400 µS/cm media at 0 hr; minimal changes were observed between trials after 1 hr of cells sitting in suspension.

Optimization of RBC Concentration: RBC concentration is an important factor influencing ζ-potential measurement due to the possibility for increased RBC aggregation. In clinical practice, RBC concentration is traditionally represented by hematocrit, the percentage by volume of red cells in whole blood, with a baseline hematocrit for healthy human donors of 40-45%[37–39]. At times the volume of whole blood needed to achieve 40% may be difficult to maintain due to large volume needs for some experiments and limitations of single donor blood volume availability. Considering this need, an experiment was carried out to determine if the results obtained using 10% hematocrit can be translated to real-world 40% hematocrit applications. Further, for downstream electrophysiological measurement, RBC samples are typically prepared at a concentration of ~10^6 cells/mL[34,36,40]. This, however, can vary based on the density of the packed RBC pellet (and number of cells available due to hemolysis) after washing. Since ζ-potential

measurement relies on ELS, cell concentration may influence the results. Therefore, a second experiment was carried out to compare cell concentrations of 10^5, 10^6, 10^7, and 10^8 cells/mL, to determine reproducibility of results within and across experiments which may vary in experimental cell concentration.

Human whole blood was freshly drawn intravenously into 10 mL sodium-heparin tubes and stored in refrigeration overnight. On the day of experiments, whole blood was transferred to 15 mL conical tubes containing approximately 2 mL whole blood in 5 mL Hank's Buffered Saline Solution (HBSS). Whole blood suspensions were centrifuged for 5 minutes @ 700 x g for three cycles to produce a packed RBC pellet. Following isolation, RBC suspensions were stored at 30-40% hematocrit in a refrigerator at 4±1°C.

Measurement of surface ζ-potential was conducted using a Zetasizer Pro Red Label (Malvern Analytical, UK). For each hematocrit group, ζ-potential measurements were collected in triplicate for three biological replicates (i.e., n=9 technical replicates) per hematocrit group. The final RBC concentration for each sample was at least ~10^6 cells/mL.

From the first experiment, no changes in ζ-potential magnitude were observed between 10% and 40% hematocrit, **Figure 3.9A**, suggesting that results obtained in this dissertation can be translated to real-world 40% hematocrit applications. For the concentration experiment, while significant differences in ζ-potential magnitude were observed at both low (10^5 cells/mL) and high (10^8 cells/mL) concentrations, **Figure 3.9B**, no changes were observed at 10^6-10^7 cells/mL which is the typical range of starting cell concentration from the standard method of taking 10 µL from an RBC pellet and resuspending in 5 mL of buffer[31,33].

This work confirms two important conclusions for the work carried out in subsequent chapters. First, our experiments conducted at 10% hematocrit for the sake of single donor usage should yield physiological relevant results with regards to the normal 40% hematocrit found in whole blood. Second, standard protocols used in previous DEP and ζ-potential studies for sampling 10 µL of RBC pellet (and the normal range of cell concentrations this produces) should not impact final ζ-potential results. However, care should be taken in interpreting any ζ-potential measurements where cell concentration falls below 10^6 cells/mL, and dilution steps should be considered for any concentrations above 10^7 cells/mL.

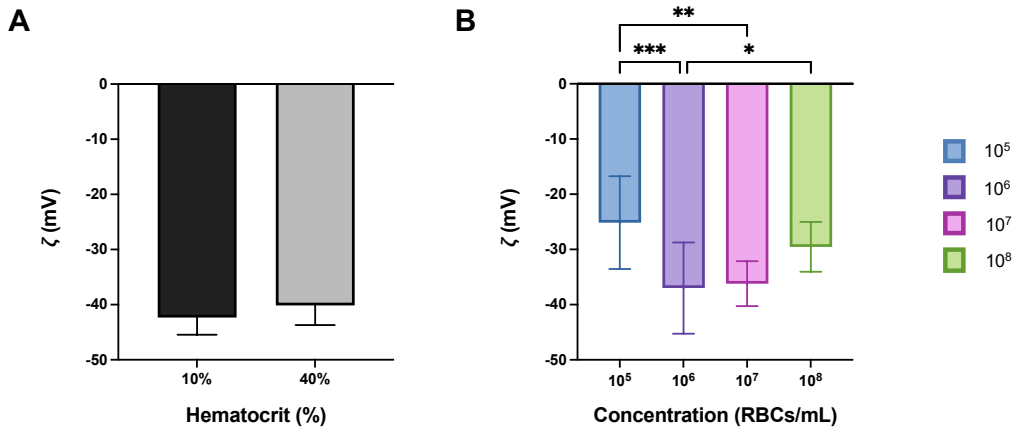

Figure 3.9: (A.) Hematocrit Experiment - No changes in ζ-potential magnitude were observed between 10% to 40%. (B.) Cell Concentration Experiment - Changes in ζ-potential magnitude were observed at cell concentrations from 10^5-10^8 cells/mL.

REFERENCES

1. Simon, F. Electrokinetic Phenomena. *Leibniz Institute of Polymer Research, Dresden, Germany* (2009).

2. Sze, A., Erickson, D., Ren, L. & Li, D. Zeta-potential measurement using the Smoluchowski equation and the slope of the current–time relationship in electroosmotic flow. *Journal of colloid and interface science* **261**, 402–410 (2003).

3. Chan, D. & Halle, B. The Smoluchowski-Poisson-Boltzmann description of ion diffusion at charged interfaces. *Biophysical Journal* **46**, 387–407 (1984).

4. Sennett, P. & Olivier, J. Colloidal dispersions, electrokinetic effects, and the concept of zeta potential. *Industrial & Engineering Chemistry* **57**, 32–50 (1965).

5. Sennett, P. & Olivier, J. Colloidal dispersions, electrokinetic effects, and the concept of zeta potential. *Industrial & Engineering Chemistry* **57**, 32–50 (1965).

6. Allagui, A., Benaoum, H. & Olendski, O. On the Gouy–Chapman–Stern model of the electrical double-layer structure with a generalized Boltzmann factor. *Physica A: Statistical Mechanics and its Applications* **582**, 126252 (2021).

7. Sharp, K. A. & Brooks, D. E. Calculation of the electrophoretic mobility of a particle bearing bound polyelectrolyte using the nonlinear Poisson-Boltzmann equation. *Biophysical Journal* **47**, 563–566 (1985).

8. Clogston, J. D. & Patri, A. K. Zeta potential measurement. in *Characterization of nanoparticles intended for drug delivery* 63–70 (Humana press Totowa, NJ, 2010).

9. Lunardi, C. N., Gomes, A. J., Rocha, F. S., De Tommaso, J. & Patience, G. S. Experimental methods in chemical engineering: Zeta potential. *The Canadian Journal of Chemical Engineering* **99**, 627–639 (2021).

10. Henry, D. The electrophoresis of suspended particles. IV. The surface conductivity effect. *Transactions of the Faraday Society* **44**, 1021–1026 (1948).

11. Xiong, B. *et al.* Electrophoretic mobility measurement by laser Doppler velocimetry and capillary electrophoresis of micrometric fluorescent polystyrene beads. *Analytical Methods* **4**, 183–189 (2012).

12. Tucker, I. *et al.* Laser Doppler Electrophoresis applied to colloids and surfaces. *Current opinion in colloid & interface science* **20**, 215–226 (2015).

13. Cotner, P., Serrallach, E., Catsimpoolas, N. & Valeri, C. *Electrophoretic Light Scattering: Instrumentation and Application to the Measurement of the Electric Charge of Human Blood Cells.* (1982).

14. Avsievich, T., Zhu, R., Popov, A., Bykov, A. & Meglinski, I. The advancement of blood cell research by optical tweezers. *Reviews in Physics* **5**, 100043 (2020).

15. Bernecker, C. *et al.* Biomechanics of ex vivo-generated red blood cells investigated by optical tweezers and digital holographic microscopy. *Cells* **10**, 552 (2021).

16. Silva, D. C. *et al.* Optical tweezers as a new biomedical tool to measure zeta potential of stored red blood cells. *PloS one* **7**, e31778 (2012).

17. Avsievich, T., Zhu, R., Popov, A., Bykov, A. & Meglinski, I. The advancement of blood cell research by optical tweezers. *Reviews in Physics* **5**, 100043 (2020).

18. Riddick, T. M. Control of colloid stability through zeta potential. *Blood* **10**, 52–68 (1968).

19. Mohammadi-Jam, S., Greenwood, R. W. & Waters, K. E. An overview of the temperature dependence of the zeta potential of aqueous suspensions. *Results in Engineering* **27**, 105698 (2025).

20. Anbu, P., Gopinath, S. C., Yun, H. S. & Lee, C.-G. Temperature-dependent green biosynthesis and characterization of silver nanoparticles using balloon flower plants and their antibacterial potential. *Journal of Molecular Structure* **1177**, 302–309 (2019).

21. Sudsiri, C. J. & Ritchie, R. J. Energy absorption of human red blood cells and conductivity of the cytoplasm influenced by temperature. *Biophysical Chemistry* **273**, 106578 (2021).

22. Chien, S. *et al.* Blood viscosity: influence of erythrocyte aggregation. *Science* **157**, 829–831 (1967).

23. Chevalier, G., Sinatra, S. T., Oschman, J. L. & Delany, R. M. Earthing (grounding) the human body reduces blood viscosity—a major factor in cardiovascular disease. *The Journal of Alternative and Complementary Medicine: Paradigm, Practice, and Policy Advancing Integrative Health* **19**, 102–110 (2013).

24. Colognesi, C., Maia, R., Hajjar, L. & Galas, F. Red blood transfusion is a predictor of poor outcome in pediatric cardiac surgery. *Critical Care* **16**, P443 (2012).

25. Schmid-Schönbein, H., Heidtmann, H. & Grebe, R. Spectrin, red cell shape and deformability: II. The antagonistic action of spectrin and sialic acid residues in determining membrane curvature in genetic spectrin deficiency in mice. *Blut* **52**, 149–164 (1986).

26. Huang, Y. *et al.* Human red blood cell aging: correlative changes in surface charge and cell properties. *Journal of cellular and molecular medicine* **15**, 2634–2642 (2011).

27. Eylar, E. H., Madoff, M. A., Brody, O. & Oncley, J. The contribution of sialic acid to the surface charge of the erythrocyte. *Journal of Biological Chemistry* **237**, 1992–2000 (1962).

28. Tokumasu, F., Ostera, G. R., Amaratunga, C. & Fairhurst, R. M. Modifications in erythrocyte membrane zeta potential by Plasmodium falciparum infection. *Experimental parasitology* **131**, 245–251 (2012).

29. Tzounakas, V. L. *et al.* Beta thalassemia minor is a beneficial determinant of red blood cell storage lesion. *Haematologica* **107**, 112 (2021).

30. Tokumasu, F. *et al.* Altered membrane structure and surface potential in homozygous hemoglobin C erythrocytes. *PloS one* **4**, e5828 (2009).

31. Henslee, E. A. *et al.* Rhythmic potassium transport regulates the circadian clock in human red blood cells. *Nature communications* **8**, 1978 (2017).

32. Hughes, M. P. *et al.* V m-related extracellular potentials observed in red blood cells. *Scientific reports* **11**, 19446 (2021).

33. Hoettges, K. F. *et al.* Ten–Second Electrophysiology: Evaluation of the 3DEP Platform for high-speed, high-accuracy cell analysis. *Scientific reports* **9**, 19153 (2019).

34. Henslee, E. A. Optimisation of dielectrophoretic based molecular targeting for blood chronobiology. (2016).

35. Gaikwad, S. S., Avari, J. G. & Patil, M. L. Zeta potential as a diagnostic tool to determine the angina risk. *Apolipoproteins, Triglycerides and Cholesterol* 1–8 (2020).

36. Hughes, M. P. The cellular zeta potential: cell electrophysiology beyond the membrane. *Integrative Biology* **16**, zyae003 (2024).

37. Elzik, M. E., Dirschl, D. R. & Dahners, L. E. Correlation of transfusion volume to change in hematocrit. *American journal of hematology* **81**, 145–146 (2006).

38. Isbister, J. P. Blood volume, hematocrit and hemorheology: the interrelationships. *Clinical Hemorheology and Microcirculation* **14**, 305–319 (1994).

39. Billett, H. H. Hemoglobin and hematocrit. *Clinical Methods: The History, Physical, and Laboratory Examinations. 3rd edition* (1990).

40. Hughes, M. P. The surface conductance of red blood cells and platelets is modulated by the cell membrane potential. *Electrophoresis* **44**, 845–853 (2023).

Chapter 4: Surface Zeta Potential as a Biomarker for Monitoring Human Red Blood Cells Under Oxidative Stress

INTRODUCTION

RBCs play a critical role in maintaining homeostasis via transport of oxygen from the lungs to tissues in the body, in exchange for carbon dioxide. To accomplish this function, RBCs possess high intracellular concentrations of hemoglobin (Hb) which serve as 'vehicles' by which to transport oxygen. However, an unfortunate consequence of oxygen transport is continuous exposure of RBCs to a high-oxygen tension environment, which leads to oxidative stress (OS) via free radicals, molecules containing one or more unpaired electrons. Oxygen free radicals that react with RBCs are referred to as reactive oxygen species (ROS). Although numerous ROS exist, primary oxidants responsible for producing damage in RBCs are, superoxide, hydroxide radical, and hydrogen peroxide[1]. Superoxide ($O_2^{\bullet -}$) is a single-electron byproduct of oxygen resulting from Hb autoxidation (reducing oxyHb to ferrylHb via the Fenton reaction). Alone $O_2^{\bullet -}$ is not a very potent or damaging oxidant, however, when reacting with nitric oxide, a highly toxic oxidant peroxynitrite, is produced. Hydrogen peroxide (H_2O_2), produced by $O_2^{\bullet -}$ via the reaction shown in Equation 4.1, is responsible for numerous cellular processes, including cell survival and proliferation[2,3].

$$2O_2^{\bullet -} + 2H^+ \rightarrow H_2O_2 + O_2 \quad (4.1)$$

Due to the ability of H_2O_2 to rapidly cross the cell membrane and damage other tissues, as well as its ability to be reduced into the highly reactive hydroxyl radical, it is

deemed a potent oxidant. Hydroxyl radical ($HO^{\bullet}$) is considered the most harmful free radical in biology due to its high degree of reactivity. Production of $HO^{\bullet}$ is accomplished by reducing H_2O_2 via reduction of iron (Fe), from Fe(III) to Fe(II) via the Fenton reaction[2] (Equation 4.2). Additionally, the presence of excess free iron in the RBC membrane, as seen in sickle cell disease, can further precipitate $HO^{\bullet}$-induced oxidative damage.

$$H_2O_2 + Fe^{II} \rightarrow HO^{\bullet} + HO^{-} + Fe^{III} \quad (4.2)$$

Tert-Butyl hydroperoxide (denoted chemically by $(CH_3)_3COOH$, and abbreviated tBHP) is a commercially synthesized oxidizing agent produced by combining an equimolar amount of tert-butyl alcohol ($(CH_3)_3COH$) with 30-50% H_2O_2 in the presence of a catalytic agent such as sulfuric acid (H_2SO_4), shown in Equation 4.3:

$$(CH_3)_3COH + H_2O_2 \xrightarrow{H_2SO_4} (CH_3)_3COOH + H_2O \quad (4.3)$$

In RBCs, tBHP targets and damages the cell membrane by binding hemoglobin to the inner surface of the cell membrane. This produces long protein chains that cross-link with cytoskeletal proteins (e.g., spectrin and actin) which results in protein denaturing and clustering, rigidifying the membrane and decreasing deformability. For example, through the fluorescence-labelling of spectrin and actin, Caprari *et al* observed that tBHP selectively targets actin junctional sites on the RBC membrane causing detachment of spectrin[4]. This can subsequently result in both membrane degradation and the formation of membrane pores (and subsequent intracellular Ca^{2+} leakage from the cytoplasm).

Another commercially synthesized oxidizing agent used in this chapter, cumene hydroperoxide, (denoted chemically by $C_9H_{12}O_2$, and abbreviated COOH) is produced by mixing cumene (C_9H_{12}) with air used as an oxidant to precipitate the chemical conversion at temperatures ranging from 45–130°C and reaction times up to 12 hours (Equation 4.4).

$$C_9H_{12} + O_2 \xrightarrow{\text{Heat}} C_9H_{12}O_2 \tag{4.4}$$

Like tBHP, COOH is a membrane-targeting OS agent that directly penetrates the lipid bilayer triggering the formation of high molecular weight aggregates of RBC membrane proteins, decreasing RBC deformability. As a direct consequence of this lipid peroxidation, exposure to COOH has been shown to increase the dipole potential of the RBC membrane by up to 14%, increasing flux of intracellular calcium (Ca^{2+}) and triggering cell shrinkage through Gardos channel activation[5]. This shift in the intracellular dipole potential also has potential impacts on the surface ζ-potential based on the observed relationship between ζ-potential and membrane potential (V_m) discussed in *Chapter 2*.

To counteract the damaging effects of ROS, RBCs possess a robust antioxidant defense system comprised of enzymes that work to neutralize and break down ROS[6]. Specifically, catalase (CAT) is an important enzyme responsible for protecting cells and tissues from the toxic effects of H_2O_2 via decomposition of H_2O_2 into water and oxygen[7,8]. Additionally, glutathione peroxidase (GPX) is responsible for preventing H_2O_2 accumulation within the cell[9,10]. Despite this robust defense system, in diseases such as red cell anemias (e.g., sickle cell and malaria), diabetes, and cardiovascular disease, ROS levels often exceed that of natural antioxidant defenses, resulting in OS. Exposure of RBCs

to an overabundance of ROS results in OS with deleterious impacts to the RBC membrane, including irreversible membrane damage, as well as impaired oxygen delivery through Hb autoxidation[11,12].

The most readily observed impact of OS in RBCs are changes to membrane morphology, characterized by increasing echinocytes. Considering this, *ex vivo* studies have primarily evaluated the effects of OS on RBC mechanical properties (e.g., shear stress[13], deformability[11,14], etc.). Mechanical properties, while effective at distinguishing differences between healthy and damaged cells, only reveal significant changes once irreversible membrane damage or complete hemolysis has occurred. However, because OS causes gradual, cumulative impacts to RBCs, **there is a significant need to apply alternative techniques capable of providing greater measurement sensitivity for detecting subtle shifts in the biophysical response of RBCs during OS.**

RBC electrical properties have been shown to occur prior to shifts in mechanical properties, and may provide insights into the progression of OS[15]. Thus, the aim of this study was to apply ζ-potential as a tool for monitoring human RBCs exposed to OS. To carry out this aim, the following study objectives were performed:

<u>Study Objective 1:</u>

Determine sensitivity of surface ζ-potential for monitoring RBCs in H_2O_2 induced-OS.

<u>Study Objective 2:</u>

Probe the biophysical and OS agent-specific mechanisms that modulate the surface ζ-potential response of human RBCs under OS.

METHODS

Human Subjects: Studies were conducted in accordance with 45 CFR 46 and the principles of the Declaration of Helsinki, with approval from the Institutional Review Board (Wake Forest University, Winston-Salem, NC). Participants in the study were screened for relevant self-reported health issues. All participants provided written, informed consent after having received a detailed explanation of the study procedures.

Blood Procurement and Isolation of RBCs: Human whole blood was freshly drawn intravenously into 10 mL sodium-heparin tubes and stored in refrigeration overnight. For all experiments conducted for Objective 1 and Objective 2, blood samples were drawn from a single, Caucasian healthy female donor (no underlying chronic conditions) with the following characteristics: O+ blood type and less than 50 years old. On the day of experiments, whole blood was transferred to 15 mL conical tubes containing approximately 2 mL whole blood in 5 mL Hank's Buffered Saline Solution (HBSS). Whole blood suspensions were centrifuged for 5 minutes @ 700 x g for three cycles to produce a packed RBC pellet. Following isolation, RBC suspensions were stored at 30-40% hematocrit in a refrigerator at 4±1°C during drug preparation.

Hydrogen Peroxide Drug Treatment: To determine the electrophysiologic response of RBCs under OS conditions, RBCs were exposed to a graded H_2O_2 drug treatment regime. The H_2O_2 concentrations shown in **Table 4.1** were chosen just beyond the physiologic threshold of 50 μm observed in RBCs.

Table 4.1: ***Hydrogen Peroxide Treatment Groups (prepared in 1 mL total volume)***

Treatment Group	**HBSS 1x (w/o PR)**	**NaN_3 [100 mM]**	**Washed RBCs (10% HCT)**	**tBHP Stock**	
				CONCENTRATION	VOLUME
Control	860 µL	40 µL	100 uL	-------	-------
0.5 mM	758 µL			4.9mM	102 µL
1 mM				9.8mM	102 µL
5 mM				49mM	102 µL
10 mM				98mM	102 µL

The drug response was developed with collaborators, Regina Cordy and Heather Colvin-Binns (whose work was conducted at the 50 µM, above the physiologic threshold) and the final concentrations selected represent both healthy and unhealthy concentrations of H_2O_2. This was done to achieve a dose-dependent response in H_2O_2-induced OS. Briefly, RBC suspensions were prepared in the dark in light-sensitive Eppendorf tubes by diluting stock 3% H_2O_2 in HBSS to 4.9-98 mM stock (depending on treatment concentration), prepared at 10% hematocrit in total volume of 1 mL. To inhibit CAT, sodium azide (NaN_3) was added to each sample at a final concentration of 4 mM prior to introducing H_2O_2 treatment. A control, without H_2O_2 treatment was prepared by adding 860 µL of HBSS to 10% hematocrit suspension of packed RBC pellet and 4 mM of NaN_3 in total volume of 1 mL. All samples were incubated in light-sensitive Eppendorf tubes in the dark at 37°C for 2 hours. Following incubation, samples were washed twice by centrifugation at 700 x g for 5 minutes to stop the oxidization reaction.

Tert-Butyl and Cumene Hydroperoxide Dose Optimization: To probe the biophysical mechanisms responsible for modulating the ζ-potential response in OS, RBCs were

exposed to increasing concentrations of tBHP and cumene hydroperoxide COOH. Treatment groups for each oxidizing agent were prepared from a 100 mM stock in a total volume of 1 mL from stock solutions at a hematocrit of 10% with NaN_3 at final concentration of 4 mM. Considering that both tBHP and COOH have been reported to induce an OS response via lipid peroxidation treatment protocols were first developed to measure ζ-potential response at several tBHP and COOH concentrations below the I_{C50} values found in literature, **Figure 4.1: A** and **Figure 4.1: B.** Since no significant changes ($p<0.05$) in ζ-potential response were observed below these I_{C50} values, I preceded with the final tBHP and COOH treatment regime, shown in **Table 4.2** and **Table 4.3, which is** above the I_{C50} values and up to the concentrations where complete hemolysis has been reported to occur.

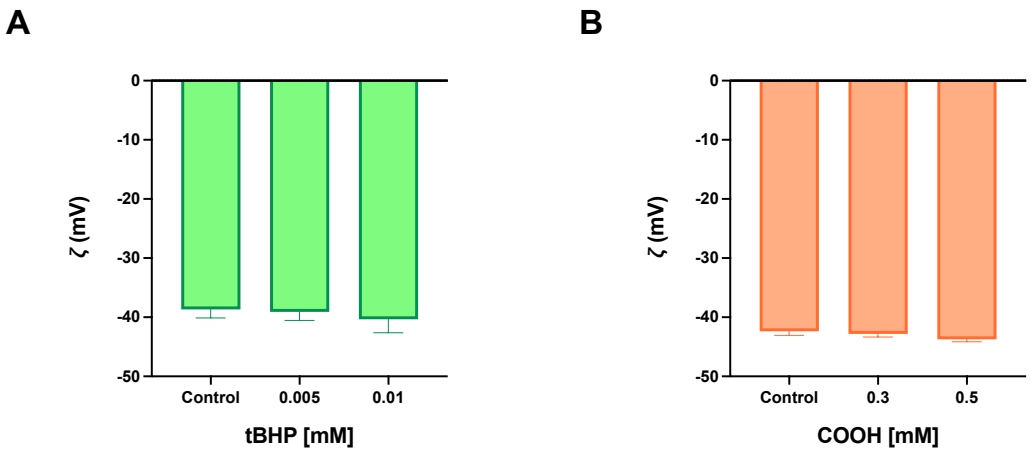

Figure 4.1: Optimization of drug treatments below I_{C50} values did not reveal changes in ζ-potential response in (A.) tert-Butyl (tBHP) and (B.) COOH concentrations compared to control.

Table 4.2: Final Treatment Regimen for Tert-Butyl Hydroperoxide (prepared in 1 mL total volume)

Treatment Group	HBSS 1x (w/o PR)	NaN_3 [100 mM]	Washed RBCs (10% HCT)	tBHP Stock	
				CONCENTRATION	VOLUME
Control	860 µL	40 µL	100 uL	-------	-------
1mM	760 µL			10 mM	100 µL
5 mM				50 mM	100 µL
10 mM				100 mM [Bulk stock]	100 µL

Table 4. 3: Final Treatment Regimen for Cumene Hydroperoxide (prepared in 1 mL total volume)

Treatment Group	HBSS 1x (w/o PR)	NaN_3 [100 mM]	Washed RBCs (10% HCT)	COOH Stock	
				CONCENTRATION	VOLUME
Control	860 µL	40 µL	100 uL	-------	-------
0.5 mM	760 µL			5mM	100 µL
1 mM				10 mM	100 µL
3 mM				30 mM	100 µL

Measurement of Surface ζ-potential: Measurement of surface ζ-potential was conducted using a Zetasizer Pro Red Label (Malvern Analytical, UK) system as previously described in *Chapter 3*. For each treatment sample, ζ-potential measurements were collected in triplicate for three biological replicates (i.e., n=9 technical replicates) per treatment group for H_2O_2, tBHP, and COOH. ζ-potential measurements were taken immediately following removal of the treatment and resuspension in the low conductive, iso-osmotic media described in *Chapter 3.*

Measurement of DEP-based Electrical Properties: As mentioned in Chapter 2, Dielectrophoresis (DEP) is another electrokinetic technique that has been extensively used to characterize RBCs. Taken together with ζ-potential, these properties help describe the entire cell "electrome"[16,17]. Measurement of dielectrophoresis (DEP)-based electrical properties was conducted using a commercial three-dimensional DEP (3DEP) system (**Figure 4.2A**). For each control and treatment group ~80 μL of RBC sample were pipetted into a 20-well DEP chip. All wells were energized simultaneously for 10 s with each well producing a different frequency response ranging from 10kHz-20MHz (**Figure 4.2 B-C**). The frequency responses from each well produced a corresponding DEP force, which was plotted to obtain a DEP "spectrum" curve (Force vs. frequency) for each RBC sample (**Figure 4.2D**). Measurements of effective membrane conductance (G_{EFF}), effective membrane capacitance (C_{EFF}), and cytoplasmic conductivity (σ_{CYT}) were extracted from the DEP data by first inputting the average weighted cell radius, *r* (obtained by microscopy, described below) and media conductivity into the 3DEP software and then fitting a single-shell model to this data[18]. At least five technical replicates for each control and treatment sample with an R^2 of at least 0.9 for each dataset were obtained.

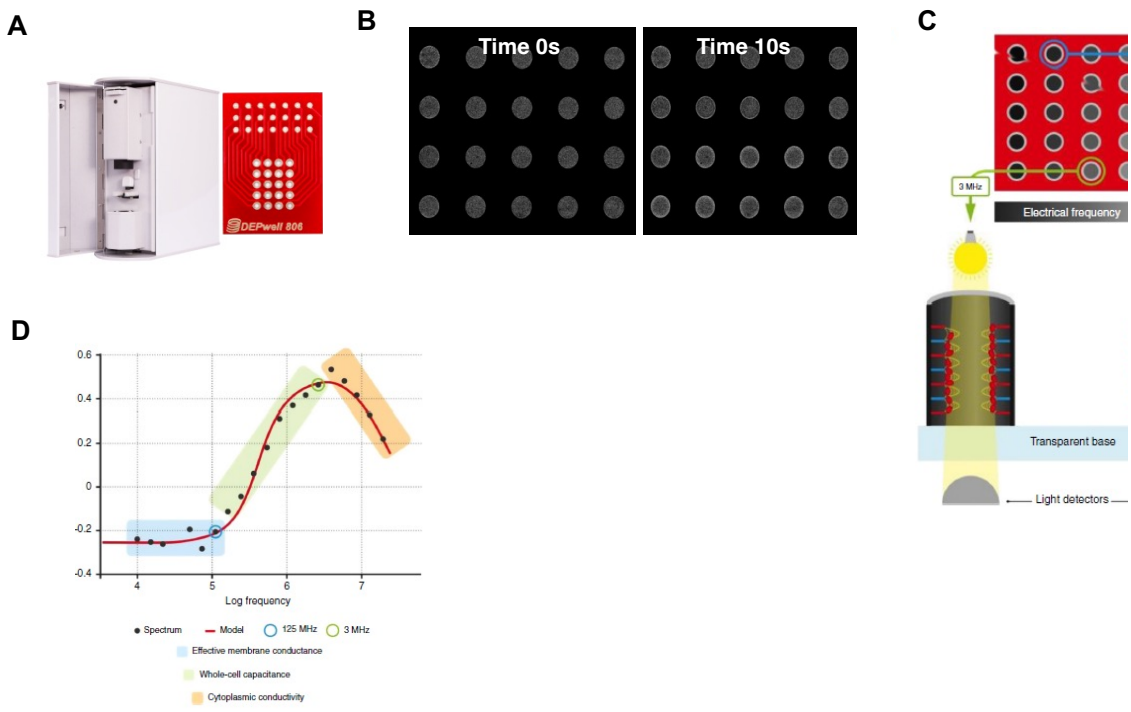

Figure 4.2: (A.) Schematic showing 3DEP system and 20-well chip used to collect DEP-based electrical properties of RBCs. (B-C.) Experimental workflow for obtaining DEP force data based on applied frequencies. (D). Exemplar DEP spectrum curve from which effective membrane capacitance, effective membrane conductance, and cytoplasmic conductivity properties are obtained.

Measurement of Cell Radius and RBC Count: To determine the cell radius, the image scale was set using ImageJ software (National Institute of Health) where the side length of a single box within the 4 x 4 grid measured 50μm (**Figure 4.3: A**). Based on this scale, the diameters of up to 10 cells for each sub-population were measured (each measurement was divided in half to obtain the radius). To get an average weighted radius measurement, the population % of each sub-population was multiplied by the average of the 10 cells for each

sub-population. The weighted radius for each sub-population was added together to get the total weighted radius for each control and treatment group.

RBC concentration was determined from hemocytometer images at x20 magnification using brightfield microscopy (ECHO Technologies, San Diego, CA), **Figure 4.3A**. For each hemocytometer image, for each control and treatment sample group cells on 0.2 mm x 0.2 mm grids were tagged green for "healthy" (exhibiting a normal concave RBC shape) or tagged red for echinocytes (e.g., cells with spikes formed on membrane surface), **Figure 4.3: B**. The RBC count was determined as the total number of cells within a 4 x 4 grid. The population % for each sample was determined as the ratio of each sub-population to the total cell concentration. ImageJ was also used to perform all cell counting measurements.

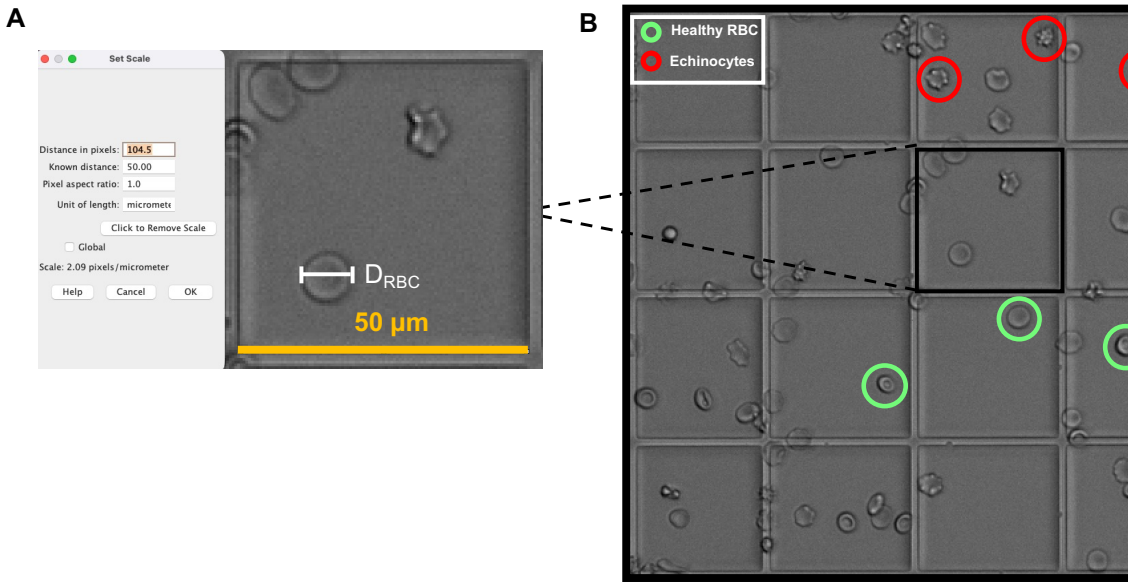

Figure 4.3: Experimental workflow used to (A.) measure RBC radius and (B.) distinguish cell sub-populations using ImageJ software.

Flow Cytometry Preparation and Analysis: To measure ROS presence in control and treatment samples using flow cytometry analysis, RBCs were tagged with a 2',7'-dichlorofluorescin diacetate (DCFDA) ROS-sensitive fluorescent probe (Abcam, Cambridge, UK) at a final concentration of 5 μM in total volume of 200 uL at final cell concentration of 2 x 10^6 cells/mL. DCFDA-tagged samples were prepared in light-sensitive Eppendorf tubes and incubated for 30 minutes at 37 °C. Following incubation ~30,000 RBCs were analyzed using the BD Fortessa X20 flow cytometer system (BD Biosciences, San Jose, CA). As noted in DCFDA manufacture's protocols, excess DCFDA stain does not impact flow cytometry signal, therefore, the samples were not washed to avoid additional cell loss. The flow cytometry data was gated Forward Scatter Area (FSC-A) versus Forward Scatter Height (FSC-H) to isolate RBC populations and eliminate signal artifact. Following analysis, flow cytometry data was plotted as histogram with individual treatment groups overlaid, with the y-axis displaying total cell count and the x-axis displaying fluorescent intensity.

Additionally, to measure eryptosis in control and treatment samples using flow cytometry analysis, RBCs were tagged with Annexin-V, a fluorophore used to detect early eryptosis by binding to phosphatidylserine (PS), a protein that translocates to the outer leaflet of RBCs during cell death. Annexin-stained RBC control and treatment samples were prepared in light-sensitive Eppendorf tubes by adding 10 μL of Annexin-V FITC stain to Annexin Binding Buffer in total volume of 1 mL at a final cell concentration of 2 x 10^6 cells/mL. Annexin-stained samples were incubated in the dark at room temperature for 10 minutes. Halfway through this incubation 10 μL of 7-AAD Following incubation,

RBCs were analyzed using the BD Fortessa X20 flow cytometer system using the same methods for DCFDA stain, described above.

SEM Sample Preparation: To prepare control and treatment samples for imaging analysis by scanning electron microscopy (SEM), RBCs must be fixed in glutaraldehyde on glass coverslips. Briefly, osmolality-controlled buffer for each sample was prepared in light-sensitive Eppendorf tubes by combining 300 μL of Phosphate Buffered Saine (PBS) with 200 μL of distilled water (dH_2O). RBCs from each control and treatment group were added to osmolality-controlled buffer at a final cell concentration of 2 x 10^6 cells/mL for each sample. A 2% glutaraldehyde fixing solution was prepared by diluting 20 μL of 50% glutaraldehyde stock in 240 μL dH_2O and 240 μL PBS. Next, 500 μL of the 2% glutaraldehyde fixing solution was added to each sample tube, pipetting up-and-down slowly to mix each tube. The glutaraldehyde-fixed samples were incubated in the dark at room temperature for 30 minutes. Following incubation, glutaraldehyde-fixed samples were washed twice with dH_2O by centrifugating at 900 xg for 5 minutes with reduced centrifuge acceleration and braking (Acc: 4/9, Dec: 2/9). For the final SEM sample preparation step 100μL of each washed, glutaraldehyde-fixed sample was pipetted onto 12 mm round glass coverslips and left drying overnight on a slide warmer set at 60 °C.

Before performing SEM imaging, the prepared RBC samples were attached to 15 mm diameter metal stubs via black double-sided round stickers. Samples were gold-coated with 5-10 nm of cold powder using a LUXOR Goldcoater system (Lambda Photometrics Ltd, United Kingdom). After gold coating, samples were loaded onto the tray of the

Phenom XL G3 Desktop SEM system (Thermo Fisher Scientific, Waltham, MA) and subsequently imaged.

Measurement of Free Sialic Acid Concentration: The free sialic acid (SA_{free}) concentration of RBCs was determined using a commercial assay kit. Briefly, 40 μL of supernatant was removed from RBC samples and mixed with 10 μL of 10% trichloroacetic acid (TCA), a precipitant used to treat samples and separate SA residues from supernatant protein to enhance colorimetric signal. Next, RBC samples were vortexed and centrifuged at 14,000 revolutions per minute (RPM) for 10 minutes. Following centrifugation 25 μL of supernatant was added to a clean light-sensitive Eppendorf tube and labeled "FSA". FSA tubes were prepared in triplicate for each treatment group. Next, an **oxidation step** was performed to convert non-colored SA_{free} into formylpyruvic acid, which reacts with thiobarbituric acid (TBA) to form pink-colored product that can be measured via spectrophotometer, after adding dye. Oxidation was carried out by mixing 15 μL of Hydrolysis Reagent with 50 μL of dH_2O, and 65 μL of Oxidation Reagent. Next, 125 μL of this working reagent was added to each tube and let stand at room temperature for 1 hour.

Following the oxidation step, the **color reaction step** was performed by adding 50 μL Dye Reagent to each tube, mixing, and heating at 100 °C for 10 minutes. Lastly, 100 μL of dimethyl sulfoxide (DMSO) was added to each tube, samples were mixed and centrifuged at 14,000 RPM for 5 minutes. Measurement of sample color intensity, used to quantify SA_{free}, was performed by pipetting 250 μL of sample into separate wells of a clear

96-well microplate. The optical density (OD) was measured at 549 nm. In parallel with RBC treatment samples, a stock SA standard was prepared at 1000 μM by mixing 50 μL of 10 mM "Standard" included in the assay kit with dH_2O at a final volume of 250μL in a light-sensitive Eppendorf tube. From this stock tube, calibration standards were prepared in triplicate based on concentrations shown in **Table 4.4**, adding 5 μL of 10% TCA to each tube. To obtain the OD data used to produce the experimental calibration curve depicted in **Figure 4.4A**, the same oxidation, color reaction, and color intensity measurement steps were performed. Quantification of SA_{free} concentration of RBC samples was determined by the Warren Method[19] (Equation 4.4):

$$SA_{free}\ [\mu M] = \frac{OD_{sample} - OD_{blank}}{Slope\ [\mu M^{-1}]}\ x\ n \tag{4.4}$$

Where OD_{sample} and OD_{blank} are the optical density readings of the RBC sample and blank dH_2O sample (No. 4 in **Table 4.4**) respectively, and *n* is the sample dilution factor (i.e., *n*=1 for FSA assays).

Table 4.4: Standard Concentrations for Sialic Acid Calibration Curve

No.	Premix + dH_2O	Total Volume	Sialic Acid Concentration
1	100 μL + 0 μL	100 μL	1000 μM
2	60 μL + 40 μL		600 μM
3	30 μL + 70 μL		300 μM
4 (Blank)	0 μL + 100 μL		0 μM

The slope was determined from the experimental calibration curve (**Figure 4.4A**), created by subtracting the OD for each standard from the OD of blank dH_2O sample and then plotting the ΔOD against the standard SA concentrations. For validation purposes, the experimental calibration curve was compared to the representative calibration curve provide in the manufacturer's protocol (**Figure 4.4B)**.

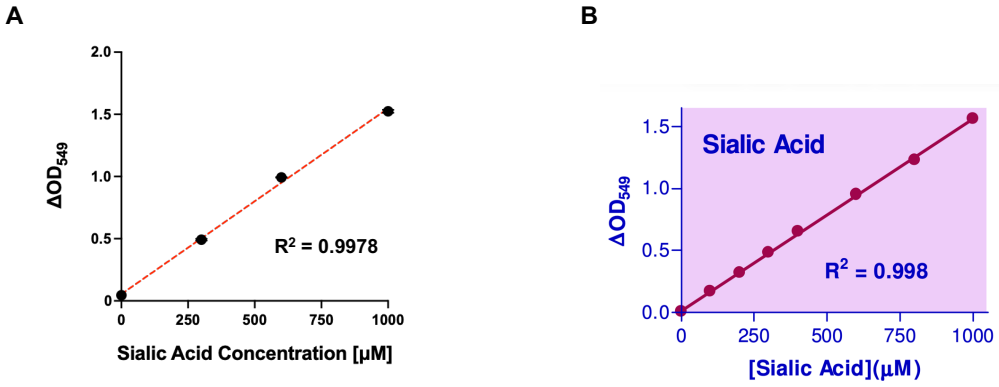

Figure 4.4: (A.) Calibration plot from experimental sialic acid (SA) measurements obtained from SA Standards #1-4. (B.) Calibration plot provided in manufacturer protocol.

Measurement of RBC Hemolysis: To measure hemolysis, following centrifugation at 700 xg for 5 minutes, the supernatants of each RBC sample were collected and resuspended in a clear 96-well plate at 10x dilution in HBSS at a total volume of 200 µL per well. The percent hemolysis was determined at an OD of 541 nm using a microplate reader (SynergyH1, BioTek Agilent Technologies, Durham, NC) and calculated by Equation (4.5):

$$\text{Hemoslysis} = 100 \text{ x } \left(\frac{A_s - A_b}{A_p - A_b}\right) \tag{4.5}$$

where A_S, A_p, and A_b are the absorbances of the supernatant, a 100% hemolysis reference sample (prepared by suspending 10% packed RBCs in 1 mL total volume of dH_2O), and the pure buffer solution, respectively[3].

Measurement of Intracellular Calcium: Packed RBCs were re-suspended in Phosphate Buffered Saline (PBS) in 1 mL total volume at a final concentration of ~2 x 10^6 cells/mL. Fluo-4 AM, a calcium-sensitive fluorescent dye[20], was added from stock (prepared from 100g powder in 88 μL DMSO) at a final concentration of 1 μM. Samples were incubated in the dark at 37 °C for 1 hour. Following incubation, fluorescently labeled RBCs were pipetted into a black 96-well microplate. Intracellular calcium (Ca^{2+}) was determined by measuring fluorescent intensity at emission/excitation wavelengths of 485 nm/526 nm using a microplate reader (SynergyH1, BioTek Agilent).

RESULTS AND DISCUSSION

With increasing H_2O_2 treatment concentration there was a significant decrease ($p<0.05$) in ζ-potential magnitude (**Figure 4.5A),** further corroborated by significant decreases ($p<0.05$) in cytoplasmic conductivity, σ_{CYT} (**Figure 4.5B**) and significant increases ($p<0.05$) in effective membrane conductance, G_{EFF} (**Figure 4.5C**). Mechanistically, the observed changes in σ_{CYT} and G_{EFF} are indicative of ion leakage (membrane conductance increase with a decrease in bulk cytoplasmic conductivity). Further, these shifts in DEP parameters directly correlate to the decreases in ζ-potential magnitude observed beginning at 1 mM treatment, due to activation of the Gardos channel causing potassium (K^+) leakage out of the cell. This efflux of K^+ increases the bulk concentration of cations in the suspending media and shielding the RBC negative surface charge.

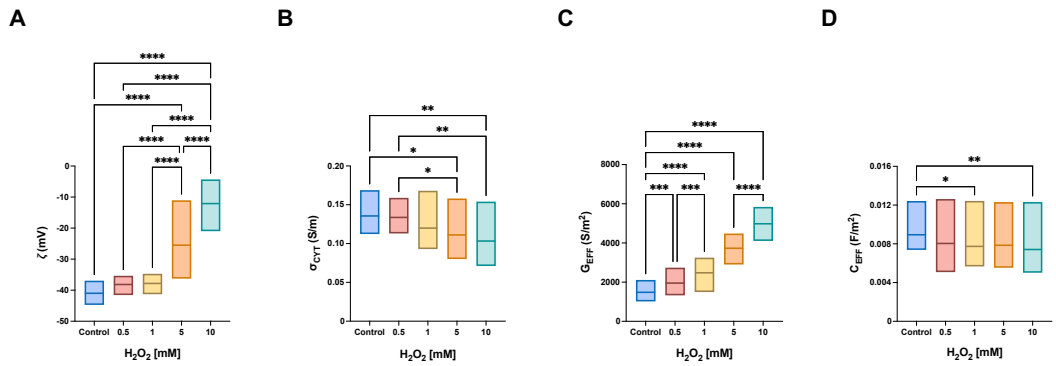

Figure 4.5: Comparing RBC σ_{CYT} under OS conditions revealed significant difference ($p<0.05$) between H_2O_2 treatment groups. (B). Comparing RBC C_{EFF} under OS conditions revealed significant difference ($p<0.05$) between H_2O_2 treatment groups. (C). Comparing RBC G_{EFF} under OS conditions revealed significant difference ($p<0.05$) between H_2O_2 treatment groups. (D). Comparing RBC ζ-potential under OS conditions revealed significant difference ($p<0.05$) between H_2O_2 treatment groups. Data presented in represents the mean ± (s.d.) of (N=3) donors.

Interestingly, a "stepwise" progression in RBC viability due to OS can be observed by two distinct shifts in ζ-potential magnitude. The first shift, indicating the onset of OS, occurs between the upper inter-quartile range of the 1 mM treatment group and the lower inter-quartile of the 5 mM treatment group. The second shift, occurring between the upper inter-quartile rage of 5 mM and the 10 mM H_2O_2 treatment groups indicates a further progression in OS response—from OS to eryptosis. The observed shifts in the ζ-potential response are indicative of altered cell morphology which can be explained by the observed decrease in effective membrane capacitance, C_{EFF}, **Figure 4.5D**. This is consistent with other work from our group investigating eryptosis (unpublished).

Further, from scanning electron microscopy (SEM) images there is a progressive increase in echinocytes at 0, 1 and 10 mM H_2O_2 treatment concentrations, (**Figure 4.6: A-C**). Although changes in weighted RBC radius, indicative of cell shrinkage, were not

observed (likely due to the heterogeneity of the RBC bulk populations) the morphological progression from biconcave to echinocytes seen on SEM was confirmed quantitatively by a decrease in total RBC count (**Figure 4.6: E**) and an increase in population % of echinocytes from control to 10 mM treatment (**Figure 4.6: F**).

Flow cytometry plots of DCFDA ROS (**Figure 4.7*:* A**) and Annexin-V eryptosis (**Figure 4.7*:* B**) provide a visual confirmation of the "shifts" in biophysical response of RBCs to H_2O_2-induced OS. Specifically, there was progressive increase in ROS signal intensity (x-axis) from 0 mM to 1 mM followed by a rapid decrease in ROS signal peak from 5 mM to 10 mM. This corresponded to a large peak in the Annexin-V signal at 10 mM, indicating cell death. This demonstrates the transition from ROS to cell death between 5mM and 10mM. The shifts in ROS and eryptosis were also confirmed by fluorescence analysis using a microplate reader (**Figure 4.7C-D**). Lastly, changes in RBC viability in H_2O_2-induced OS were quantitatively confirmed by significant increases ($p<0.05$) in both hemolysis (**Figure 4.7E**) and eryptosis (**Figure 4.7F**) measurements.

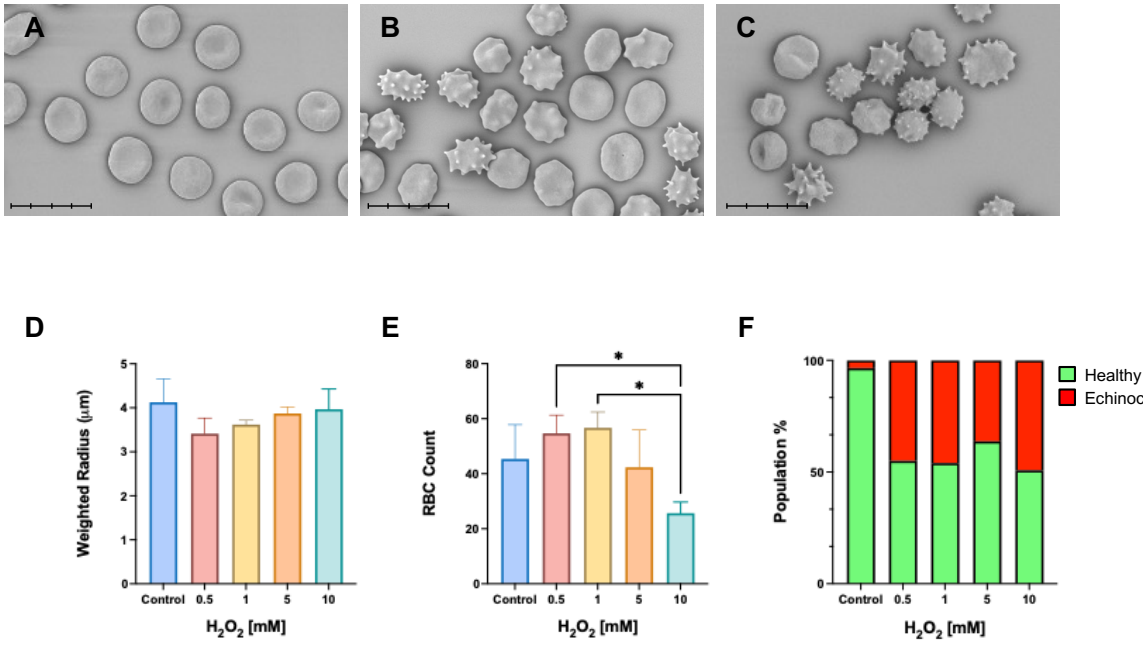

Figure 4.6: Scanning electron microscopy (SEM) images of RBC morphology for (A.). Control and (B) 1 mM and (C.) 10 mM treatment with hydrogen peroxide (H_2O_2) for 2 hours at 37 °C (10 µm scale bar). (D.) No changes in (D.) weighted cell radius was observed with increasing H_2O_2 treatment concentration. (E.) Changes in total RBC count were observed with increasing H2O2 treatment concentration. (F.) Changes in the population % of echinocytes were observed with increasing H_2O_2 treatment concentration. Data presented in Panels D-F represents the mean ± (s.d.) of (N=3) donors.

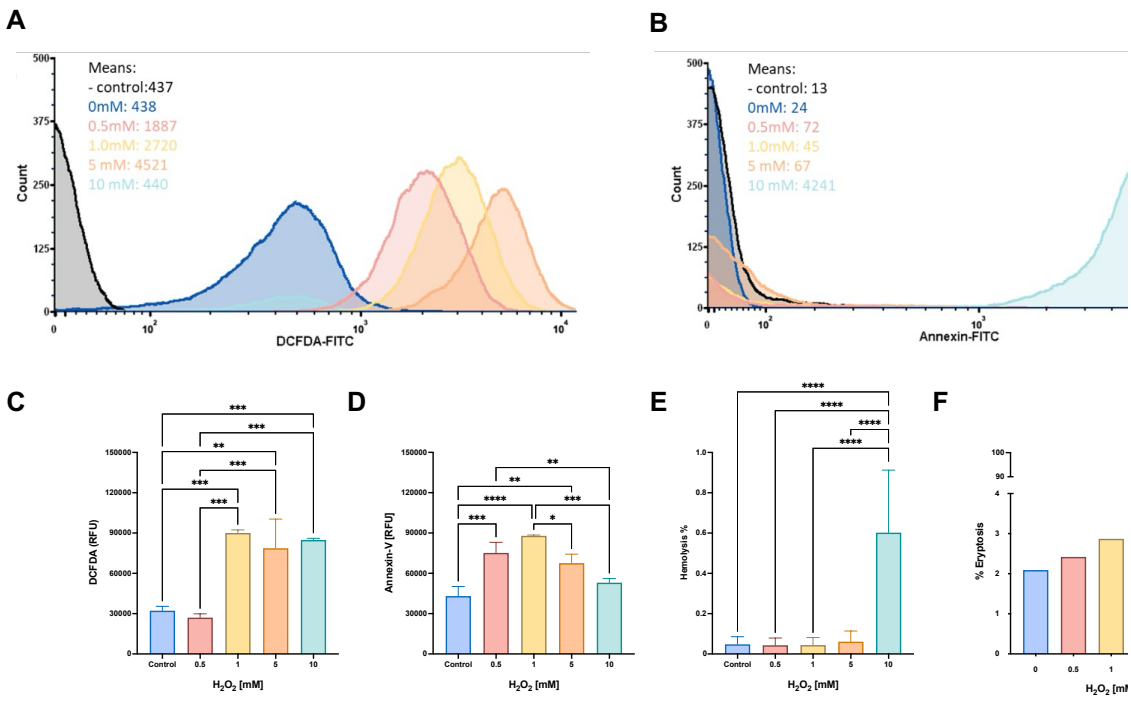

Figure 4.7: (A.) DCFDA-FITIC and (B.) Annexin-FTIC stain flow cytometry histograms of RBCs treated with NaN_3 (dark blue) and 0.5 mM (pink), 1 mM (yellow), 5 mM (orange), 10 mM (light blue) H_2O_2 and a negative control using (C.) DCFDA and (D.) Annexin-V fluorescence measurements confirming OS shifts. (E.). Hemolysis % and (F.) Eryptosis % of RBCs exposed to H_2O_2-induced OS. Data presented in Panels C-D represents the mean ± (s.d.) for a single (N=1) representative donor. Data presented in Panels E-F represents the mean ± (s.d.) of (N=3) donors.

Snyder *et al*[21] also reported an increase in echinocyte formation at H_2O_2 concentrations up to five-times lower than those presented in the current work. Interestingly, the authors attributed morphological changes to the formation of spectrin-globin complexes, which elsewhere has been shown to reduce the number of available sialic acid binding sites, reducing the maximum surface charge density on the RBC membrane. Collectively these

studies may further explain the link between shifts in ζ-potential response and morphological changes in OS processes.

Probing Mechanisms of ζ-potential Response in Oxidative Stress: While no significant changes ($p>0.05$) were observed in ζ-potential magnitude with increasing tBHP concentration (**Figure 4.8A**), there was a shift in ζ-potential occurring between the upper inter-quartile range of the 5 mM treatment group and the upper inter-quartile of the 10 mM treatment group. Like the shift and spread of data observed in the H_2O_2 treatment, but with no significant change ($p<0.05$) , the shift in tBHP-based ζ-potential likely suggests changes in the RBC bulk population in which sub-populations are beginning to influence the bulk ζ-potential response , as was observed with increasing H_2O_2 treatment concentrations.

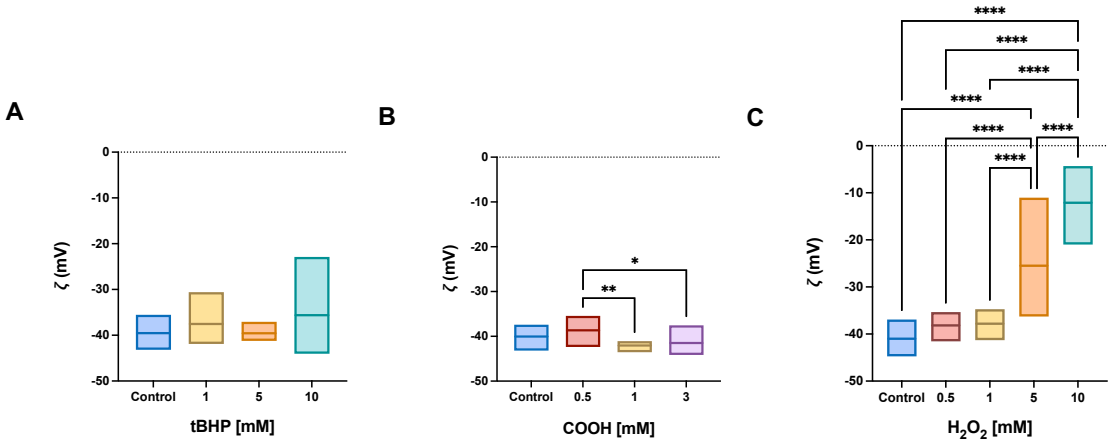

Figure 4.8: Comparison of changes in ζ-potential response with treatment concentration between (A.) tert-Butyl hydroperoxide (tBHP), (B.) cumene hydroperoxide (COOH), and (C.) hydrogen peroxide (H_2O_2) revealed significant differences ($p<0.05$) with concentration, and across OS agents. Data represents mean ± s.d. of (N=3) donors.

Interestingly the tBHP shifts in ζ-potential coincide with spikes in free sialic acid (SA_{free}) at both 1 mM and 10 mM (**Figure 4.9A**). Typically, increasing SA_{free} is corroborated by a decrease in ζ-potential magnitude and due to reduced surface charge density caused via enzymatic cleavage of negatively charged SA from the RBC membrane surface. In tBHP-induced OS, lipid peroxidation causes cytoplasmic stores of sialic acid to leak out of the cell, spiking SA_{free} in suspending medium, independent of membrane SA (surface charge) removal. This can help explain why we do not see shifts in ζ-potential for the tBHP treatment group though OS is present.

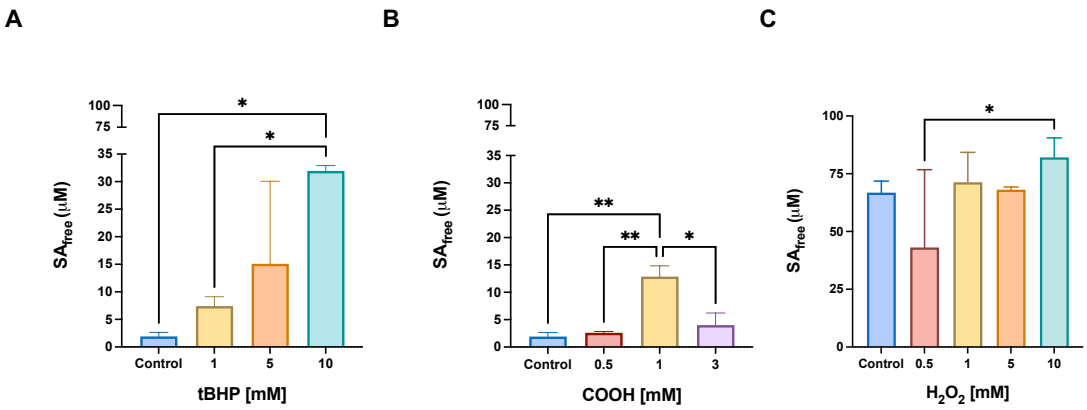

Figure 4.9: Comparison of changes in free sialic acid (SA_{free}) with treatment concentration between (A.) tert-Butyl hydroperoxide (tBHP), (B.) cumene hydroperoxide (COOH), and (C.) hydrogen peroxide (H_2O_2) revealed significant differences ($p<0.05$) with concentration, and across OS agents. Data represents mean ± s.d. of n=3 technical replicates for single (N=1), representative donor.

Given the hemolysis measures at COOH concentrations of 1 mM and 3 mM, I expected to see a spike in SA_{free} in both treatment groups. While I observed a spike in 1 mM, I saw a reduction in SA_{free} at 3mM, which is likely due to experimental error.

Additionally, no differences were observed in weighted radius, RBC counts, or differences between echinocyte sub-populations (**Figure 4.10**).

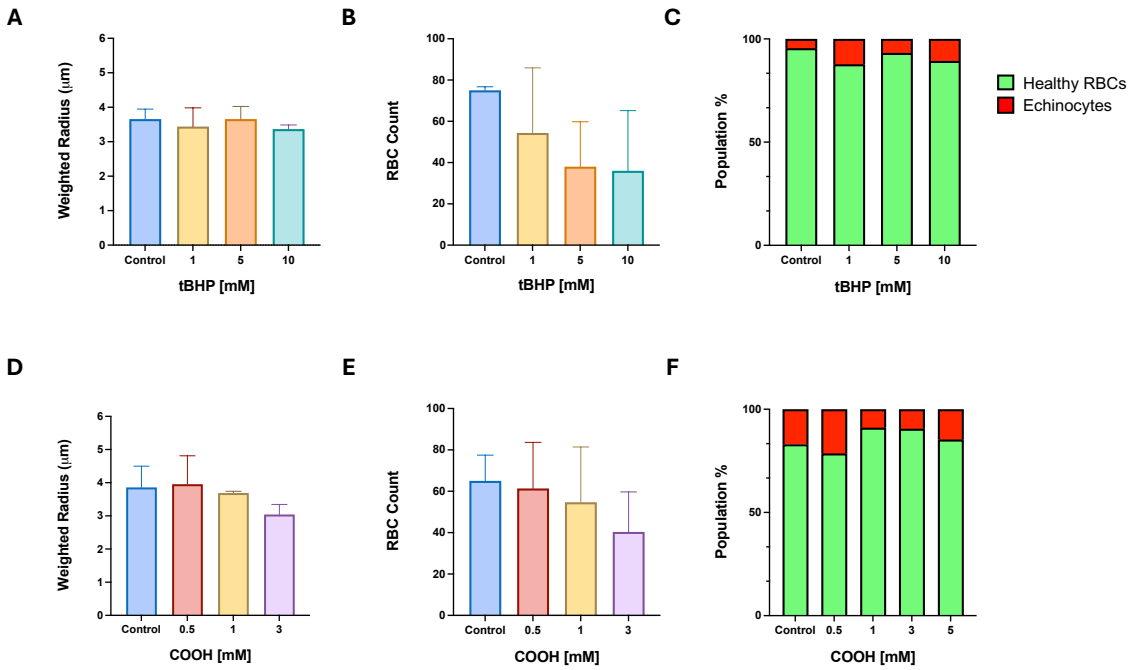

Figure 4.10: Tert-Butyl hydroperoxide (tBHP) induced changes in (A.) weighted radius, (B.) RBC count, and (C.) sub-population % with increasing treatment concentration. Cumene hydroperoxide (COOH) induced changes in (D.) weighted radius, (E.) RBC count, and (F.) sub-population % with increasing treatment concentration. Data represents mean ± s.d. of N=3 donors.

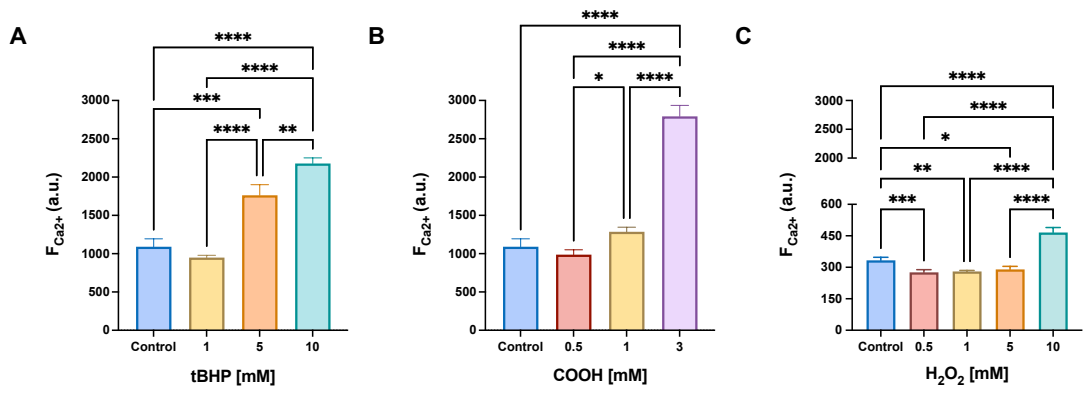

Figure 4.11: Comparison of changes in intracellular calcium (Ca^{2+}) with treatment concentration between (A.) tert-Butyl hydroperoxide (tBHP), (B.) cumene hydroperoxide (COOH), and (C.) hydrogen peroxide (H_2O_2) revealed significant differences ($p<0.05$) with concentration, and across OS agents. Data represents mean ± s.d. of n=3 technical replicates for single (N=1) representative donor.

Mechanistically, tBHP also inhibits the clearance of excess cytoplasmic calcium (Ca^{2+}) by "locking" the enzyme Ca^{2+}-pump ATPase into an inactivated state. In the present study this mechanism was quantitatively observed via an increase intracellular Ca^{2+} with tBHP treatment concentration (**Figure 4.11A**). Similarly, in COOH-treated RBCs, a concentration-dependent increase in intracellular Ca^{2+} was observed (**Figure 4.11B**). Further, a higher Ca^{2+} fluorescent signal in COOH treatments (**Figure 4.11B**) compared to both tBHP and H_2O_2 can be attributed to increased membrane solubility of COOH, resulting in more extensive lipid peroxidation of the RBC membrane[22]. Several authors have shown that RBCs treated with H_2O_2 exhibit a slow, pre-hemolytic increase in intracellular Ca^{2+}[23] compared to the rapid spikes in Ca^{2+} observed in tBHP and COOH[24,25]. This is corroborated by the lower magnitude in fluorescent signal observed in **Figure 4.11C**. The mechanism of Ca^{2+}-pump ATPase inhibition described above may, in part,

explain the significant increase (more negative) in mean ζ-potential response with COOH treatment observed in **Figure 4.8B**. Specifically, an influx of Ca^{2+} has been shown to make the extra-cellular medium more electro-negative which increases the thickness of electric double layer, increasing both ζ-potential magnitude and the repulsive strength between RBCs.

Lastly, a significant dose-dependent increase ($p<0.05$) in hemolysis was observed in both tBHP (**Figure 4.12A**) and COOH (**Figure 4.12B**) OS agents. Interestingly, both tBHP and COOH exhibit a greater magnitude of hemolysis than the H_2O_2 samples. This response is likely due to rapid cell destruction caused by lipid peroxidation, considering that both tBHP and COOH are membrane-targeting OS agents.

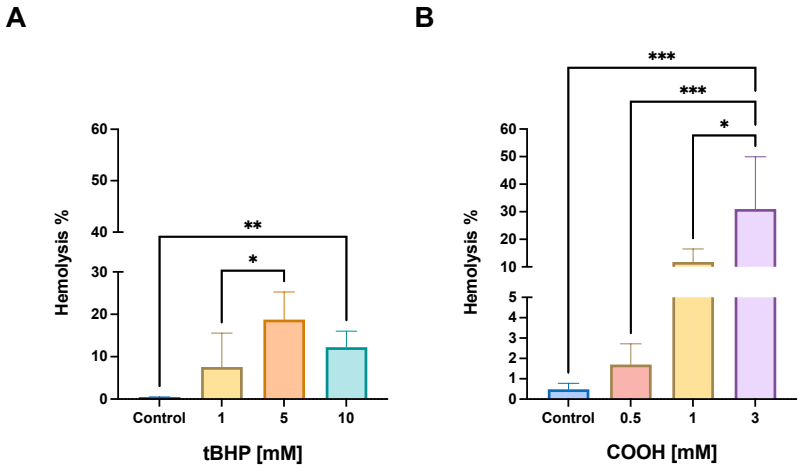

Figure 4.12: Comparison of changes in hemolysis % of (A.) Tert-Butyl hydroperoxide and (B.) Cumene hydroperoxide (COOH) at increasing treatment concentrations. Data represents mean ± s.d. of N=2 donors.

STATISTICAL ANALYSIS

All statistical analysis was carried out using Prism 11 (GraphPad Software, La Jolla, CA).

To address Objective 1 of Chapter 4—*determine sensitivity of surface ζ-potential for monitoring RBCs in H_2O_2 induced-OS*—I analyzed ζ-potential response of human RBCs across four H_2O_2 concentrations: Control, 0.5, 1, 5, 10 mM. Using one-way analysis of variance (ANOVA) I compared the mean ζ-potential technical replicates for N=3 separate blood draws from the same donor on different days across treatment groups to determine "concentration effect". Follow up post-hoc analysis was performed using Tukey's Multiple Comparisons Test to identify specific differences between drug concentration groups. Across concentration groups, all p-values <0.05 were statistically significant. To control for blood draw (i.e., biological replicate) variability and repeated measures we fitted a mixed-effects linear model.

To address Objective 2 of Chapter 4—*probe the biophysical and OS agent-specific mechanisms that modulate the surface ζ-potential response of human RBCs under OS*—I analyzed ζ-potential response of human RBCs to increasing drug treatment for tert-Butyl hydroperoxide (tBHP) and cumene hydroperoxide (COOH) OS agents independently. For each OS agent, ζ-potential response of human RBCs across control and three treatment concentrations (tBHP: 1, 5, 10 mM, and COOH: 0.5, 1, 3 mM). Using One-Way ANOVA, I compared the mean ζ-potential of technical replicates for N=3 separate blood draws from the same donor on different days across treatment groups to determine "concentration effect" for each OS agent independently. Follow up post-hoc analysis was performed using

Tukey's Multiple Comparisons Test to identify specific differences between drug concentration groups. For each OS agent, across concentration groups, all p-values <0.05 were statistically significant. To control for blood draw (i.e., biological replicate) variability and repeated measures we fitted a mixed-effects linear model.

STUDY LIMITATIONS, IMPLICATIONS, AND FUTURE WORK

The primary aim of this study was to **determine the ζ-potential response of RBCs OS, considering dose-dependent changes and mechanistic differences between OS agents**. For Objective 1**,** I showed that ζ-potential can detect subtle shifts in the gradual progression of OS, including the biophysical transition of RBCs from OS to complete cell death—confirmed by flow cytometry. Limitations of the H_2O_2 study include inconsistencies in cell concentration during imaging. While significant dose-dependent changes in ζ-potential were observed with H_2O_2, these changes are likely influenced by the high degree of multi-population heterogeneity present in the bulk cell population. Therefore, an alternative approach would be to first isolate the oxidized cells from the bulk population and re-suspend them in iso-osmotic buffer prior to conducting ζ-potential measurements. Doing this would ensure a fully homogenous treatment sample, which would further increase ζ-potential sensitivity under OS conditions.

Objective 2 focused on probing mechanistic differences between OS agents, significant changes ($p<0.05$) in both intracellular Ca^{2+} and SA_{free} were observed, however,

no significant changes ($p<0.05$) were observed in ζ-potential magnitude of tBHP-treated RBCs. Additionally, only minimal changes were observed in COOH treated RBCs, compared with ζ-potential from H_2O_2 results. Because H_2O_2 is a cytoplasm-targeting OS agent and both tBHP and COOH are membrane-targeting OS agents, differences in ζ-potential response may be due to widespread membrane damage with H_2O_2 (via spectrin-globin crosslinking) compared to only localized lipid peroxidation in tBHP and COOH. Another possible reason for the observed differences in ζ-potential between OS agents, and a limitation of tBHP and COOH studies, was the lack of GPX inhibition.

Recall from the *Introduction* that RBCs possess two antioxidant defense mechanisms, catalase (CAT), and glutathione peroxidase (GPX). While both antioxidants help to combat OS processes in RBCs, CAT is the primary antioxidant defense against H_2O_2[7,26]. In the present study sodium azide (NaN_3), a potent CAT inhibitor, was incubated with H_2O_2-treated samples to block repair and enhance the OS response. However, in tBHP and COOH OS processes, catalase acts as a secondary antioxidant defense with GPX serving as the primary antioxidant defense mechanism[27,28]. This likely explains the minimal ζ-potential response observed tBHP and COOH treatments compared to H_2O_2. However, to compare OS mechanisms of tBHP and COOH with prior H_2O_2 findings, it was necessary to add NaN_3 to tBHP and COOH treatments.

To address this study limitation, in future studies the addition of a GPX inhibitor in the tBHP and COOH treatment regimens should be included. For example, following incubation of isolated RBCs with 1.5 mM mercaptosuccinate, a potent GPX inhibitor,

along with tBHP concentrations, Rohn *et al* demonstrated a decrease in Ca^{2+}-ATPase activity up to 50%[24]. Considering that the tBHP study revealed a dose-dependent increase in intracellular Ca^{2+}, and that increases in intercellular Ca^{2+} can shift the ζ-potential response by expanding the electric double layer, the addition of a GPX inhibitor would allow for greater amplification and detection of changes in ζ-potential response in RBCs exposed to both tBHP and COOH.

Collectively, my findings presented here in *Chapter 4* demonstrate that ζ-potential can detect subtle shifts in H_2O_2-induced OS progression in human RBCs. This ζ-potential response was further corroborated by shifts in both DEP properties and secondary biophysical parameters (e.g., SA_{free} and intracellular Ca^{2+}). Previously *ex vivo* studies monitoring OS response in human RBCs relied on assessing morphological changes and were unable to distinguish subtle shifts in RBC function (e.g., ion channel inhibition) occurring with OS progression. The presents work helps to address this unmet need by demonstrating the applicability of ζ-potential as an alternative technique for RBC monitoring in OS, providing greater measurement sensitivity. This in turn offers the potential to inform monitoring of OS-related processes (e.g., cardiovascular disease and blood-artificial material surface interactions) where high measurement sensitivity is critical to deciphering the underlying biophysical mechanisms contributing to OS progression, especially in the midst of often compounding factors (e.g., flow-induced shear stress and blood storage duration, etc.).

REFERENCES

1. Moller, M. N. *et al.* Oxidants and antioxidants in the redox biochemistry of human red blood cells. *ACS Omega* **8**, 147–168 (2022).

2. Orrico, F. *et al.* Oxidative stress in healthy and pathological red blood cells. *Biomolecules* **13**, 1262 (2023).

3. McKenney, J. *et al.* Decreased in vivo survival of hydrogen peroxide-damaged baboon red blood cells. *Blood* **76**, 206–211 (1990).

4. Caprari, P. *et al.* Junctional sites of erythrocyte skeletal proteins are specific targets of tert-butylhydroperoxide oxidative damage. *Chem. Biol. Interact.* **94**, 243–258 (1995).

5. Jewell, S. A., Petrov, P. G. & Winlove, C. P. The effect of oxidative stress on the membrane dipole potential of human red blood cells. *Biochim. Biophys. Acta BBA-Biomembr.* **1828**, 1250–1258 (2013).

6. Melo, D., Rocha, S. & Coimbra, S. Interplay between Erythrocyte. *Erythrocyte* 65 (2019).

7. Scott, M. D., Lubin, B. H., Zuo, L. & Kuypers, F. A. Erythrocyte defense against hydrogen peroxide: preeminent importance of catalase. *J. Lab. Clin. Med.* **118**, 7–16 (1991).

8. Agar, N. & Baker, M. Role of catalase in H2O2-induced oxidant stress in marsupial erythrocytes. *Comp. Haematol. Int.* **6**, 32–34 (1996).

9. Bessa, S. S., Ali, E. M. & Hamdy, S. M. The role of glutathione S-transferase M1 and T1 gene polymorphisms and oxidative stress-related parameters in Egyptian patients with essential hypertension. *Eur. J. Intern. Med.* **20**, 625–630 (2009).

10. Cohen, G. & Hochstein, P. Glutathione peroxidase: the primary agent for the elimination of hydrogen peroxide in erythrocytes. *Biochemistry* **2**, 1420–1428 (1963).

11. Aydogan, S., Yapislar, H., Artis, S. & Aydogan, B. Impaired erythrocytes deformability in H2O2-induced oxidative stress: protective effect of L-carnosine. *Clin. Hemorheol. Microcirc.* **39**, 93–98 (2008).

12. Mohanty, J. G., Nagababu, E. & Rifkind, J. M. Red blood cell oxidative stress impairs oxygen delivery and induces red blood cell aging. *Front. Physiol.* **5**, 84 (2014).

13. McNamee, A. P., Horobin, J. T., Tansley, G. D. & Simmonds, M. J. Oxidative stress increases erythrocyte sensitivity to shear-mediated damage. *Artif. Organs* **42**, 184–192 (2018).

14. Bayer, R. & Waßer, G. Effects of oxidative stress on erythrocyte deformability. in vol. 2678 333–341 (SPIE, 1996).

15. Yaram, S. D. R., Bostic, A., Smalley, A. & Srivastava, S. K. Simulated Microgravity Induces Rapid Dielectric Shifts in Erythrocytes of Pancreatic Cancer Patients. *ACS Nanosci. Au* (2026).

16. Hughes, M. P. The cellular zeta potential: cell electrophysiology beyond the membrane. *Integr. Biol.* **16**, zyae003 (2024).

17. Hughes, M. P. *et al.* V m-related extracellular potentials observed in red blood cells. *Sci. Rep.* **11**, 19446 (2021).

18. Henslee, E. A. Dielectrophoresis in cell characterization. *Electrophoresis* **41**, 1915–1930 (2020).

19. Jana, P. *et al.* Detection of sialic acid and imaging of cell-surface glycan using a fluorescence–SERS dual probe. *ACS Sens.* **8**, 1693–1699 (2023).

20. Kaestner, L., Tabellion, W., Weiss, E., Bernhardt, I. & Lipp, P. Calcium imaging of individual erythrocytes: problems and approaches. *Cell Calcium* **39**, 13–19 (2006).

21. Snyder, L. *et al.* Effect of hydrogen peroxide exposure on normal human erythrocyte deformability, morphology, surface characteristics, and spectrin-hemoglobin cross-linking. *J. Clin. Invest.* **76**, 1971–1977 (1985).

22. van den Berg, J. J., den Kamp, J. A. O., Lubin, B. H., Roelofsen, B. & Kuypers, F. A. Kinetics and site specificity of hydroperoxide-induced oxidative damage in red blood cells. *Free Radic. Biol. Med.* **12**, 487–498 (1992).

23. Chen, M., Sorette, M. P., Chiu, D. T.-Y. & Clark, M. R. Prehemolytic effects of hydrogen peroxide and t-butylhydroperoxide on selected red cell properties. *Biochim. Biophys. Acta BBA-Biomembr.* **1066**, 193–200 (1991).

24. Rohn, T. T., Hinds, T. R. & Vincenzi, F. F. Inhibition of the Ca pump of intact red blood cells by t-butyl hydroperoxide: importance of glutathione peroxidase. *Biochim. Biophys. Acta BBA-Biomembr.* **1153**, 67–76 (1993).

25. Tretter, L. & Adam-Vizi, V. Early events in free radical-mediated damage of isolated nerve terminals: effects of peroxides on membrane potential and intracellular Na+ and Ca2+ concentrations. *J. Neurochem.* **66**, 2057–2066 (1996).

26. Anwar, S. *et al.* Exploring therapeutic potential of catalase: Strategies in disease prevention and management. *Biomolecules* **14**, 697 (2024).

27. Sullivan, S. G. & Stern, A. Membrane protein changes induced by tert-butyl hydroperoxide in red blood cells. *Biochim. Biophys. Acta BBA-Biomembr.* **774**, 215–220 (1984).

28. Dremza, I., Lapshina, E., Kujawa, J. & Zavodnik, I. Oxygen-related processes in red blood cells exposed to tert-butyl hydroperoxide. *Redox Rep.* **11**, 185–192 (2006).

Chapter 5: Surface Zeta Potential as a Biomarker for Monitoring Human Red Blood Cells in Extracorporeal Membrane Oxygenation

INTRODUCTION

Extracorporeal membrane oxygenation (ECMO) is a type of cardiopulmonary bypass (CPB) system that provides temporary artificial heart and lung functionality to critically ill patients, also serving as a bridge to heart and lung transplantation[1]. ECMO systems consist of either a roller pump (used primarily for pediatric and neonatal patients) or centrifugal pump (used in both pediatric and adult patients) and an artificial lung (membrane oxygenator) which facilitates gas exchange and reoxygenation of the blood. These components are connected via heparin-coated tubing, forming a complete circuit. Unlike traditional CPB systems which are used on a short-term basis (up to 6-8 hours) during cardiac surgical procedures, ECMO systems frequently provide support for at least 12 hours or even days to weeks. Due to prolonged blood circulation, complications of bleeding and red blood cell (RBC) aggregation leading to thrombosis remain significant clinical challenges for ECMO patients[2,3]. In ECMO circuits, inflammatory and coagulation responses are exacerbated due to the increased interaction of cells with foreign surfaces and materials, resulting in blood clot formation. A comparison of primary differences between traditional CPB and ECMO systems is depicted in **Table 5.1**.

Table 5.1: Comparison of Cardiopulmonary Bypass versus ECMO Systems

Characteristics	Cardiopulmonary Bypass System	ECMO System
Priming Volume	Large	Small
Oxygenator Use	Short term (<10 hr.)	Short or Long term (>10 hr.)
Pump Type	Roller or Centrifugal (both adult and pediatric/neonate)	Centrifugal (adult) Roller (pediatric/neonate)
External Reservoir	Yes – present	No
Heparin Bolus Dose	300-400 U/kg	50-100 U/lg
Target Clotting Time	>480 seconds	160-200 seconds

In addition to inflammatory and coagulation responses, other mechanisms of cell damage occur in ECMO circulation. One *in vivo* study showed a 60% loss of RBCs in ECMO systems due to bleeding and pump-induced hemolysis[4]. Other *ex vivo* studies have investigated the effects of flow rate for detecting thrombus formation, drug sequestration and pharmacokinetics, as well as differing pump and membrane oxygenator device models to inform ECMO circuit configuration and clinical treatment planning[5–8]. Over the past decade, blood storage and RBC aging have gained considerable attention due to the reported >96% of patients who require blood transfusions during in-hospital ECMO support[9]. Prolonged blood storage causes storage lesions which deleteriously affect cellular function and RBC membrane integrity, including cleavage of sialic acid and decreased cell membrane elasticity and deformability[10,11].

To my knowledge, no *ex vivo* studies to date have focused exclusively on monitoring RBCs in ECMO circuits despite the critical role of RBCs for oxygen delivery. Clinical laboratory techniques for monitoring RBCs during *in vivo* clinical ECMO support, which include plasma free hemoglobin (PfHb), a measure of cell damage and hemolysis,

and red cell distribution width (RDW) for monitoring systemic inflammatory response, are limited to once-daily measurement to limit blood loss from frequent phlebotomy[12]. These measurements vary widely across clinical centers, yielding inconsistent results[13,14]. Anticoagulants, while often a first-line therapy for managing thrombosis in ECMO circuits, elevate the potential risk for cannula site bleeding and intracranial hemorrhage due to systemic anticoagulation effects[15]. **Thus, a significant clinical need exists to monitor RBCs in ECMO systems, providing greater temporal measurement resolution and sensitivity, to better predict blood clot formation, blood transfusion and blood volume management in ECMO patients.** Additionally, information on how prolonged storage may impact RBCs in ECMO will provide further insights to inform this management and address unmet clinical needs.

Impacts of Blood Circulation on Red Blood Cells: During normal blood circulation RBCs are continuously exposed to mechanical shear stresses as they transverse the vascular network to deliver oxygen to tissues and remove CO_2 waste products[16,17]. To maintain homeostasis, blood circulation must be fast enough to provide adequate tissue perfusion and oxygen delivery, while not becoming too turbulent to irreversibly alter the RBC's ability to deform through the microvasculature and impair oxygen exchange. Under "normal", physiologic flow, RBCs are exposed to a range of mechanical shear stresses, from 0.1-10 Pa [18–20]. However, in patients with heart valve prostheses or mechanical blood pumps (e.g., ventricular assist devices, VADs) the flow behavior can become turbulent generating high shear stresses (>100 Pa) and resulting in RBC lysis [21–24].

In ECMO systems, the peak mechanical shear stress can reach, and even exceeds, 400 Pa, particularly in roller pumps when both rollers simultaneously occlude the tubing (**Figure 5.1:**). Moreover, not only do extreme peak shear stresses increase the severity of RBC lysis, worsening hemodilution and bleeding in critically ill ECMO patients, they have been shown to increase platelet activation and neutrophil expression over timescales of just 0.5s. These effects, in addition to the already elevated inflammatory response to underlying viral infection seen in ECMO patients, have the potential to produce a highly pro-thrombotic environment. **Thus, understanding the role of RBC surface charge in this ECMO environment is of critical importance.**

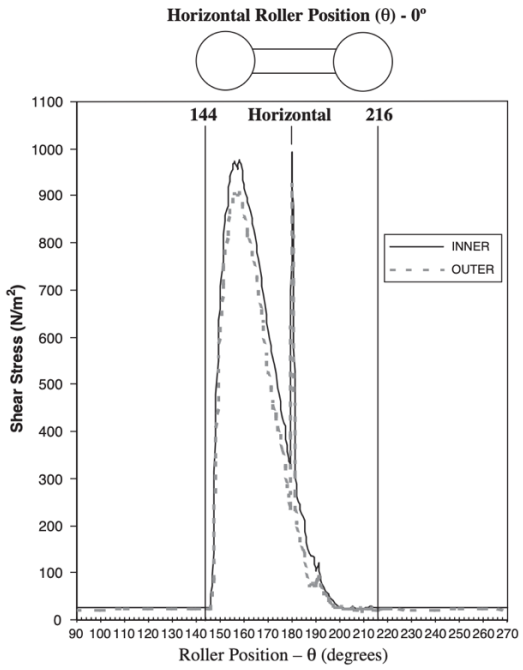

Figure 5.1: Schematic showing peak wall shear stress profile with respect to the position of leading and trailing rollers in an ECMO circuit, as described by Mulholland et al[25].

Red Blood Cell Aggregation: RBC aggregation is characterized by a reversible process whereby cells form stacks or branch networks, often resembling "pearl chains", due to

either low/stagnant flow conditions or physical alterations to the cell membrane's surface (e.g., removal of sialic acids) resulting in cell-to-cell adhesion[26,27]. In contrast to aggregation, coagulation or agglutination of blood is an irreversible process resulting from polymerization of proteins on the RBC surface. The propensity for RBCs to aggregate is closely governed by the balance between pro-aggregating factors (e.g., concentration of prothrombotic factors and fibrinogen in the blood) and dis-aggregating factors (e.g., shear stress magnitude and strength of cell-to-cell repulsive forces). As described in *Chapter 3*, the largest determinant of RBC repulsive strength is the concentration of electro-negative glycoproteins (sialic acid) present on the cell surface.

While cell aging and RBC-related diseases (e.g., malarial anemia, sickle cell disease, etc.) have been shown to decrease the cells' overall electronegative charge, resulting in cell aggregation[28,29], so too has ECMO circulation. Specifically, Lansink-Hartgring *et al*, reported an increase in RBC aggregation due the extended blood circulation time required during ECMO support compared to shorter CPB runs[30].

In the present study, I investigated the applicability of ζ-potential as an alternative tool for RBC monitoring in ECMO circuits. I evaluated the effects of blood circulation time, and blood storage duration on the ζ-potential response of RBCs circulating through a benchtop ECMO circuit. Considering the importance of membrane oxygenators in ECMO support systems, I further hypothesized that the addition of a membrane oxygenator into the benchtop circuit will compound the ζ-potential response due to increased RBC damage. Additionally, I investigated the effects of the maximum shear exposures on RBCs

in ECMO circulation through a miniaturized system, allowing for examination of a more homogeneous cell population. Although the effects of mechanical shear stress have been studied extensively in the context of RBC deformability and hemolysis (Faghih & Sharp, 2019; Huisjes et al., 2018), limited studies exist on the effects of mechanical shear stress on the electrokinetic surface charge of RBCs. Further, none have considered the compounding effects of blood storage duration on shear-induced RBC damage, which is important especially for patients requiring blood transfusions. Together, these research studies will:

ECMO Circuit Study:

Objective #1: Develop an understanding of the ζ-potential response of human RBCs circulating through a benchtop ECMO circuit.

Objective #2: Determine the compounding effects of blood circulation time and blood storage duration on the ζ-potential response of human RBCs circulating through a benchtop ECMO circuit.

Objective #3: Determine the additional effects of membrane oxygenator on the ζ-potential response of human RBCs circulating through a benchtop ECMO circuit.

Shear Stress Study:

Objective #1: Determine how compounding effects of blood storage and duration of mechanical shear stress exposure effects the ζ-potential response of human RBCs.

Objective #2: Determine how the duration of mechanical shear stress shear exposure effects the ζ-potential response of human RBCs.

Objective #3: Determine how the magnitude of mechanical shear stress exposure effects the ζ-potential response of human RBCs.

METHODS

IRB Approval for Human Subjects Studies: All studies were conducted in accordance with 45 CFR 46 and the principles of the Declaration of Helsinki, with approval from the Institutional Review Board (Wake Forest University, Winston-Salem, NC). Participants in the study were screened for relevant self-reported health issues. All participants provided written, informed consent after having received a detailed explanation of the study procedures.

Blood Procurement and Preparation for ECMO Experiments: In the ECMO study, for both Pump-Only and Pump+PIXIE flow groups, units of whole blood (~450 mL) were drawn from a total of 7 donors (4 male and 3 female) drawn by venipuncture into blood collections bags containing sodium heparin anticoagulant and shipped overnight from the blood bank (Zen-Bio, Inc., Durham, NC). Six of the donors were of African American ethnicity (the other donor was Hispanic). All donors were healthy (no underlying comorbidities). The age of all donors ranged from 26-55, and blood type (A+) was controlled across donors. Upon receipt, units were immediately stored as whole blood at 4°C in refrigeration for up to 49 days. At the blood storage date of interest (e.g., day 7, 14, 21, 30, and 49) approximately 25 mL of whole blood was aliquoted into conical tubes and RBCs were isolated by centrifugation (700 xg @ 5 minutes) washing twice with normal saline (0.9% NaCl). Following isolation, packed RBCs were resuspended at 10%

hematocrit in 100 mL of total blood volume. The reduced hematocrit was selected to allow for comparison across multiple blood storage dates using a single.

Additionally, while whole blood is conventionally used *in vivo*, isolated RBCs were selected to evaluate the bulk ζ-potential response of RBCs, without compounding effects of other blood components (e.g., platelets, leukocytes, etc.). Prior to initiation of blood circulation, a 1 mL blood sample was removed from the circuit, pelleted by centrifugation, and kept at room temperature (e.g., 19±2°C) as a static reference control.

Blood Procurement and Preparation for Shear Experiments: Fresh human whole blood (~3 mL) was drawn by venipuncture into blood collection tubes containing sodium heparin anticoagulant. Blood was drawn from two different donors, both healthy females (no underlying chronic conditions). Both donors had blood type O+ and the age of donors ranged from 26-40 years old. One donor was African American ethnicity and the other was Caucasian ethnicity. Collection tubes were immediately stored as whole blood at 4°C in refrigeration for up to 49 days. Following 7 days of blood storage, approximately 1 mL of whole blood was aliquoted, and the remaining blood was placed back in refrigeration for use in subsequent blood storage experiments (e.g., 21- and 49-days post-draw). RBCs were isolated from the whole blood by centrifugation, washing twice with normal saline (0.9% NaCl).

Following isolation, packed RBCs were resuspended in 1 mL Eppendorf tubes at 40% hematocrit in normal saline at a total volume of 175 uL per sample. Although a reduced hematocrit was needed for the ECMO experiments, as described above, we were

able to increase the hematocrit to physiologic levels (e.g., 40%) due to smaller blood volumes required for shear experiments. Additionally, while whole blood is conventionally used *in vivo*, isolated RBCs were selected to evaluate the bulk ζ-potential response of RBCs, without compounding effects of other blood components (e.g., platelets, leukocytes, etc.).

Benchtop ECMO Circuit Design: Benchtop ECMO circuits (**Figure 5.2:**) were constructed, each consisting of a roller pump (COBE Cardiovascular, Inc., Arvada, CO) and 100-mL blood bag connected by heparin-coated silicone tubing (ID: 1/4 in, OD: 3/8 in) and a volume-equivalent, 3D-printed reservoir to mimic the oxygenator, referred to in the *Results and Discussion* as the Pump-only group. An Affinity Pixie™ Pediatric hollow-fiber membrane oxygenator (Medtronic Plc, Minneapolis, MN) was placed between the pump outlet and blood bag inlet in one circuit, referred to in the *Results and Discussion* as the Pump+PIXIE group, to investigate the compounding effects of membrane oxygenators on the biophysical response of human RBCs.

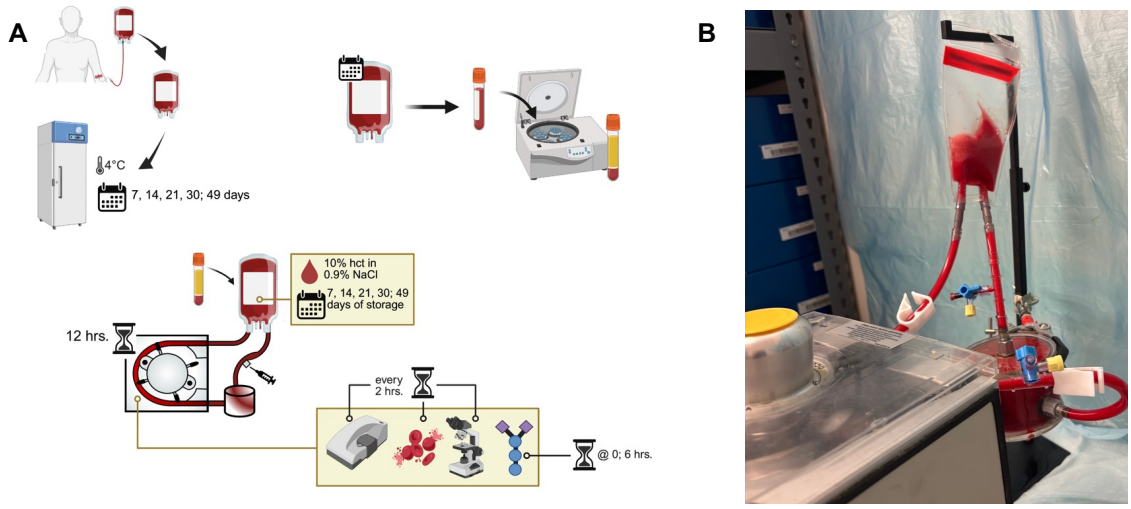

Figure 5.2: Workflow and set up for benchtop ECMO experiments. (A.) Experiments were repeated on Day 7, 14, 21, 30, and 49 of blood storage for donors with blood type A+, age matched (<55 y.o.). ζ-potential, percent hemolysis, and cell concentration and population % analysis was immediately performed for the static and flow-exposed samples every 2 hours, whereas sialic acid analysis was performed every 6 hours. (B.) Benchtop ECMO circuit with volume-equivalent chamber to mimic the oxygenator (Pump-only group).

On the oxygenator circuits, pre-and post-oxygenator pressure monitoring was carried out using Model 6069 DELTRAN® disposable pressure transducers (Utah Medical, Inc, Salt Lake City, UT) connected to a two-channel PendoTech Pressure MAT data acquisition system (Mettler-Toledo International Inc, Columbus, OH). Flow rate was monitored in real-time using the digital display on the roller pump's front control panel. Before starting each experiment, the circuits were primed with normal saline to remove any air bubbles from the tubing and oxygenator.

Roller Pump Flow Rate and Pressure Transducer Calibration: The roller pumps that I used in the benchtop ECMO circuits were graciously donated by Dr. Jim Jordan from the surplus supplies in his research laboratory at Atrium Health-Wake Forest Baptist Medical Center. Each of these pumps had previously been in clinical service with the Department of Perfusion at Atrium Health-Wake Forest Baptist Medical Center but now retired from clinical service due to upgrades to clinical equipment. Due to the age and extended clinical use of the roller pumps (Prior maintenance date: circa 2015 and clinical life: >10,000 circulating hours) manual flow calibration was necessary to ensure each roller pump provided the expected flow rate ±0.2 L/min prior to conducting *ex vivo* experiments.

Flow rate calibration was carried out by first inserting a segment of ¼-ich tubing into the roller pump raceway with the tubing end from the pump inlet inserted into a reservoir filled with ~3 L of distilled water, and the tubing end from pump outlet placed into another empty 3 L reservoir (**Figure 5.3A**). Next, the volume of water dispensed into the outlet reservoir over 1 minute was recorded with a stopwatch and volumes were confirmed using graduated cylinders recorded to ±0.05 L/min. Flow rates were measured at pump speeds of 50, 100, 150, and 200 revolutions/min (RPM) based on reference values displayed on the back of the pump (**Figure 5.3B**). The measured values were plotted against the reference values to ensure that the pump was operating within 5-10% of the expected flow rate (**Figure 5.3C**).

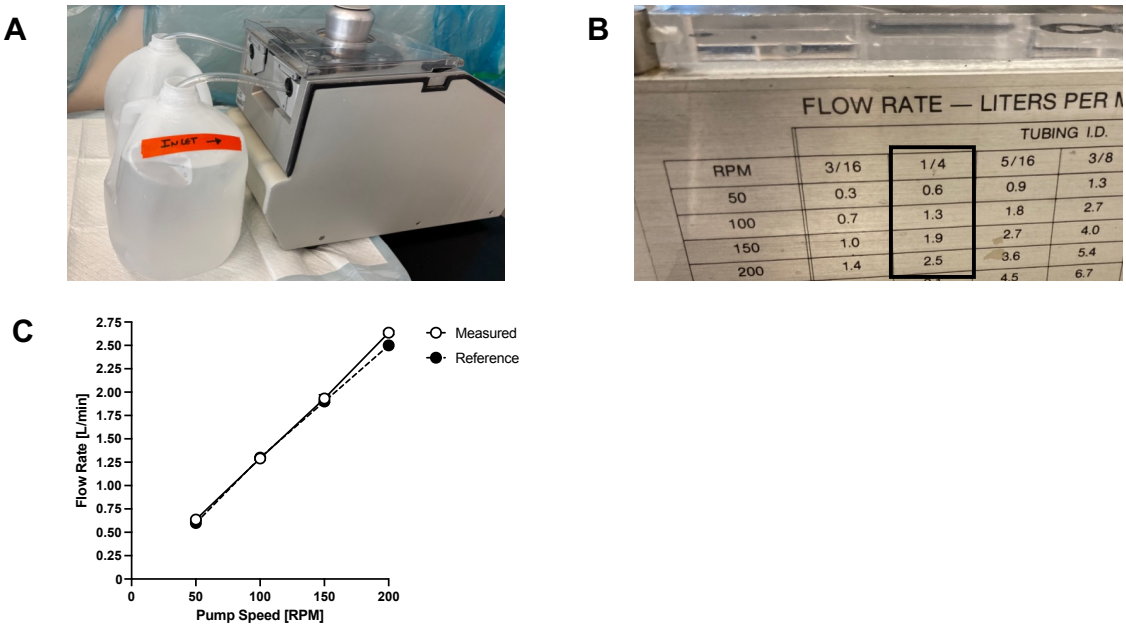

Figure 5.3: (A.) Schematic of pump flow calibration set up. (B.) Reference values provided by manufacturer. (C.) Linear regression plot comparing reference versus measured flow rate values for n=12 technical replicates per RPM interval.

Pressure transducer calibration was carried out by first opening the distal stopcock on each pressure transducer to expose it to atmospheric pressure (with the second stopcock closed to avoid introducing air into the ECMO circuit) and then pressing the TARE button on the PendoTech Pressure MAT data acquisition system to "zero out" the transducer readings. Each distal stopcock was then closed to atmosphere, and the second stopcock (proximal to the tubing) was opened to expose the transducers to the static pressure of the primed circuit (**Figure 5.5: A**). Proper pressure calibration was achieved with a static pressure differential of 1 pound/in^2 (psi) between oxygenator inlet (P_1) and oxygenator outlet (P_2) transducers (**Figure 5.5: B**).

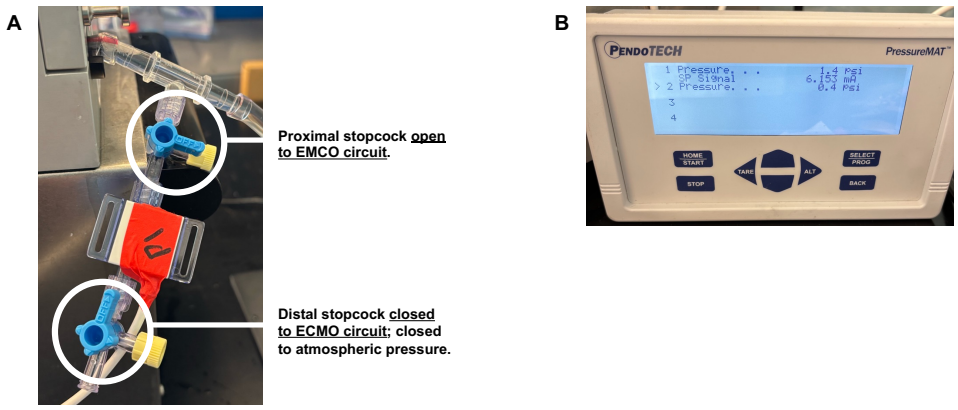

Figure 5.4: (A.) Representative stopcock configurations for measurement of static pressure in ECMO circuit. (B.) Pressure readings for properly calibrated DELTRAN® pressure transducers.

ECMO Circuit Operating Conditions: Blood was continuously circulated through the ECMO circuit for a total of 12 hours on the pre-determined blood storage experiment day. Every two hours, the sampling port was flushed with normal saline (0.9% NaCl). An initial 1 mL "waste" blood sample was drawn off each circuit's sampling port and discarded. This was done to avoid hemodilution from saline left in the stopcock during flushing, and to ensure that 100% of blood sampled from the circuit was exposed to pump flow. The stopcock "arm" has a volume of ~0.2 mL, so there is potential for stagnant cells to be included in the sample, unless the stopcock was purged with saline. After purging the sampling port, an additional 1 mL of blood was immediately drawn off each circuit and dispensed into labeled Eppendorf tubes. All blood samples were pelleted by centrifugation (700 x g @ 5 minutes) and let to stand at room temperature throughout the duration of experiments.

RBC Shearing System Setup and Operation: To induce the appropriate shear stress duration and magnitude, a linear Poiseuille shearing system was constructed in the manner

like that described by McNamee *et. al*, comprised of 38 mm segment of 400 µm I.D. polyethylene tubing (**Figure 5.6:**).

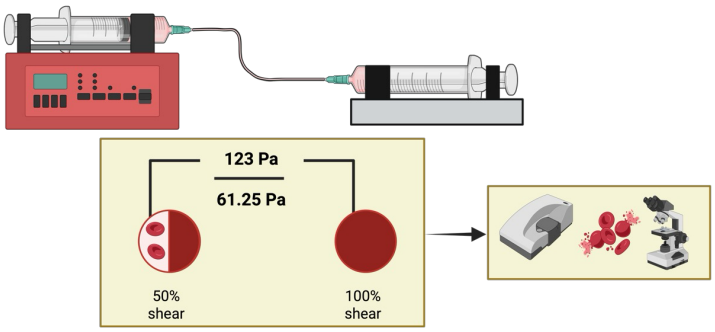

Figure 5.5: Schematic of benchtop shearing system designed to expose 100% of RBCs to maximum shear stress levels in ECMO, adapted from McNamee *et al.*

The shear stress magnitudes and shear durations used in this dissertation Chapter were based on the work of Mulholland *et al*. (to determine maximum shear in ECMO) and McNamee *et al* described subsequently. Through extensive optimization of shear magnitude-duration combinations (shown in **Figure 5.6**) McNamee *et al* found that shear durations beyond 10 seconds, at and above 50 Pa magnitude, produced sublethal mechanical trauma leading to overt hemolysis. For their study, a shear magnitude of 125 Pa stressed at durations of 1.5, 3, and 4.5 seconds were selected to (i.) avoid overt hemolysis, and (ii.) be representative of clinical mechanical circulatory support systems (e.g., >100 Pa). Considering the potential long-term and repetitive shear exposure of RBCs circulating through ECMO, I chose to investigate shear duration beyond that of McNamee *et al*. However, to avoid overt hemolysis, I limited the maximum shear duration to 6 seconds for both high and low shear magnitudes.

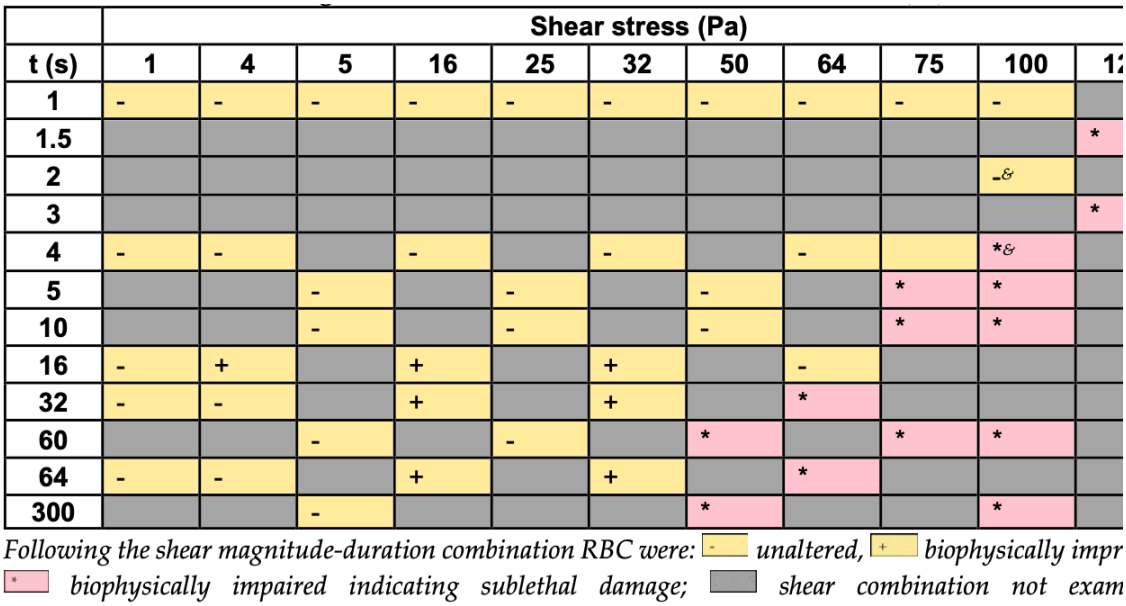

	Shear stress (Pa)										
t (s)	1	4	5	16	25	32	50	64	75	100	1
1	-	-	-	-	-	-	-	-	-	-	
1.5											*
2										-&	
3											*
4	-	-		-		-		-		*&	
5			-		-		-		*	*	
10			-		-		-		*	*	
16	-	+		+		+		-			
32	-	-		+		+		*			
60			-		-		*		*	*	
64	-	-		+		+		*			
300			-				*			*	

Following the shear magnitude-duration combination RBC were: - unaltered, + biophysically impr
** biophysically impaired indicating sublethal damage; shear combination not exam*

Figure 5.6: Shear stress-magnitude combinations identified by McNamee *et al*[31].

Following extensive optimization of my pump configuration/operating conditions, it was determined that, achieving the high shear stress magnitudes of 150 Pa and 400 Pa described by Mulholland *et al*., while also replicating the microfluidic shearing setup used by McNamee *et al* (e.g., tubing ID: 200 µm, tubing length: 0.94 m, and shear duration: 1.5 seconds/pass) would not be feasible because they required flow rates which exceeded the maximum allowable load applied to the motor (proprietary manufacturer information), causing the pump to stall. To mitigate this risk, through further optimization, a large (60mL) syringe as well as an increased tubing diameter (ID :400 µm) was selected to generate a flow rate necessary to still produce "high shear" within the ranges studied by McNamee *et al*, while preventing the built-in stall/shut-off mechanism from being triggered due to excessive force applied to the motor. To further mitigate stalling risk in my pump system, the final fluid viscosity was limited to 1.386 cP (by comparison whole blood viscosity is ~3-4 cP) which was determined as the viscosity of normal saline at 25°C,

(~1.12 cP), plus the viscosity of washed RBCs at 40% hematocrit, estimated at ~0.266 cP, based on values derrived from literature[31,32].

High (123 Pa) and low shear stress (61.25 Pa) magnitudes were produced using a syringe pump (NE-8000X, New Era Pump Systems Inc., New York, USA) programmed to operate at continuous flow rates of 33.45 mL/min (high shear) and 13.73 mL/min (low shear). The pump was programmed for a 60 mL syringe (barrel ID: 28.90 mm) at a fixed infuse/withdraw volume of 121.3 uL yielding a shear duration of 0.24 seconds per pass through the tubing. The shear stress magnitudes produced by the the microfluidic system were calculated by combining the Darcy-Weisbach and Hagen-Poiseuille equation(s) as described below:

$$\tau = \frac{32\eta Q}{\pi D^3} \quad (5.1)$$

Where η is the fluid viscosity, Q is the pump flow rate, and D is the internal diameter of the microfluidic tubing. In our system, the applied shear stress is calculated to be 123 Pa at fluid viscosity of 1.2 Pa.s (equating to ~10% hematocrit packed RBCs in normal saline). Additionally, the corresponding tubing length (L_{tube}) needed to produce a shearing duration (t_{shear}) of 1 seconds, based on the known flow rate (Q) and tubing internal diameter, was calculated by:

$$L_{tube} = \frac{Q \cdot t_{shear}}{\pi \left(\frac{D}{2}\right)^2} \quad (5.2)$$

To investigate the effects of shear duration on ζ-potential response of human RBCs, 175 uL of unsheared RBC suspension was removed from the Eppendorf tube via aspiration into a 1 mL syringe. Next, the sample syringe was attached to the free end of the pump tubing via a 31-gauge needle tip. RBCs were manually dispensed from the syringe into the tubing. Once the tubing was filled, WITHDRAW and PUMP cycles were alternated followed by START. The total number of cycles for each shearing duration is shown in **Table 5.2**. To prevent syringe back filling and ensure 100% of sample was exposed to shear, the plunger on the 1 mL syringe remained manually pressed during pump operation.

Table 5.2: Pump Operation Parameters for Shearing RBCs

Sample	Applied Shear Stress	Actual Shear Duration	# Cycles (alternating button presses)
HIGH SHEAR			
0 seconds	----	----	----
3 seconds	123 Pa	3.12	13
6 seconds		6.00	25
LOW SHEAR			
6 seconds	61.25 Pa	6.24	13

Following shear exposure, RBCs were removed from the pump through the 1 mL syringe, rapidly pulling back on the syringe plunger, followed by clamping the tubing distal to the needle tip with metal forceps to prevent negative backpressure from causing the tubing to refill. Sheared cells were dispensed back into the Eppendorf tube and ζ-potential measurements were immediately performed as described in *Chapter 3*.

To further investigate the effects of shear stress magnitude (e.g., high versus low shear stress) on the ζ-potential response of human RBCs, the pump flow rate was reduced to 16.73 mL/min (~61.25 Pa applied shear stress) and the experimental protocol was repeated for 6-second shear duration. Lastly, to investigate the sensitivity of ζ-potential measurement for detecting shear damage within a bulk cell population, a 50% sheared-to-unsheared mixture was prepared by suspending 5uL of 100% high-sheared and 5uL of unsheared (control) RBCs in 5mL of iso-osmotic buffer, for the 6-second shear duration group.

Buffer and Sample Preparation: For both ECMO and shear stress experiments, samples were prepared for electrokinetic and morphological analysis by resuspending 10 μL of packed RBC pellet in 5 mL of iso-osmotic, low conductivity buffer, prepared as described in *Chapter 4*. Cell concentrations for sheared/flow-exposed and static samples in both ECMO and shear stress experiments were at least 2 x 10^6 cells/mL over 49 days of blood storage duration.

Measurement of Surface ζ-potential: Measurement of surface ζ-potential was conducted using a Zetasizer Pro Red Label (Malvern Analytical, UK) system as previously described in *Chapter 3*. For ECMO experiments, ζ-potential measurements were collected in triplicate for up to N=7 biological replicates (separate donors) for static samples, and up to N=3 biological replicates for both Pump-only and Pump+PIXIE groups. For shear stress experiments ζ-potential measurements were collected in triplicate for N=3 biological replicates for all RBC sample groups

Measurement of Cell Radius and RBC Count: For all RBC sample groups in both ECMO and shear stress experiments, weighted cell radius and RBC count were determined from hemocytometer images using ImageJ software, as described in *Chapter 4*. The only variation from previously described methods is that for ECMO studies, RBC count is presented in the form of concentration, in cells/mL, and can be calculated from the total RBC count (same as *Chapter 4*) and volume of a 4 x 4 square grid, Equation 5.3:

$$C_{RBC}\ [\text{cells/mL}] = \left(\frac{\text{RBC Count}}{0.004\ \mu L}\right) x \left(\frac{1000 \mu L}{1\ \text{mL}}\right) \tag{5.3}$$

Where C_{RBC} is the RBC concentration, in cells/mL and RBC Count is the total number of RBCs counted in a 4 x 4 square grid. In clinical practice RBC count is represented in this manner. Thus, it allows for ease of interpretation of my findings in the broader scope of clinical practice.

Measurement of Free Sialic Acid Concentration: The free sialic acid (SA_{free}) concentration of all RBC sample groups in ECMO experiments were determined using a commercial assay kit based on methods described in *Chapter 4*. However, because there were no significant differences observed in ζ-potential response to shear, and considering the length and complexity of methods for quantification, SA_{free} measurements were not carried out for shear experiments.

Measurement of Intracellular Ca^{2+}: Measurements of intracellular calcium Ca^{2+} for both ECMO and shear stress experiments were carried out using a commercial assay kit based on methods from *Chapter 4.*

RESULTS AND DISCUSSION

Surface ζ-potential response in ECMO Circuits: In clinical practice, ECMO circuits are operated for 12 hours or longer and use whole blood stored for up to 42 days. The experiments were designed to mimic these conditions; however, RBCs were isolated from whole blood, and ECMO circuits were operated at 10% hematocrit. This allowed use of a single donor (from one 450 mL blood bag) across the entire storage duration (removing donor to donor variability over storage times). Surface ζ-potential measurements were performed immediately for the "static" and "flow-exposed" samples every 2 hours. **Error! Reference source not found.** shows the effects of blood storage duration and ECMO blood circulation on the surface ζ-potential response of RBCs.

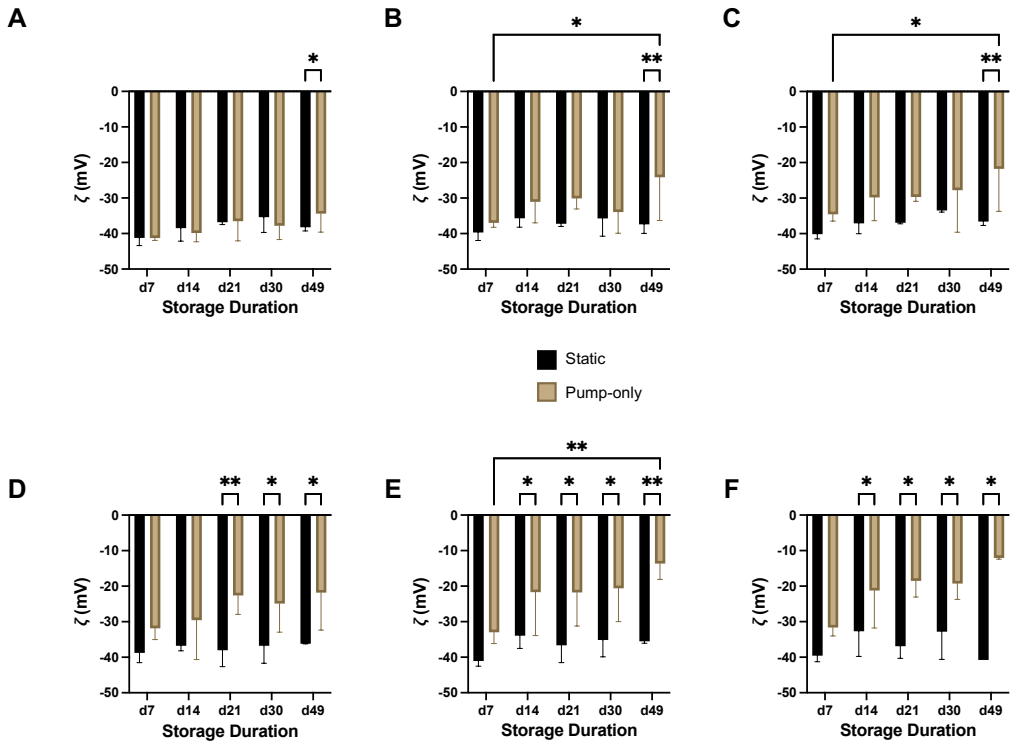

Figure 5.7: Changes in RBC surface ζ-potential over increasing blood storage duration at (A.) 2 hours, (B.) 4 hours, (C.) 6 hours, (D.) 8 hours, (E.) 10 hours, and (F.) 12 hours of ECMO blood circulation, comparing flow and static samples. Data presented represents the mean ± (s.d.) for all donors (static: N=7; flow: N=3). Statistical comparisons between static and flow-exposed samples were made via Two-way ANOVA using Tukey's Multiple Comparison test; *p<0.05, **p<0.01, ***p<0,001. All values with p<0.05 were considered statistically significant.

A significant decrease in surface ζ-potential with blood storage duration was observed (**Figure 5.7A**). I also observed a significant change in surface ζ-potential with increasing blood circulation time, and the response was further compounded by blood storage duration (**Figure 5.7B-F**). Specifically, at Storage Day 14 there was a significant change in surface ζ-potential due to flow effects after 10 hours. Further, at Storage Days 21 and 30, surface ζ-potential changes occurred after 8 hours, and at just 4 hours in the

oldest blood (Storage Day 49). These observations suggest that changes in the RBCs' physiology, impacting their ability to repel one another, are occurring within standard ECMO protocol timescales (circuit flow time and storage duration). Considering this, surface ζ-potential may be an early indicator of these changes, which has clinical implications for early prediction of cell aggregation and clot formation in ECMO circuits.

When probing the biophysical factors contributing to the observed changes in surface ζ-potential, the hemolysis in flow-exposed RBCs increased compared to the static samples after 6 hours (**Figure 5.8A**). Following 12 hours of blood circulation, an even more pronounced increase in hemolysis was observed for flow-exposed RBCs compared with static samples (**Figure 5.8B**). Longer storage time exacerbated hemolysis, with the most prevalent occurring at 49 days storage for both 6 and 12-hour blood circulation timepoints.

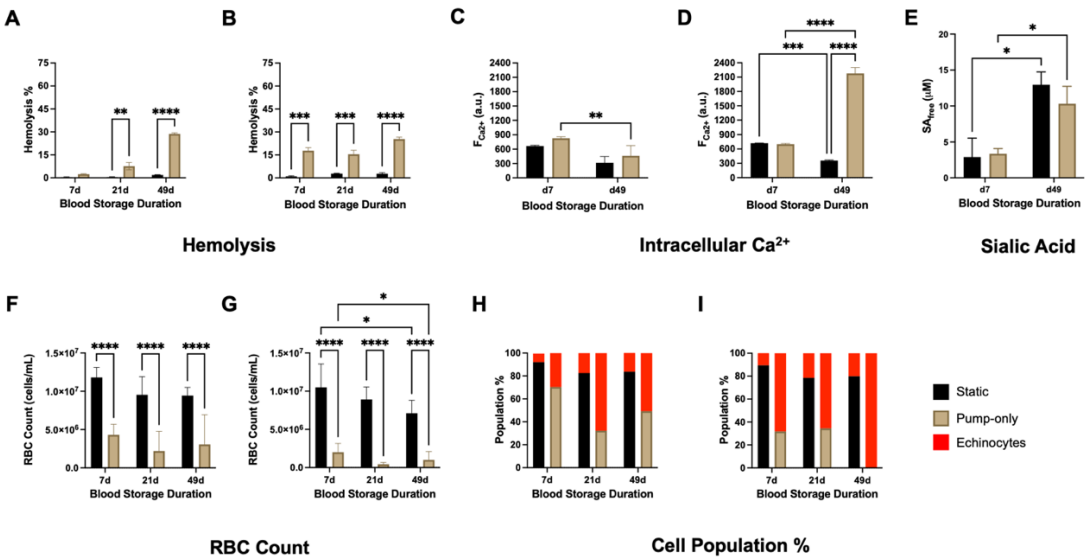

Figure 5.8: Change in RBC Hemolysis over increasing blood storage duration from 7 to 49 days following (A.) 6 hours and (B.) 12 hours of ECMO blood circulation. Change in Intracellular Ca^{2+}

over increasing blood storage duration following (C.) 6 hours and (D.) 12 hours. (E.) Change in free sialic acid (SA_{free}) concentration following 6 hours of ECMO blood circulation. Change in RBC count over increasing blood storage duration following (F.) 6 hours and (G.) 12 hours. Change in sub-population % over increasing blood storage duration following (H.) 6 hours and (I.) 12 hours. Data presented for all panels represents the mean ± (s.d.) for a single (N=1) donor. Statistical comparisons between static and flow (Pump-only) samples were made via Two-way ANOVA using Tukey's Multiple Comparison test; *p<0.05, **p<0.01, ****p<0.0001. All values with p<0.05 were considered statistically significant.

In addition to hemolysis %, both intracellular Ca^{2+} and sialic acid are important biophysical parameters used to characterize blood damage in human RBCs. Intracellular Ca^{2+} regulates cell volume and deformability, while bound sialic acid contributes up to 70% of the RBC's negative surface charge[33]. As demonstrated by McNamee *et al*[32], repeated exposure to flow-induced mechanical shear stress even over short durations (e.g., < 5s) cleaves sialic acid glycoproteins from the cell surface, reducing the electronegative charge density of the cell membrane, subsequently decreasing ζ-potential magnitude [31]. Here, the Ca^{2+} fluorescent intensity did not change between static or flow-exposed groups after 6 hours (**Figure 5.8C**). However, after 12 hours, a significant increase ($p<0.05$) in intracellular Ca^{2+} intensity was observed for flow-exposed RBCs following 49 days of blood storage (**Figure 5.8D**). The concentration of SA_{free} also increased with blood storage duration following 6 hours in ECMO circulation (**Figure 5.8E**).

Total RBC concentration decreased (**Figure 5.8F**) following 6 hours of blood circulation, with a similar but more pronounced shift following 12 hours of blood circulation (**Figure 5.8G**). Conversely, the percentage of echinocytes in the bulk cell

population increased for flow-exposed RBCs compared to static RBCs following 6 hours of blood circulation (**Figure 5.8H**), with a more pronounced shift following 12 hours of blood circulation (**Figure 5.8I**). I suspect both results are due to flow exposure in the ECMO circuit. Taken together with the observed increase in hemolysis, this suggests sequestering of lysed RBCs from circulation, as well as the presence of RBC oxidative damage as the drivers for the changes observed in surface ζ-potential. It should be emphasized that storage time was a significant factor when comparing static samples and flow-exposed samples to one another.

From the broader perspective of RBC biophysical properties, several authors have shown decreases in surface ζ-potential to be associated with blood storage[34] and RBC aging[35], as well as increasing fibrinogen-RBC binding and subsequent blood clotting risk[36]. Collectively, these studies support the hypothesis that blood storage compounds shear exposure effects to the surface ζ-potential response in RBCs and has the potential to elevate blood clotting risk in ECMO circuits due to the decrease in repulsive forces.

To further probe this hypothesis, a membrane oxygenator was added to the ECMO circuits. Membrane oxygenators are a critical component of the ECMO system providing artificial lung functionality by reoxygenating RBCs. However, as RBCs pass through the oxygenator, they are repeatedly subjected to periodic squeezing between membrane fibers. This squeezing mechanism as demonstrated by Pan *et al*, causes a multi-stage progression of cell membrane fatigue, characterized by initial elastic deformation and progressing to hemolysis[37]. Considering the increased shear exposure, it was expected to see a more

pronounced change in the surface ζ-potential response in RBCs. Interestingly, the converse response was observed, where the addition of the Affinity Pixie™ oxygenator caused an increase in ζ-potential (**Figure 5.9**).

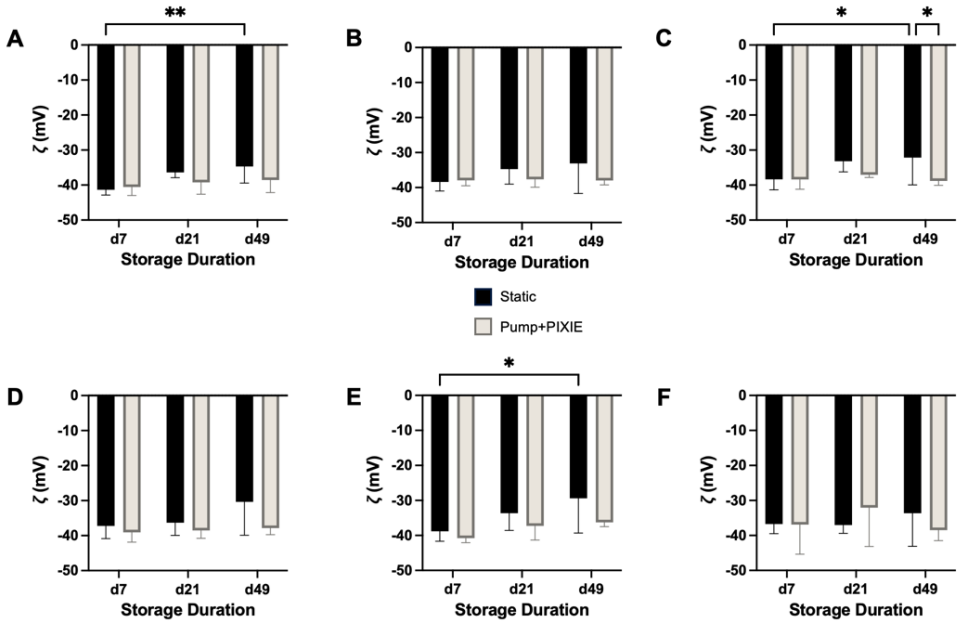

Figure 5.9: Changes in RBC surface ζ-potential through the Affinity Pixie™ Oxygenator circuit over increasing blood storage duration at (a). 2 hours, (b). 4 hours, (c). 6 hours, (d). 8 hours, (e). 10 hours, and (f). 12 hours of ECMO blood circulation. Data presented represents the mean ± (s.d.) for all donors (static: n=7; flow: n=4). Statistical comparisons between static and flow-exposed Pump+PIXIE samples were made via Two-way ANOVA using Tukey's Multiple Comparison test. All values with p<0.05 were considered statistically significant. Statistical comparisons between static and flow (Pump+PIXIE) samples were made via Two-way ANOVA using Tukey's Multiple Comparison test; *p<0.05, **p<0. 0.001. All values with p<0.05 were considered statistically significant.

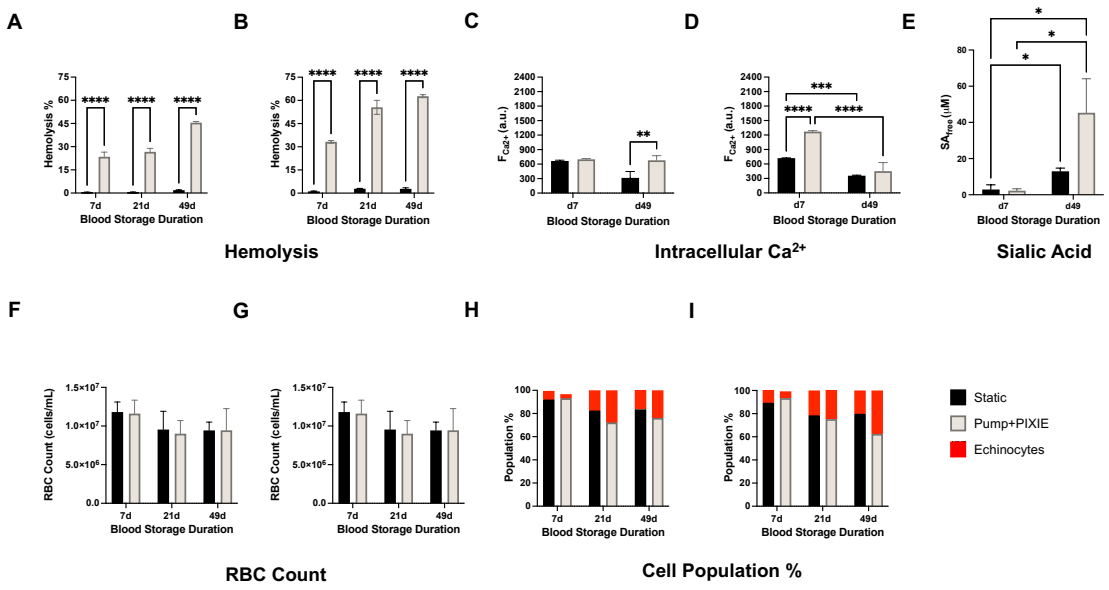

Figure 5.10: Change in RBC Hemolysis over increasing blood storage duration from 7 to 49 days following (A.) 6 hours and (B.) 12 hours of ECMO blood circulation. Change in Intracellular Ca^{2+} over increasing blood storage duration following (C.) 6 hours and (D.) 12 hours. (E.) Change in free sialic acid (SA_{free}) concentration following 6 hours of ECMO blood circulation in Affinity Pixie™ Oxygenator circuit. Data presented for all panels represents the mean ± (s.d.) for a single (N=1) donor. Statistical comparisons between static and flow (Pump+PIXIE) samples were made via Two-way ANOVA using Tukey's Multiple Comparison test; *p<0.05, **p<0. 0001*p<0. 0.001, ****p<0.0001. All values with p<0.05 were considered statistically significant.**

<u>Potential Considerations in Observed ζ-potential Response During ECMO:</u> I originally hypothesized that the observed surface ζ-potential response in ECMO flow was due to shear exposure on the RBCs. With the addition of the oxygenator, I expected to see those effects compound the observed response in surface ζ-potential. Interestingly, I did not observe that response, leading me to question to what extent is ζ-potential influenced by shear exposure? Mulholland *et al* showed that in a roller pump ECMO circuit, a peak shear stress of 150-400 Pa is experienced by approximately 1.17-1.49 x 10^{-7} dL of blood

volume occurring at the point when both rollers simultaneously occlude the tubing [24]. The hypothetical maximum percentage of shear damage experienced by red blood cells (RBCs) from the roller pump after 12 hours of continuous circulation in my ECMO circuit can be calculated. **Figure 5.11** depicts a schematic of the tubing geometry exposed to pump rollers.

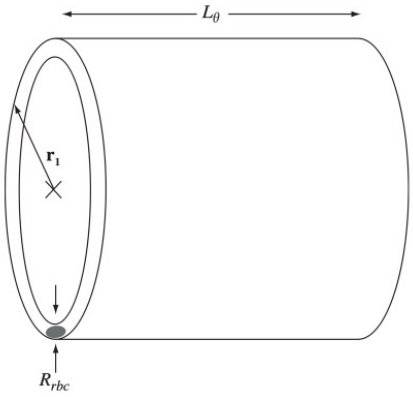

Figure 5.11: Tubing geometry exposed to pump rollers. Reproduced from Mulholland *et al*[25]. In the schematic, R_{rbc} represents a single RBC being compressed between the walls of the tubing during occlusion by the roller.

<u>Calculated Total RBC Exposure at 150 Pa Shear Stress:</u> Based on this range and the experimental parameters (e.g., circuit volume and pump speed) the total % of RBCs in the ECMO circuits exposed to nominal shear stress (e.g., 150 Pa) over 12 hours of blood circulation was calculated as follows:

$$\mathrm{P_{rbc\ @\ 150Pa}\ [\%]} = \left[\frac{(\mathrm{V_d\ x\ RPM\ x\ t_{circ}})}{\mathrm{V_{tot}}}\right] \mathrm{x}\ 100 \qquad (5.4)$$

Where RPM is the speed of the roller pump in revolutions per minute measured during ECMO experiments, t_{circ} is the ECMO blood circulation time (in hours), and V_{tot} is the

total blood volume (~100 mL) in the circuit. V_d is the volume (in deciliters) of RBCs damaged per revolution, given by:

$$\mathrm{V_d} = \sum_{\theta=0^\circ}^{360^\circ} \mathrm{L_\theta}[\pi(\mathrm{r_1^2} - (\mathrm{r_1} - \mathrm{R_{rbc}})^2)] \tag{5.5}$$

Where L_θ is the length of cells along the pump boot wall exposed to damaging shear stresses during that degree of rotation, θ, as described by Mulholland *et. al*. Additionally, r_1 and R_{rbc} are the radii of tubing and RBCs respectively.

Using an RBC volume of 1.49 x 10^{-7} dL, calculated from Mulholland *et. al*, and a pump speed of 156 RPM (equivalent to 2 L/min, measured during ECMO studies) the volume of damaged RBCs per minute is determined:

$$(1.49 \text{ x } 10^{-7} \text{ dL x } 156 \text{ RPM}) = 2.32 \text{ x } 10^{-5} \frac{\text{dL}}{\text{min}} \tag{5.6}$$

Converting ECMO circulation time to minutes, and volume to mL:

$$\left(2.32 \text{ x } 10^{-5} \frac{\text{dL}}{\text{min}} \text{x } 60 \frac{\text{min}}{\text{hr}} \text{x } 12 \text{ hr}\right) = 1.67 \text{ mL} \tag{5.7}$$

Finally, the maximum percentage of RBCs damaged in 100mL under 150 Pa is calculated as:

$$P_{rbc}\,[\%] = \left[\frac{(3.35\ \text{mL})}{(100\ \text{mL})}\right] \text{x}\ 100 = 1.67\% \tag{5.8}$$

Calculated Total RBC Exposure at 400 Pa Shear Stress: Inputting an RBC volume of 1.17 x 10^{-7} dL, calculated from Mulholland *et. al*, and ECMO circuit parameters described above, the total % of RBCs in my ECMO circuits exposed to high shear stress (e.g., 400 Pa) over 12 hours of blood circulation was calculated as:

$$(1.17 \text{ x } 10^{-7}\ \text{dL x } 156\ \text{RPM}) = \ 1.83 \text{ x } 10^{-5}\ \frac{\text{dL}}{\text{min}} \tag{5.9}$$

Converting ECMO circulation time to minutes, and volume to mL:

$$\left(1.83 \text{ x } 10^{-5}\ \frac{\text{dL}}{\text{min}} \text{x } 60 \frac{\text{min}}{\text{hr}} \text{x } 12\ \text{hr}\right) = \ 1.32\ \text{mL} \tag{5.12}$$

Finally, the maximum percentage of RBCs damaged in 100mL under 400 Pa is calculated as:

$$P_{rbc}\,[\%] = \left[\frac{(3.35\ \text{mL})}{(100\ \text{mL})}\right] \text{x}\ 100 = 1.32\% \tag{5.13}$$

Although it is unlikely that the low percentage of sheared RBCs is responsible for the observed decrease in the bulk surface ζ-potential response in ECMO circuits, I was interested to know what level of shear stress (and percentage of total cells exposed) would alter surface ζ-potential to a detectable level. To accomplish this, a microfluidic-based shearing system adapted from McNamee *et al*[38], described in the *Methods* section above,

was constructed to expose 100% of RBCs in suspension to a known level of mechanical shear stress.

As shown in **Figure 5.13 (A-C),** the magnitude of ζ-potential remained unchanged with increasing shear exposure time over 49 days of blood storage. Additionally, no changes in RBC count were observed due to either increased blood storage or increased exposure time to high shear stress. Interestingly, however, the percentage of echinocytes did increase due to both blood storage duration and increased exposure time. This was also corroborated by decreases in weighted cell radius under the same conditions.

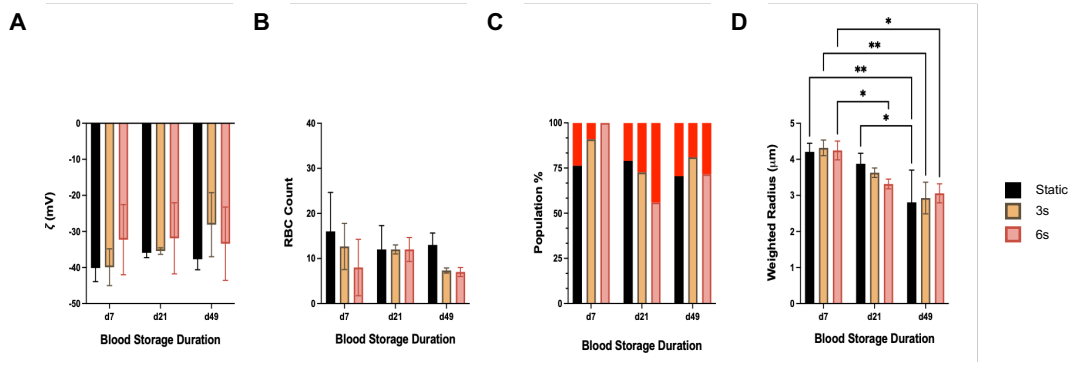

Figure 5.12: No changes observed in (A.) RBC surface ζ-potential (B.) RBC count, (C.) and Population % over increasing blood storage duration following exposure to 3 seconds and 6 seconds of high (H.S.=123 Pa) mechanical shear stress. (D.) Changes observed in weighted cell radius over increasing blood storage duration following exposure to 3 seconds and 6 seconds of high (H.S.=123 Pa) mechanical shear stress. Data presented represents the mean ± (s.d.) for (N=3) donors. Statistical comparisons between static, 3 seconds, and 6 seconds shear stress duration groups were made via One-way and Two-way ANOVA using Tukey's Multiple Comparison test; *p<0.05, **p<0.01. All values with p<0.05 were considered statistically significant.

Further evaluating the effect of shear stress magnitude on RBC electrokinetic and biophysical properties (**Figure 5.13**), no changes in either ζ-potential response or RBC

count were observed with increasing shear magnitude or blood storage duration. Interestingly, in addition to the expected decrease in RBC radius in static samples due to prolonged blood storage, there was a significant ($p<0.05$) decrease in RBC radius at low shear magnitude with increased blood storage. This suggests that blood storage compounds the effects of mechanical shear on RBCs, making them susceptible to damage even at the lower shear magnitude.

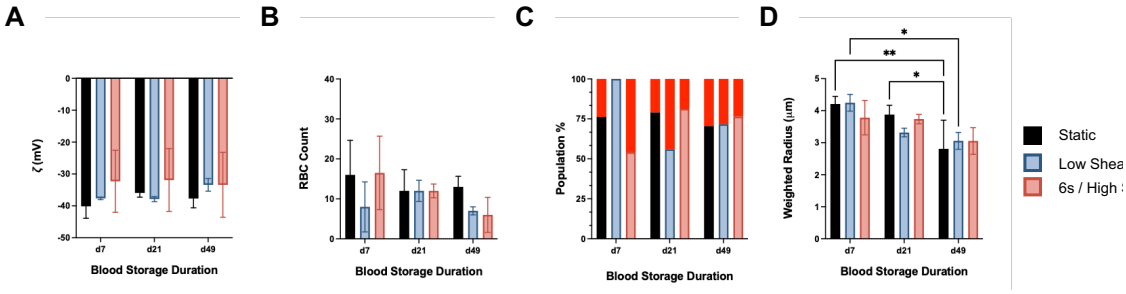

Figure 5.13: No changes observed in (A.) RBC surface ζ-potential (B.) total RBC count, (C.) and Population % over increasing blood storage duration following exposure to low (L.S. = 61.25 Pa) and high (H.S.=123 Pa) mechanical shear stress. (D.) Changes observed in weighted cell radius over increasing blood storage duration following exposure to low and high mechanical shear stress. Data presented represents the mean ± (s.d.) for (N=3) donors. Statistical comparisons between static, low shear stress, and high shear stress magnitude groups were made via One-way and Two-way ANOVA using Tukey's Multiple Comparison test; *p<0.05, **p<0.01. All values with p<0.05 were considered statistically significant.

On Day 7 of blood storage there was a decrease in intracellular Ca^{2+} fluorescence with increasing shear exposure time (compared to static samples), and with increasing shear stress magnitude (**Figure 5.14**). Biophysically, this increase in intracellular Ca^{2+}, corroborated by an observed decrease it RBC radius, indicates the activation of PIEZO-1 Ca^{2+}ion channels.

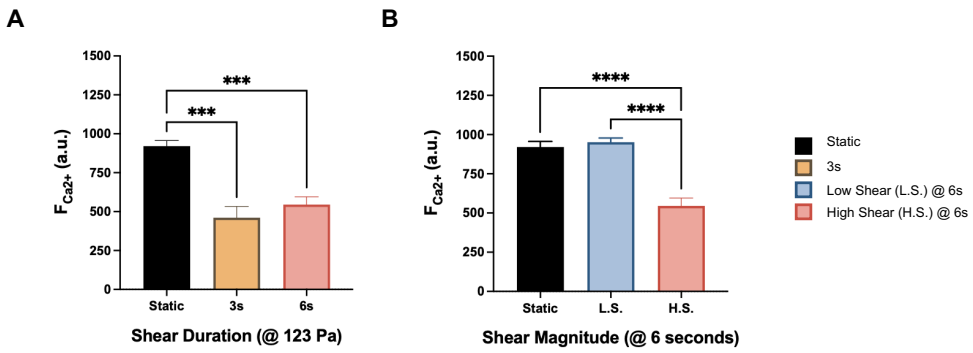

Figure 5.14: Change observed in intracellular Ca^{2+} over increasing blood storage duration following exposure to (A.) increasing shear exposure. (B.) Change observed in intracellular Ca^{2+} over increasing blood storage duration following exposure to low (61.25 Pa) and high (123 Pa) mechanical shear stress at 6 seconds of shear duration. Data presented represents the mean ± (s.d.) for a single (N=1) donor. Statistical comparisons between static, low shear stress, and high shear stress magnitude groups were made via One-way ANOVA using Tukey's Multiple Comparison test; *** p<0.001, ****p<0.0001. All values with p<0.05 were considered statistically significant.

While Day 49 timepoints could not be obtained due to experimental limitations and time constraints, blood storage has been shown to compound PIEZO1 channel activity, accelerating Ca^{2+} flux. Thus, I would expect an even more pronounced decrease in Ca^{2+} at high shear stress (as well as low shear stress, based on decreases in RBC radius) at Day 49 of blood storage.

Although I originally hypothesized that the ζ-potential of RBCs is altered by increasing shear stress exposure time and with shear stress magnitude, neither of these conditions resulted in ζ-potential changes. One possible explanation can be seen in the work of Merlo *et al*. and Kobuchi et al[39,40] who both showed that the viscosity and composition of suspending media impact the motion and shear response on isolated RBCs. Suspension of RBCs in polyvinyl-propylene (PVP) solution results in more uniform shear

exposure (eliminating the non-Newtonian effects of blood). Comparing the present study with prior work by McNamee *el al*[32,41], despite applying similar high shear stress magnitude (123 Pa in our study versus 125 Pa from McNamee *et al*) and shear stress duration (3 seconds of shear exposure in both studies) I did not changes in ζ-potential magnitude, compared to significant decrease in ζ-potential observed by McNamee *et al*. I suspect that these differences are because the RBC suspensions exhibited Newtonian, shear-thinning behavior due to the low blood viscosity.

Another experimental parameter I considered that could be responsible for the observed changes in ζ-potential in the Pump-only group was chemical exposure to the custom 3D printed chamber used to volume-match the oxygenator in the original experiments. Printed plastic components, such as that used in the Pump-only group, have been shown to cause oxidative stress (OS) and cytotoxicity to RBCs[42], thus, I also tested blood circulating without the reservoir (silicone tubing only). No changes in ζ-potential was observed in the Tubing-only group compared to the flow group with the 3D-printed reservoir (**Figure 15.15A**). Further, I visually observed a progression of blood color from bright red to dark brown over 12 hours of circulation in both circuits (**Figure 15.15E**). This blood discoloration suggests that the tubing and other plastic components inflict significant OS in RBCs[43] over just 12-hours of ECMO blood circulation, an important consideration when monitoring inflammatory and coagulation response in ECMO patients.

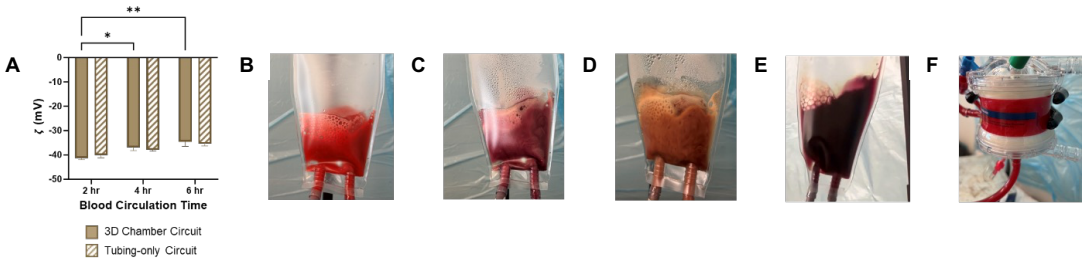

Figure 5.15: Comparison of circuits with and without a 3D printed reservoir. (A.) Changes in RBC surface ζ-potential between Pump-only circuit configurations at 7 days blood storage. Data presented represents the mean ± (s.d.) for a single (n=3 technical replicates) donor. Statistical comparisons between 3D Chamber and Tubing-only circuit groups, and over 6 hours of blood circulation time, were made via Two-way ANOVA using Tukey's Multiple Comparison test; *p<0.05, **p<0.01. Comparison of blood color changes following (B.) 2 hours, (C.) 6 hours and (D.) 12 hours of blood circulation for Pump-only ECMO circuits.

Although a higher percent hemolysis was observed in the Pump+PIXIE group, indicating increased shear stress due to RBCs squeezing through membrane fibers, I suspect that the membrane oxygenator may provide chemical protection against OS, based on no changes in blood discoloration (**15.15F**) or surface ζ-potential (**Figure 5.7**) compared to Pump-only flow samples. Recall from *Chapter 4* that surface ζ-potential decreased with chemical OS damage in H_2O_2 , confirmed by flow cytometry analysis.

This further confirmed my hypothesis that OS is a likely mechanism responsible for the ζ-potential changes in flow samples I observed in the Pump-only group. Many membrane oxygenators are coated with synthetic polymers to enhance biocompatibility and mitigate the formation of blood clots. In fact, the Affinity Pixie™ oxygenator used in this study is coated with Balance™ Biosurface, a heparin-free coating comprised of a negatively

charged hydrophilic layer with bonded (negative) sulphonated polymer groups, which mimic the native endothelium[44]. Armstong *et al*[45] demonstrated that sulphonated polymer groups (also referred to as polyethylene glycol, PEG) lower the viscosity of RBCs in plasma via binding to blood group-specific antigens on the membrane surface, inhibiting cell agglutination (clustering) and enhancing RBC survival in circulation. Jovtchev *et al* also showed that binding of PEG polymer particles to the RBC membrane can elevate the steric (negative) charge of RBCs increasing repulsive force between cells[46]. This phenomenon might explain the increase in surface ζ-potential that I observed in the Affinity Pixie™ oxygenator circuit, compared to the Pump-only flow samples. Another possible explanation is that the because the RBCs Pump-Only are poorly oxygenated, they are undergoing rapid more rapid autooxidation of metHb leading to a greater response via lipid peroxidation. Since the oxygenator serves as a "little lung" the surface area to volume ratio is greater for O_2 diffusion, acting as a re-oxygenation and protective effect to limit oxidative damage to the RBC membrane.

STATISTICAL ANALYSIS

All statistical analysis was carried out using Prism 11 (GraphPad Software, La Jolla, CA).

ECMO Circuit Study: To address Objectives 1 and 2 of the ECMO Study— (1) *develop an understanding of the ζ-potential response of human RBCs circulating through a benchtop ECMO circuit*, and (2) *determine the compounding effects of blood circulation time and blood storage duration on the ζ-potential response of human RBCs circulating through a benchtop ECMO circuit*—I investigated the main effects of two independent

variables on the ζ-potential response of human RBCs: overall flow effect (e.g., static versus flow for each time point), and blood storage effect (e.g., Day 7 versus Day 14 for both flow and static samples).

To analyze flow effects and blood storage effects, a Two-Way analysis of variance (ANOVA) was used to compare the mean ζ-potential of three technical replicates for N=7 donors for static samples, and mean of three technical replicates for N=3 donors for flow samples, at each flow timepoint, across five storage dates. This analysis specifically looked at both main effects, and interaction effects (e.g., does the effect of flow depend on the duration of blood storage?). Follow up post-hoc analysis was performed using Tukey's Multiple Comparisons Test to identify specific differences between blood circulation timepoints. Across blood circulation timepoints and blood storage conditions, all p-values <0.05 were statistically significant.

To address Objective 3 of the ECMO Study—*determine the additional effects of membrane oxygenator on the ζ-potential response of human RBCs circulating through a benchtop ECMO circuit*—I investigated the main effects of two independent variables on the ζ-potential response of human RBCs: overall flow effect (e.g., static versus flow for each time point), and blood storage effect (e.g., Day 7 versus Day 14 for both flow and static samples) in the PIXIE Oxygenator ECMO circuit.

To analyze the effects of oxygenator-induced flow and blood storage effects, a Two-Way analysis of variance (ANOVA) was used to compare the mean ζ-potential of

three technical replicates for N=7 donors for static samples, and mean of three technical replicates for N=3 donors for flow samples, at each timepoint, across four storage dates. This analysis specifically looked at both main effects, and interaction effects (e.g., does the effect of flow depend on the duration of blood storage?). Follow up post-hoc analysis was performed using Tukey's Multiple Comparisons Test to identify specific differences between blood circulation timepoints. Across blood circulation timepoints and blood storage conditions, all p-values <0.05 were statistically significant. To control for donor-to-donor variability and repeated measures we fitted a mixed-effects linear model.

Shear Stress Study: Mechanical Shear Study Objective 1—*determine how compounding effects of blood storage and duration of mechanical shear stress exposure effects the ζ-potential response of human RBCs*—was addressed in parallel with analysis for both Objective 2 and Objective 3. Specifically, for Objective 2—*determine how the duration of mechanical shear stress shear exposure effects the ζ-potential response of human RBCs*—a Two-Way analysis of variance (ANOVA) was used to compare the mean ζ-potential three technical replicates for total of N=3 donors across three shearing durations (0, 3, and 6 seconds) at three different storage dates. This analysis specifically looked at both main effects and interaction effects (e.g., does the effect of shear stress duration on ζ-potential depend on the duration of blood storage?). Follow up post-hoc analysis was performed using Tukey's Multiple Comparisons Test to identify specific differences between shear stress durations. Across shear stress durations and blood storage conditions, all p-values <0.05 were statistically significant.

Similarly, for Mechanical Shear Study Objective 3—*determine how the magnitude of mechanical shear stress exposure effects the ζ-potential response of human RBCs*—a Two-Way analysis of variance (ANOVA) was used to compare the mean ζ-potential three technical replicates for total of N=3 donors across low shear stress (61.25 Pa) and high shear stress (123 Pa) magnitudes at 6 seconds of shear duration, at three different blood storage dates. This analysis specifically looked at both main effects and interaction effects (e.g., does the effect of shear stress magnitude on ζ-potential depend on the duration of blood storage?). Follow up post-hoc analysis was performed using Tukey's Multiple Comparisons Test to identify specific differences between shear stress durations. Across shear stress durations and blood storage conditions, all p-values <0.05 were statistically significant.

STUDY LIMITATIONS, IMPLICATIONS, AND FUTURE WORK

This study has several limitations, both in the physical experimental design, and limitations of current knowledge, prompting further investigations. The following sections, sub-divided between ECMO and shear stress experiments, address these limitations and propose future studies to address critical gaps.

ECMO Circuit Study: Experimentally, ζ-potential was evaluated in isolated RBCs in the absence of interactions with other blood components commonly found in whole blood (e.g., fibrinogen, platelets and leukocytes). Furthermore, while the compounding effects of a

membrane oxygenator were investigated from the perspective of inflicting greater mechanical shear stresses on the cell membrane, oxygen flow was not incorporated into the membrane oxygenator during ECMO circulation. Not only is low oxygen delivery a strong predictor of acute kidney injury (AKI) and mortality risk in ECMO patients, but the oxygen-deoxygenation process causes RBC aggregation through CO_2-mediated increases in pH [16]. Considering this biophysical response, I would expect the ζ-potential response of RBCs to be directly altered by the presence of oxygen, which should be incorporated into the ECMO circuit in subsequent studies.

The present ECMO study was limited to four individual donors for flow-based studies and seven individual donors for static/storage experiments. Although all donor characteristics were matched for age (<55 years old), and blood type (A+), I observed significant donor-to-donor variability especially at longer blood circulation times and storage durations. Expanding the donor pool, I would expect lower variability across ζ-potential and other measurements due to an increased sample size. Additional studies with other blood types would not result in differences in ζ-potential response because, the surface proteins responsible for blood type do not contribute to the negative surface charge of RBCs [47].

Shear Stress Study: This study has several limitations, both in the physical experimental design, and limitations of our current knowledge, prompting further investigations. Due to the concerns for pump stalling discussed previously, I did not incorporate PVP into our samples to increase the viscosity of RBC suspensions to physiological levels, and to fully

eliminate the non-Newtonian properties of RBCs. Because the cell suspensions retained non-Newtonian blood properties, it is likely that the actual applied shear stresses were lower than calculated, particularly under high shear conditions due to RBC shear-thinning behavior, and vice-versa.

To address the limitations of this pilot study, future work should focus on investigating the ζ-potential response of RBCs under Newtonian rheological properties by supplementing our RBC suspensions with PVP. Interestingly, while sodium heparin is often used as anticoagulant to prevent clot formation by deactivation of thrombin, heparin has also been known to induce RBC aggregation due to binding of heparin molecules to the RBC surface, reducing the number of glycoprotein binding sites and overall net negative electrokinetic charge. Therefore, the influence of heparin concentration on cell aggregation and the ζ-potential response of RBCs under mechanical shear stress conditions should be investigated with the aim of gaining a better understanding of the interplay between anti-coagulant therapeutics, mechanical flow-induced shear stress, and cell aggregation to inform blood coagulation management in clinical practice.

Although these results show that ζ-potential can monitor human RBCs in benchtop ECMO circuits under clinically relevant flow conditions, we have yet to fully elucidate the biophysical mechanics responsible for the observed ζ-potential response to flow-induced mechanical shear stress. Recognizing that the PIEZO1 channel is mechano-activated by external mechanical stressors, I originally hypothesized that flux of K^+ and Ca^{2+}, from the cytoplasm was the mechanism responsible for the lack of a ζ-potential response, due to shielding of the electronegative charge on the RBC surface, as described in *Chapter 3 and*

Chapter 4. However, the absence of intracellular Ca^{2+} changes at both 6 and 12 hours of circulation at day 7 suggests K^+ to be the dominant cation. Further biochemical analysis, applying techniques of proteomics is needed to quantify extracellular ion concentrations to support this proposition.

Recent advancements in oxygenator technologies, including the PIXIE model used in the present study, have added surface coatings to the membrane fibers to decrease clotting risk[44,48,49]. The primary function of the surface coatings is to decrease platelet activation and inflammatory response by mimicking the hydrophobic surface properties of the native endothelium. Other studies have demonstrated a reduction in visible clot formation and RBC aggregation when using negatively charged polytetrafluorethylene (PTFE) conduits [50–52], compared to tradition polyvinylchloride (PVC) tubing. Thus, it is highly probable that the PIXIE oxygenator coating preserves the cell's repulsive strength.

To test this hypothesis further, studies would be conducted to investigate the effects of different surface coatings on the ζ-potential response of RBCs, and the degree to at which surface coating exposure would result in a significant ζ-potential response (based on the length and size of the ECMO circuit) . This would be accomplished by comparing the small ECMO circuit used in the current study (where RBCs circulated through many times over 12-hour duration) to a larger circuit, where RBC circulation/exposure to the oxygenator would likely be reduced.

Finally, this work not only provides a scientific basis for more refining the for clinical utilization of stored blood in ECMO practice (as noted by the increased risk for RBC aggregation and blood clotting at longer storage dates) , but the high temporal sensitivity of surface ζ-potential measurements (compared once-daily ACT and PfHb measurements) is clinically important because it is indicative of an increased risk of cell aggregation, clotting and potential circuit failure, and we can detect changes in RBCs at a much earlier timescales than measurements currently used in clinical ECMO practice, particularly at longer storage durations.

REFERENCES

1. Bartlett, R. *et al.* The history of extracorporeal membrane oxygenation and the development of extracorporeal membrane oxygenation anticoagulation. in vol. 50 081–090 (Thieme Medical Publishers, Inc., 2024).

2. Annich, G. Extracorporeal life support: the precarious balance of hemostasis. *J. Thromb. Haemost.* **13**, S336–S342 (2015).

3. Sniderman, J., Monagle, P., Annich, G. M. & MacLaren, G. Hematologic concerns in extracorporeal membrane oxygenation. *Res. Pract. Thromb. Haemost.* **4**, 455–468 (2020).

4. Bilodeau, K. S., Saifee, N. H. & Chandler, W. L. Causes of red blood cell loss during extracorporeal membrane oxygenation. *Transfusion (Paris)* **63**, 933–941 (2023).

5. Bertin, S. *et al.* Effects of Extracorporeal Membrane Oxygenation Circuits on Drug Sequestration: A Review of Ex Vivo Experiments. *J. Clin. Med.* **14**, 8060 (2025).

6. Heith, C. S. *et al.* Effects of an ex vivo pediatric extracorporeal membrane oxygenation circuit on the sequestration of mycophenolate mofetil, tacrolimus, hydromorphone, and fentanyl. *J. Pediatr. Pharmacol. Ther.* **24**, 290–295 (2019).

7. Meyer, A. D. *et al.* Effect of blood flow on platelets, leukocytes, and extracellular vesicles in thrombosis of simulated neonatal extracorporeal circulation. *J. Thromb. Haemost.* **18**, 399–410 (2020).

8. Sarathy, S. *et al.* Flow monitoring of ECMO circuit for detecting oxygenator obstructions. *Ann. Biomed. Eng.* **49**, 3636–3646 (2021).

9. Shin, Y. *et al.* Association between blood transfusion and early mortality in patient undergoing extracorporeal membrane oxygenation. *Sci. Rep.* **15**, 27145 (2025).

10. Godin, C. & Caprani, A. Effect of blood storage on erythrocyte/wall interactions: implications for surface charge and rigidity. *Eur. Biophys. J.* **26**, 175–182 (1997).

11. Wagner, S. J., Glynn, S. A. & Welniak, L. A. Research opportunities in optimizing storage of red blood cell products. *Transfusion (Paris)* **54**, 483 (2013).

12. Ghaleb, S. *et al.* Correlation among hemolysis biomarkers in pediatric patients undergoing extracorporeal membrane oxygenation. *J. Extracorpor. Technol.* **53**, 125–129 (2021).

13. Baghaei, R. *et al.* Red Cell Distribution Width as a Predictor of Outcome in Cyanotic Congenital Cardiac Surgery. (2022).

14. Shin, D. A., Lee, J. C., Shin, H., Cho, Y.-J. & Kim, H. C. Point-of-care testing of plasma free hemoglobin and hematocrit for mechanical circulatory support. *Sci. Rep.* **11**, 3788 (2021).

15. Nellis, M. E., Dalton, H. & Karam, O. Quantifiable bleeding in children supported by extracorporeal membrane oxygenation and outcome. *Crit. Care Med.* **47**, e886–e892 (2019).

16. Cicha, I., Suzuki, Y., Tateishi, N. & Maeda, N. Changes of RBC aggregation in oxygenation-deoxygenation: pH dependency and cell morphology. *Am. J. Physiol.-Heart Circ. Physiol.* **284**, H2335–H2342 (2003).

17. Frey, P. E. Shear Stress-Induced Alterations in Red Blood Cell Calcium Accumulation, Microvesicle Formation, and Deformability Under Mechanical Circulatory Support Conditions. (2025).

18. Barshtein, G., Ben-Ami, R. & Yedgar, S. Role of red blood cell flow behavior in hemodynamics and hemostasis. *Expert Rev. Cardiovasc. Ther.* **5**, 743–752 (2007).

19. Chien, S. Red cell deformability and its relevance to blood flow. *Annu. Rev. Physiol.* **49**, 177–192 (1987).

20. Clavería, V., Wagner, C., Connes, P., Villat, A. & Abkarian, M. Aggregating and blood flow in health and disease. in *Dynamics of Blood Cell Suspensions in Microflows* 183–213 (CRC Press, 2019).

21. Bachmann, C. *et al.* Fluid dynamics of a pediatric ventricular assist device. *Artif. Organs* **24**, 362–372 (2000).

22. Becsek, B., Pietrasanta, L. & Obrist, D. Turbulent systolic flow downstream of a bioprosthetic aortic valve: velocity spectra, wall shear stresses, and turbulent dissipation rates. *Front. Physiol.* **11**, 577188 (2020).

23. Chen, Z., Sun, A., Wang, H., Fan, Y. & Deng, X. Non-physiological shear stress-induced blood damage in ventricular assist device. *Med. Nov. Technol. Devices* **3**, 100024 (2019).

24. Scotten, L. N. & Siegel, R. Importance of shear in prosthetic valve closure dynamics. *J Heart Valve Dis* **20**, 664–72 (2011).

25. Mulholland, J. W., Shelton, J. & Luo, X. Blood flow and damage by the roller pumps during cardiopulmonary bypass. *J. Fluids Struct.* **20**, 129–140 (2005).

26. Izumida, Y., Seiyama, A. & Maeda, N. Erythrocyte aggregation: bridging by macromolecules and electrostatic repulsion by sialic acid. *Biochim. Biophys. Acta BBA-Biomembr.* **1067**, 221–226 (1991).

27. Jan, K. Electrochemical basis of heparin-induced red blood cell aggregation. in (ACS Publications, 1980).

28. Barodka, V. M. *et al.* New insights provided by a comparison of impaired deformability with erythrocyte oxidative stress for sickle cell disease. *Blood Cells. Mol. Dis.* **52**, 230–235 (2014).

29. Cooke, B. M., Mohandas, N. & Coppel, R. L. Malaria and the red blood cell membrane. in vol. 41 173–188 (Elsevier, 2004).

30. Lansink-Hartgring, A. O., Hoffmann, R., van den Bergh, W. & de Vries, A. Changes in red blood cell properties and platelet function during extracorporeal membrane oxygenation. *J. Clin. Med.* **9**, 1168 (2020).

31. McNamee, A. Physical alterations to erythrocytes following sublethal mechanical stresses. (2020).

32. McNamee, A. P., Tansley, G. D. & Simmonds, M. J. Sublethal mechanical trauma alters the electrochemical properties and increases aggregation of erythrocytes. *Microvasc. Res.* **120**, 1–7 (2018).

33. Seaman, G., Knox, R., Nordt, F. & Regan, D. Red cell aging. I. Surface charge density and sialic acid content of density-fractionated human erythrocytes. *Blood* **50**, 1001–1011 (1977).

34. Silva, D. C. *et al.* Optical tweezers as a new biomedical tool to measure zeta potential of stored red blood cells. *PloS One* **7**, e31778 (2012).

35. Huang, Y. *et al.* Human red blood cell aging: correlative changes in surface charge and cell properties. *J. Cell. Mol. Med.* **15**, 2634–2642 (2011).

36. Carvalho, F. A., de Oliveira, S., Freitas, T., Gonçalves, S. & Santos, N. C. Variations on fibrinogen-erythrocyte interactions during cell aging. *PLoS One* **6**, e18167 (2011).

37. Pan, Y., Li, Y., Li, Y., Li, J. & Chen, H. Fatigue of red blood cells under periodic squeezes in ECMO. *Proc. Natl. Acad. Sci.* **119**, e2210819119 (2022).

38. McNamee, A. P., Tansley, G. D. & Simmonds, M. J. Sublethal mechanical trauma alters the electrochemical properties and increases aggregation of erythrocytes. *Microvasc. Res.* **120**, 1–7 (2018).

39. Kobuchi, Y., Ito, T. & Ogiwara, A. A Model for Rouleaux Pattern Formation of Red Blood Cells: Enumeration of Absolutely Stable Patterns. in *Biomathematics and Related Computational Problems* 371–379 (Springer, 1988).

40. Merlo, A. *et al.* Influence of storage and buffer composition on the mechanical behavior of flowing red blood cells. *Biophys. J.* **122**, 360–373 (2023).

41. McNamee, A. P., Fitzpatrick, T., Tansley, G. D. & Simmonds, M. J. Sublethal supraphysiological shear stress alters erythrocyte dynamics in subsequent low-shear flows. *Biophys. J.* **119**, 2179–2189 (2020).

42. Luximon, A. & Luximon, Y. New technologies—3D scanning, 3D design, and 3D printing. in *Handbook of Footwear Design and Manufacture* 477–503 (Elsevier, 2021).

43. Kassa, T., Jana, S., Baek, J. H. & Alayash, A. I. Impact of cold storage on the oxygenation and oxidation reactions of red blood cells. *Front. Physiol.* **15**, 1427094 (2024).

44. Zhang, M. *et al.* Anti-thrombogenic surface coatings for extracorporeal membrane oxygenation: a narrative review. *ACS Biomater. Sci. Eng.* **7**, 4402–4419 (2021).

45. Armstrong, J. K., Meiselman, H. J. & Fisher, T. C. Covalent binding of poly (ethylene glycol)(PEG) to the surface of red blood cells inhibits aggregation and reduces low shear blood viscosity. *Am. J. Hematol.* **56**, 26–28 (1997).

46. Jovtchev, S., Djenev, I., Stoeff, S. & Stoylov, S. Role of electrical and mechanical properties of red blood cells for their aggregation. *Colloids Surf. Physicochem. Eng. Asp.* **164**, 95–104 (2000).

47. Karemore, M. N. & Avari, J. G. Alteration in zeta potential of erythrocytes in preeclampsia patients. in *Prediction of maternal and fetal syndrome of preeclampsia* (IntechOpen, 2019).

48. Marlena, J. Novel Anti-Thrombotic Coatings for Cardiovascular Medical Devices. (2020).

49. Zhao, C. *et al.* Commercial and novel anticoagulant ECMO coatings: a review. *J. Mater. Chem. B* **11**, 4832–4841 (2023).

50. Arul, R. M., Danajka, M. K., Gray, E. C., Henretta, K. P. & Pierrakos, O. A Design Feasibility Investigation for a Pulmonary ePTFE Transcatheter Pediatric Heart Valve. in 61–66 (IEEE, 2023).

51. Serna III, C. *et al.* Development of a large diameter in vitro flow loop thrombogenicity test system. *Artif. Organs* **49**, 65–73 (2025).

52. Welborn, L. H. *et al.* Design and Preliminary Testing of a Quadleaflet ePTFE Pediatric Prosthetic Heart Valve. in 95–98 (IEEE, 2022).

Chapter 6: Conclusions and Future Work

CONCLUSIONS

Although the surface ζ-potential response of cells has been studied in many biomedical applications, including across mammalian species, the underlying mechanisms responsible for changes in ζ-potential of human red blood cells (RBCs) are largely unknown. Considering the importance of RBC monitoring for studying RBC-related diseases (e.g., malaria and sickle cell anemia) and the importance of RBC monitoring to inform blood storage and blood volume management (such as in ECMO patients), the primary aim of this dissertation was to investigate changes in the surface ζ-potential response of human RBCs exposed to chemical and mechanical interventions. These included induced oxidative stress and shear stress exposure. I then determined the applicability of ζ-potential as a real-time biomarker for monitoring human RBCs in a clinically relevant setting by investigating changes in ζ-potential response to blood circulation time and blood storage duration in *ex vivo* extracorporeal membrane oxygenation (ECMO) circuits.

Optimization of ζ-potential Measurement in RBCs: To carry out robust, reliable ζ-potential experiments throughout this work, it was necessary to optimize several experimental parameters, including the conductivity of the iso-osmotic suspending medium and RBC concentration. Results of these investigations showed that higher medium conductivity produced the least amount of inter-replicate variability. Further, when comparing 10% and 40% hematocrit, no significant change was observed in ζ-

potential magnitude, suggesting that results obtained in this dissertation can be translated to real-world 40% hematocrit applications. Additionally, no significant changes in ζ-potential magnitude at cell concentrations between 10^6-10^7 cells/mL were found, however, a significant decrease in ζ-potential was observed at lower (10^5 cells/mL) and higher (10^8 cells/mL) concentrations. At lower cell concentrations there is a greater signal-to-noise ratio in bulk ζ-potential, resulting in a lower mean ζ-potential magnitude, and greater measurement spread. This has implications for conditions that may yield low final cell concentrations and suggests that whole blood RBC concentrations (>10^8 cells/ml) may require dilution These optimization experiments informed all subsequent experiments which were conducted at ~430 uS/cm medium conductivity and cell concentrations within operating range of 10^6-10^7 cells/mL.

Research Aim 1 Conclusions - RBC Monitoring in OS Processes: In Research Aim 1 I investigated the ζ-potential response of human RBCs exposed to chemical oxidative stress, probing the sensitivity of ζ-potential for informing progression of OS damage to RBCs. Following treatment of healthy RBCs with hydrogen peroxide (H_2O_2), surface ζ-potential and DEP properties (e.g., effective membrane capacitance, effective membrane conductance, and cytoplasmic conductivity) were measured, along with microscope images to assess morphological changes. Results revealed a H_2O_2 dose-dependent decrease in ζ-potential magnitude. This ζ-potential response, corroborated by changes in all DEP properties and changes in cell morphology, indicates that ion flux, specifically potassium (K^+), is a primary driver for changes in surface ζ-potential in H_2O_2 driven OS processes.

Additionally, to probe the sensitivity of ζ-potential response to different OS pathways, a follow up study investigated changes in the ζ-potential response of human RBCs exposed to different OS drug agents. OS was chemically induced by treating RBCs with tert-Butyl hydroperoxide (tBHP) and cumene hydroperoxide (COOH). Results from this experiment revealed significant changes in both intracellular Ca^{2+} and SA_{free}, however, no significant changes were observed in ζ-potential magnitude of tBHP-treated RBCs. Additionally, only minimal changes were observed in COOH treated RBCs, compared with ζ-potential from H_2O_2 results Objective 1. Considering that H_2O_2 is a cytoplasm-targeting OS agent and both tBHP and COOH are membrane-targeting OS agents, differences in ζ-potential response may be due to widespread membrane damage with H_2O_2 (via spectrin-globin crosslinking) compared to only localized lipid peroxidation in tBHP and COOH. Another possible reason for the observed differences in ζ-potential response between OS agents, and a limitation of tBHP and COOH studies, was the lack of GPX inhibition.

Collectively, my findings demonstrate that ζ-potential can detect subtle shifts in H_2O_2-induced OS progression in human RBCs. Previously, *ex vivo* studies monitoring OS response in human RBCs relied on assessing morphological changes and were unable to distinguish subtle shifts in RBC function (e.g., ion channel inhibition) occurring with OS progression. The present work helps to address this unmet need by demonstrating the applicability of ζ-potential as an alternative technique for RBC monitoring in OS, providing greater measurement sensitivity (manuscript submission expected April/May 2026 to Analyst).

Research Aim 2 and Research Aim 3 - RBC Monitoring in ECMO and Shear Stress:

In Research Aim 2 and Research Aim 3 I sought to investigate the applicability of surface ζ-potential as a real-time biomarker for monitoring human RBCs in ECMO circuits. Following setup and priming of the benchtop *ex vivo* ECMO circuit, ζ-potential measurements were obtained, along with microscopy (to measure cell count and cell radius) every two hours over 12 hours of blood circulation time, and over 49 days of blood storage. Results show a significant decrease in ζ-potential with blood storage duration, and a significant decrease in ζ-potential with blood circulation time, further compounded by blood storage duration. With the addition of the Affinity Pixie™ oxygenator, I expected to see those effects increase the observed changes in surface ζ-potential (with a reduction in overall surface potential). Interestingly, I did not observe that, leading me to question to what extent is ζ-potential response influenced by shear exposure? Applying calculations from Mulholland *et al* to experimental parameters of my ECMO circuit (see *Chapter 5*) revealed <2% of RBC's experience peak mechanical shear stress over 12 hours of ECMO blood circulation. Although it is unlikely that the low percentage of sheared RBCs is responsible for the observed decrease in the bulk surface ζ-potential response in ECMO circuits, I was interested to know what level of shear stress (and percentage of total cells exposed) would alter surface ζ-potential to a detectable level. This is important for deciphering the potential compounding factors contributing to ζ-potential response seen in Pump-only ECMO circuits, and for understanding the overall response of ζ-potential to mechanical shear stress exposure in a controlled experimental environment.

Results from the shear stress study showed that the magnitude of ζ-potential remained unchanged with increasing shear exposure time over 49 days of blood storage. Additionally, no changes in RBC count were observed due to either increased blood storage or increased exposure time to high shear stress. Further, evaluating the effect of shear stress magnitude on RBC electrokinetic and biophysical properties, no changes in either ζ-potential response or RBC count was observed with increasing shear magnitude or blood storage duration. Collectively, these findings indicate that the reduced cell-to-cell repulsive force, indicated by a decrease in ζ-potential magnitude, is due to fewer cell interactions rather than a direct reduction in cell surface charge.

The ECMO study demonstrated that surface ζ-potential can detect flow-induced changes in RBCs due to oxidative stress, however, it is limited (at least from the observations in this study) in detecting hemolysis and shear stress changes. Further, the progressive decrease in surface ζ-potential from blood storage Day 7 to Day 49, and the surface zeta potential decrease as early as 8 hours of blood circulation (on Day 21 of storage) show the impact of storage duration on RBC electrophysiology in ECMO. This highlights the use of surface ζ-potential as a biomarker to help refine blood banking guidelines for improved clinical outcomes. Lastly, the increase in surface ζ-potential in Affinity Pixie™ oxygenator flow samples suggests that membrane oxygenators protect RBCs from OS (despite increased hemolysis) which may have benefits for blood preservation. (Manuscript submitted 2/2026 and under review in Scientific Reports)

FUTURE WORK

RBC Monitoring in OS Processes: In the present work I demonstrated that surface ζ-potential can detect subtle shifts in H_2O_2-induced OS progression in human RBCs but is only able to detect minimal changes between OS agents with different mechanisms of action (i.e., comparing tbHP and COOH). It should be noted that studies in Objective 2 only accounted for inhibition of catalase with sodium azide (NaN_3), despite glutathione being an equally potent antioxidant enzyme. Further, RBCs in these studies were exposed to high levels of OS compared to physiologic levels. making translation to real-world clinical applications and applications of surface ζ-potential as a real-time biomarker for monitoring OS processes difficult. Therefore, future work focused on applying ζ-potential as an RBC biomarker in OS processes will:

Determine effects of incubation time on the ζ-potential response at physiologically relevant treatment dosage (e.g., below 0.5 mM). Longer exposure time will also better mimic exposure in the body.

Determine mechanistic contributions of glutathione and catalase for RBC repair, observed through the lens of ζ-potential modulation. This will also include the addition of other OS agents such as superoxide and diamide.

Determine biophysical mechanisms responsible for sialic acid removal in oxidative processes. This will focus on comparing sialic acid removal by viral agents to drug-induced ROS mechanisms of removal.

Mechanical Shear Stress Experiments: There are several opportunities to continue investigating the ζ-potential in monitoring mechanical shear stress exposure in human RBCs as follows:

Determine ζ-potential response of human RBCs to mechanical shear stress in physiologically relevant fluids, to accurately mimic rheological properties observed in *vivo*. This alternative study can be accomplished by supplementing RBC suspensions with polyvinyl-propylene (PVP) solution to increase fluid viscosity and remove non-Newtonian properties, to produce more uniform shear exposure (eliminating the non-Newtonian effects of blood).

Determine the effects of heparin concentration on ζ-potential response of human RBCs exposed to mechanical shear stress. While sodium heparin is often used as anticoagulant to prevent clot formation by deactivation of thrombin, heparin has also been known to induce RBC aggregation due to binding of heparin molecules to the RBC surface, reducing the number of glycoprotein binding sites and overall net negative electrokinetic charge. Therefore, the influence of heparin concentration on cell aggregation and the ζ-potential response of RBCs under mechanical shear stress conditions should be investigated with the aim of gaining a better understanding of the interplay between anti-coagulant therapeutics, mechanical flow-induced shear stress, and cell aggregation to inform blood coagulation management in clinical practice.

Determine the ζ-potential response of human RBCs exposed to peak mechanical shear stress. This will be accomplished by using a microfluidic syringe pump with a higher force-load tolerance (e.g., New Era-8000 Syringe Pump), allowing for application of shear stresses at 150 Pa and 400 Pa, as originally proposed, prior to pump optimization.

ECMO Experiments: Considering the multi-faceted response of human RBCs to mechanical and oxidative stress (OS) and blood storage effects future ECMO studies will:

Determine the time-based response of oxygenator protective effects, and effects of blood storage additives. This will be accomplished by expanding the size of the Affinity Pixie™ oxygenator circuit (to more clinically relevant lengths) to determine if less time through the oxygenator produces the same protective effects. Additionally, to mimic *in vivo* blood storage, and evaluate the compounding effects of additives, whole blood will be utilized in our circuit, as well as comparing blood storage effect with and without the addition of storage additives (e.g., CPDA). Lastly the hemoglobin state in PIXIE oxygenator circuits will be evaluated based on absorbance spectroscopy using a microplate reader.

Determine the compounding effect of oxygen on ζ-potential response in ECMO. To enable closer clinical correlation and investigate the relationship between oxygen binding and RBC surface charge, oxygen will be introduced into the circuit at varied O_2 gas rates to investigate the relationship between oxygen binding and RBC surface charge.

Additionally, considering the potent antioxidant properties of nitric oxide, this can also be introduced into the circuit to investigate repair of tubing-based OS damage.

Determine effects of circuit components on ζ-potential response in ECMO. Considering the wide variability of clinical ECMO circuit configurations and ECMO oxygenators available on the market, the effects of membrane fiber orientation, membrane material, and oxygenator size can be investigated.

Curriculum Vitae

(See subsequent pages)

DR. BRANDON K. EBERL, PHD

Winston-Salem, North Carolina

803-646-9906 | drbrandoneberlphd@gmail.com

PROFESSIONAL EXPERIENCE

Graduate Research Engineer, Cardiovascular Perfusion & Blood Management **February 2023 to Present**

Wake Forest University (Winston-Salem, North Carolina)

- Completed 300+ hours in extracorporeal circulatory equipment preparation, maintenance, and *in vitro* ECMO circuit monitoring (e.g., building pumps, blood priming, and hemolysis monitoring) to facilitate successful execution of *in vitro* ECMO experiment protocols.
- Developed experiment protocols and training materials informed by Extracorporeal Life Support Organization (ELSO) and Food and Drug Administration technical standards.
- Skilled in aseptic laboratory techniques for processing, isolation, and recovery of human red blood cells.

Graduate Research Engineer, Prosthetic Heart Valve Hemodynamics **August 2019 to December 2022**

Wake Forest University (Winston-Salem, North Carolina)

- Served as lead point-of-contact for daily operations of the nascent Cardiovascular Fluid Dynamics Laboratory.
- Managed $20,000 grant funding portfolio across breath of cardiovascular research areas, including purchase requisitions and budget management to facilitate efficient laboratory operations.
- Managed and trained 5 inter-disciplinary teams of engineers, senior scientists, and student researchers on optimal configuration and operation of heart simulator flow apparatus.
- Evaluated *in vitro* hemodynamic performance of pediatric prosthetic valve therapies through hemodynamic waveform analysis and data post-processing.

CLINICAL CARDIOVASCULAR EXPERIENCE

Pediatric and Adult Cardiovascular Perfusion **September 2025 to January 2026**

Atrium Health Levine Children's Hospital (Charlotte, North Carolina)

Observation duration: 8 hours

- Shadowed certified Pediatric Perfusionist Jillian Holler, CCP during congenital heart defect surgical procedures, including ASD and Partial Anomalous Pulmonary Venous Return repair, and Bidirectional Glenn procedure (Hypoplastic Right Heart Syndrome staged repair).
- Gained first-hand exposure to the major components of cardiopulmonary bypass circuit (e.g., roller pumps, membrane oxygenator). Observed process for initiation of cardiopulmonary bypass and "coming off pump".
- Learned about specific considerations for pediatric/congenital heart cases, including need for circuit pre-priming with packed RBCs in neonates to mitigate hemodilution. Learned about importance of patient anatomy for cannulation (e.g., placement of cannulas in SVC and IVC to fully drain atrium during atrial septal defect repair).
- Gained appreciation for importance of inter-disciplinary collaboration and communication between perfusionists and other members of OR team through discussions with nurse anesthetist and scrub tech.

Atrium Health Cabarrus Hospital (Concord, North Carolina)

Observation Duration: 5 hours

- Shadowed certified Adult Perfusionist Zach Lambert, CCP during surgical repair of triple coronary artery bypass, as well as surgical mitral valve replacement (with MITRIS RESILIA bioprosthesis).
- Gained hands-on exposure with cardioplegia equipment set-up prior to going on bypass.
- Discussed benefits of using retrograde analogous priming (RAP) technique during bypass to limit hemodilution.
- Discussed strategies for monitoring coagulation risks (e.g., heparin dosing and measurement of activated clotting time) during cardiopulmonary bypass, and discussed approaches to adjust mean arterial pressure (e.g., administering calcium for vasoconstriction) to facilitate refilling of the heart when coming off bypass.

ECMO Support and Cardiac Intensive Care Unit **November 2023**
Duke University Healthcare (Durham, North Carolina)

Observation duration: 2 hours
- Shadowed cardiothoracic surgeon Joseph Turek, MD, in Cardiovascular ICU. Gained first-hand exposure to patients supported on ECMO.
- Gained insight into clinical decision-making (e.g., blood product administration, circuit monitoring) to improve treatment outcomes for ECMO patients.
- Developed appreciation for the importance of inter-disciplinary collaboration and communication in cardiac critical care through interactions with ICU nurses and advanced practice providers.

Pediatric Cardiology **January 2021 to December 2022**
Brenner Children's Hospital (Winston-Salem, North Carolina)

Observation duration: 30 hours
- Shadowed pediatric cardiologists, Michael Walsh, MD and Carmen Kiper, MD multiple days each semester across outpatient clinic, echocardiography imaging laboratory, and during inpatient rounds to gain clinical exposure and inform clinical significance and translation of Ph.D. thesis research.
- Gained hands-on experience with reading and interpreting ECHO and cMRI patient scans and interpretation of clinical findings in the context of engineering hemodynamic performance and ventricular energy loss principles.
- Applied understanding of cardiovascular imaging modalities (e.g., ECHO and cMRI) through extensive case review with attending physicians.
- Disseminated fundamental knowledge of cardiovascular anatomy, physiology, and congenital heart pathophysiology through facilitation of case discussions with pediatric cardiologists and medical students.
- Fostered clinician-engineer collaborations by providing engineering perspectives to inform clinical case planning.

LEADERSHIP EXPERIENCE

Graduate Student Body President, School of Medicine Campus **April 2021 to April 2023**
Wake Forest University (Winston-Salem, North Carolina)
- Appointed by Senior Associate Dean of Graduate School, and Director of Biomedical Graduate Programs to represent 300+ M.S. and Ph.D. students on the Wake Forest University School of Medicine campus.
- Collaborated with University administration to secure $6,000 stipend increase for all Ph.D. graduate students on the Wake Forest University School of Medicine campus.
- Partnered with Reynolda Campus Graduate Student Government leadership to host joint inter-campus "WFU Graduate School Formal" social networking event during Fall 2022 semester.

Undergraduate Student Body President **March 2018 to April 2019**
University of South Carolina Aiken (Aiken, South Carolina)
- Elected by the University of South Carolina Aiken's student body to represent 3,700+ undergraduate students.
- Served as student representative on the South Carolina Collaborative working with state legislators to improve higher education opportunities for college students across the state of South Carolina.
- Served as Chancellor's appointee on Cabinet Search Committee for Executive Vice Chancellor of Student Life.

EDUCATION

Ph.D. | Biomedical Engineering **May 2026**
Wake Forest University (Winston-Salem, North Carolina)

PhD Dissertation: "Surface Zeta Potential as a Biomarker for Monitoring Human Red Blood Cells"

B.S. | Industrial Process Engineering **May 2019**
University of South Carolina Aiken (Aiken, South Carolina)

Bachelor's Thesis: "Post-processing of Metal 3D Printed Pressure Vessels"

RESEARCH SCHOLARSHIP AND DISSEMINATION

Oral Presentations:

- **Eberl, BK**, "Surface Zeta Potential as a Biomarker for Monitoring Human Red Blood Cells in Extracorporeal Membrane Oxygenation". Sanibel Symposium | May 10, 2025; Fort Meyers, FL

- **Eberl, B.K.,** "Engineering Outside the Box: An Interdisciplinary Approach and Insights from a USC Aiken Alumni". University of South Carolina Aiken | March 25, 2024; Aiken, SC

- **Eberl, B.K.,** "Electrokinetic Analysis of Oxidative Stress in Human Red Blood Cells". Biomedical Engineering Society Annual Meeting | October 14, 2023; Seattle, WA

Publications:

- **Eberl, B.K.**, Henslee, E.A., et al. " Electrophysiology as a Real-time Biomarker for Human Red Blood Cell Monitoring in Extracorporeal Membrane Oxygenation". *Nature Sci. Reports, [Manuscript submitted; under review].*

- **Eberl, B. K.,** Manferdelli, G., & Goss, K. N. Coronary Microvascular Dysfunction and Exercise-Induced ST Changes Following Trauma in a Young Adult Born Preterm: A Case Report. Case Rep Clin Cardiol J. 2025; 5 (4): 163. Case Rep Clin Cardiol J. 2025; 5 (4): 163 www. cardiologycasereportsjournal.org, 2, 22-24.

- Welborn, L. H., Himes, A. K., Greenlee, I. E., DeWitt, N. J., Burgess, A. T., **Eberl, B. K.,** & Pierrakos, O. (2022, April). Design and Preliminary Testing of a Quadleaflet ePTFE Pediatric Prosthetic Heart Valve. In 2022 Systems and Information Engineering Design Symposium (SIEDS) (pp. 95-98). IEEE.

- Main, K. L., **Eberl, B. K.,** McDaniel, D., Tikadar, A., Paul, T. C., & Khan, J. A. (2021). Nanoparticles size effect on thermophysical properties of ionic liquids-based nanofluids. Journal of Molecular Liquids, 343, 117609.

- **Eberl, B**., Mikolanis, C., Eberl, K., McKeel, C., Ketusky, E., & Krentz, T. (2020, August). Effects of Post-Manufacturing Process on Material Properties of 3D Printed Vessels. In Pressure Vessels and Piping Conference (Vol. 83884, p. V008T08A044). American Society of Mechanical Engineers.

ACADEMIC HONORS AND AWARDS

Invited Keynote Speaker, Sanibel Symposium	2025
Best Student Poster, AES/SciX Conference	2024
Outstanding Senior Student, Industrial Process Engineering	2019
Inductee, Robert E. Alexander Leadership Hall of Fame	2019
Dean's List, University of South Carolina Aiken	2014 to 2019

CERTIFICATIONS AND PROFESSIONAL MEMBERSHIPS

American Society of Extracorporeal Technology (AmSECT), Professional Member	2025 to Present
AHA Certified in CPR and Basic Life Support (Cert. #: 271261898164)	2021 to Present
American Heart Association, Professional Member | *Young Hearts Council Member*	2021 to Present
Biomedical Engineering Society (BMES), Student Member	2019 to Present